Decoding the Structural Determinants of Hemagglutinin Mediated Influenza Entry and Antigenicity

Natalie K. Garcia

A dissertation

submitted in partial fulfillment of the

requirements for the degree of

Doctor of Philosophy

University of Washington

2015

Reading Committee:

Kelly K. Lee, Chair

William M. Atkins

Abhinav Nath

Program Authorized to Offer Degree:

Pharmacy - Medicinal Chemistry

University of Washington

Abstract

Decoding the Structural Determinants of Hemagglutinin Mediated Influenza Entry and Antigenicity

Natalie K. Garcia

Chair of the Supervisory Committee:
Associate Professor Kelly K. Lee
Pharmacy - Medicinal Chemistry

The fusion glycoproteins found on the surface of enveloped viruses enable the delivery of the viral genome into the host cell by facilitating the merger of the viral membrane with the host cell membrane, an essential step for a productive infection. The thermodynamically favorable but kinetically slow process of spontaneous membrane fusion is permitted by such complex viral molecular machines, which work by releasing enough conformational energy to surmount the activation barrier associated with fusion between two separate membranes. The trimeric influenza viral fusion glycoprotein hemagglutinin (HA) binds cell surface sialic acid moieties to trigger endocytosis of the virion into the host cell. During endosomal maturation, the drop in pH induces structural rearrangements within HA, to drive membrane fusion. While the pre-fusion and fragmentary post-fusion states of HA have been crystallized, the intermediates that promote fusion are too dynamic and transient for characterization through classical methodologies. HA is also the major target for neutralizing antibodies that bind to either prevent receptor binding or membrane fusion. Understanding the fusion mechanism and antigenic profile of HA is a sought after goal for the rational design of universal therapeutics and vaccines that can prevent influenza infection. This dissertation aims to discover how HA is triggered to undergo pH-dependent membrane fusion, and how the process is inhibited by neutralizing antibodies, therapeutic proteins, and small molecules. Using a combination of solution-phase structural techniques such as hydrogen-deuterium exchange mass spectrometry, small angle X-ray scattering, and light scattering, we find the structural elements that carry out membrane fusion are isolate specific. We also find that while neutralizing antibodies prevent fusion by stabilizing the pre-fusion state, other therapeutic proteins and small molecules stabilize some structural features but also allosterically destabilize portions of the trimer. In the efforts to find a broad-spectrum inhibitor, and characterize the mechanism of acid-activation during membrane fusion, it is imperative to study multiple isolates and subtypes of HA to comprehensively survey the structural and consequently mechanistic differences between variants.

TABLE OF CONTENTS

LIST OF FIGURES

LIST OF TABLES

ACKNOWLEDGEMENTS

To all who have helped me get to this place in time, I have been so fortunate to learn, converse and gain inspiration from everyone I have met and I hope to continue to grow as a scientist, humanitarian, environmentalist and as an individual.

In no particular order; Thank You to:

University of California, Santa Cruz Banana Slugs: Professor Theodore Holman, Yulianna Ortega, Dr. Aaron Wecklser, Kenny Ikea, Professor Barry Sinervo, Professor Leslie Lancaster and Malika Bell, CAMP, UCSC SACNAS Chapter and International. Each of you have helped me start out as a fledgling scientist and shown me that I can do it even when I don't want to!

Natalie Jacuzzi and Ira Tarshis your unconditional love for one another and for some odd reason, me too, has been the greatest gift! Xoxox

Molly Adams thank you for always being OK with listening to Prince, MJ and Stevie Wonder, you have no idea how important those dance parties were!

Deena & Beatrice the memories we have made in SC and continue to make have helped keep me going especially when you visit!

Julianne Ho Summer O-Chem for life! You're such an awesome woman and I am so excited to see where your medical journey takes you.

Emily and Richie no matter where our paths take us I will always remember fondly the wonderful conversations and experiences besos.

Tim Valentic you will get there and you will be so happy, relieved, overwhelmed…all the things I am feeling right now! Keep at it buddy!

Barson, Holway, California, Walti Houses. Everyone affiliated has in one way or another gotten me to this place today, thank you for the geometry wars, rooftop jumping and all the crazy experiences that are important to realize how silly we were as kids. I grew up here!

University of Washington Huskies: Professor Kelly K. Lee, you are an incredibly patient man, a great father and constantly supportive mentor. Thank you for helping me develop into a doctor and letting me find my way. Dr. Miklos Guttman, you know what I want to say, you're the best. Without you I would probably still be toiling away at the bench, thank you for bestowing in me all your HDX knowledge and being my best friend, I love you. All the Kelly Lee Lab affiliates, Dr. Tad Davenport, Long Gui, James Williams, Dr. Nancy Hom, Hans Verkerke, soon to be Jamie Ebner, M.D. Alex Mileant, Mark Benhaim, Dr. Yu Liang, Dr. Ryan Littlefield, Modestas Filipavicius, Daniel Alvarado. Each of you have provided me a wealth of knowledge through conversation, protein expression, Din Tai Fung and thank you for putting up with my rollercoaster ride of graduate school, we truly are a lab-family.

Department of Medicinal Chemistry and Pharmaceutics: Professor William M. Atkins, you were the first person I met from UW, thank you for having faith in my abilities as a researcher and I hope I haven't disappointed you! Professor Carlos E. Catalano, thank you for being such an inspiring mentor and good friend, your work and devotion to programs like SACNAS give me hope for a richer scientific culture. Professor Abhinav Nath you have helped reinvigorate my quest for knowledge, you've been an amazing friend and mentor and I know your lab will come to do wonderful things.

Dr. Eri Nakatani and Evan Webster you two have been wonderful cat companions and friends throughout the years, thank you for never hesitating to look after the little ones. Thank you for your love of music, film and art.

Ryan Seguin thank you for always being my friend, being zen and for all the free rides.

Dr. Justin Lutz you're hilarious, crude and always know what not to say. Thank you for your constant generosity and lack of compassion.

Caleb M. Woods to me you will always be a full werewolf.

UW SACNAS Chapter thank you for all your support, love and inspiration you all are wonderful leaders and activists!

Non-University Affiliates:

Seattle Otters: thank you for letting me blow off some steam no matter how poorly I swim.

Kate Hokanson and Shadow for giving me a creative release when I needed it the most.

The Sperling, Guttman and Hooker family although we've just gotten to know each other thank you for your warmth and hospitality through the years.

The Ortiz Family I have known you all for so long and while our encounters are sometimes few and far between I am so lucky to have such wonderful people in my life who exude joy and love and respect.

The Goss and Chavannes Families thank you for all the supporting words throughout my teens.

The Corwin Family, Sonya you will always have a place in my heart.

The Strange Family you have made me laugh and continue to make me laugh keep it up!

And most importantly, thank you to my entire family there is not a single word more that I can say other than how grateful I am for your constant support, love, generosity, guidance, discipline and sarcasm. To my aunts and uncles thank you for acting as a second set of parents. To my cousins, thank you for acting as second set of siblings, we've had some wonderful experiences growing up and you are so important in my development. To my brother, sister in law and niece, thank you for letting me be your sister and aunt, I look forward to seeing your family grow. To my mother and father thank you for introducing me to oldies, Motown and good food. Your constant respect and love for my grandparents have shown me that my grandparents are the cornerstone of what makes us a great clan. You all know how much I love you and no words can express how lucky and fortunate I have been and will continue to be from knowing each and every one of you.

DEDICATION

To my Mother and Father; Yvette and Felix Garcia, this doctorate really belongs to you both. From all your sacrifices and support I have learned how to think, love, hope and dance and I will be forever grateful for you both.

CHAPTER I: Influenza Hemagglutinin pH-dependent Membrane Fusion Activation and Antigenicity

Overview

Influenza A infects a broad range of animals but replicates to high titers with little pathogenesis in the natural wild water fowl reservoir.[1,2] Annual infection in humans however, causes acute upper respiratory disease and systemic symptoms, which is rapidly spread through aerosol droplets in coughs and sneezes. Influenza A is also responsible for hundreds of thousands of deaths per year especially in high risk individuals such as the immunocompromised, elderly and young, and infection can cost billions of dollars in health care and productivity loss.[3]

Virion Architecture

Influenza belongs to the O*rthomyxoviridae*, which is a family of pleiomorphic enveloped viruses that contains a segmented single stranded negative-sense RNA genome packaged as a complex of viral polymerases and nucleoproteins.[4] An infectious virion contains unique segments of RNA that encodes eight structural and four non-structural proteins (Figure 1.1).[5-7] The viral matrix capsid protein (M1) forms a shell around the viral genome, and the host-derived viral membrane surrounds the protenaceous core acting as a physical barrier between the viral genetic material and host cell cytosol.[8,9] Protruding from the viral membrane is the ectodomain of three transmembrane surface antigens; hemagglutinin (HA), neuraminidase (NA), and the proton channel (M2).[10-12] HA is the most abundant surface protein (~85% occupancy) and major antigenic target of the immune system.[9] Furthermore, HA mediates the initial steps of viral entry, attachment and pH-dependent membrane fusion, which is essential for infection.[13,14]

The Influenza Life Cycle: Hemagglutinin Mediates Viral Entry

Engulfment of the influenza virus is triggered when HA binds extracellular sialic acids presented by the host cell surface glycocalyx, an assortment of glycoproteins/lipids and peptidoglycans (Figure 1.1).[15,16] During endosomal maturation the compartment acidifies (~6.0-5.0) and a patch of hydrophobic residues known as the fusion peptide is released from the HA core and penetrates the endosomal membrane.[17-20] Irreversible pH-dependent structural rearrangements within HA provide the conformational energy required to bring the viral and endosomal membranes together, creating a pore through which the genetic material can pass.[14,21,22] Meanwhile, protons passively transfer through M2 into the viral interior to synchronize the acid-dependent de-polymerization of M1, and the protein-genome complex is extruded into the cytosol for nuclear transport and viral replication.[23-27] The viral polymerase replicates the viral genome and creates the mRNA for host machinery to carry out protein synthesis and post-translational modifications (e.g. glycosylation and palmitoylation) and new viral components are shuttled to cholesterol rich lipid-rafts on the cell surface for viral assembly.[28-34] NA-mediated hydrolysis of terminal sialic acid moieties adjacent to the budding site release progeny viruses into the extracellular milieu ready for another round of infection.[35-37] NA sialidase activity has also been shown to be important for viral locomotion throughout the interstitial fluid by cleaving sialic acids abundant on mucins and other glycosylated secretions that compete for the HA receptor binding site (RBS).[38-40]

Surface Antigens Classify Viral Subtypes

The formal nomenclature of influenza viruses is based on: virus type (e.g. type A), non-human species from which it was isolated, isolate number, isolated year and corresponding surface antigen subtype. For example, the influenza A 2009 pandemic H1N1 isolated from humans in California is written: A/California/7/2009 (H1N1).[41] Sequence conservation of HA and NA indicate that both antigens cluster into two distinct evolutionary groups denoted 1 and 2. Out of 16 HA and 9 NA subtypes, group-1 consists of 11 HAs and 4 NAs , while group-2 includes 6 HAs and 5 NAs, all of which have been identified in the natural wild water fowl reservoir.[1,2] Recently, two influenza-like viruses H17N10 and H18N11 were discovered in South American bats, and though both antigens share overall structural similarities with other subtypes, neither strains could productively infect human cells when generated by reverse genetics.[42-44] While the new discovery of bat-derived influenza-like viruses is an emerging field that could provide insight into the evolution of influenza it is believed that these viruses currently pose little threat to humans and will not be discussed further.

Zoonotic transmission of avian viruses into humans can initiate a pandemic if the virus can efficiently replicate in the new host and adapt fast enough to spread between humans before being cleared by the immune system, a process known as antigenic shift. Antigenic shift occurs when the HA and NA gene segments from non-human viruses assemble with gene segments from other mammalian viruses to create a strain new to the human immune system. The three major pandemics of the 20th century introduced the 1918 H1N1, 1957 H2N3 and 1968 H3N2 strains into the human population through antigenic shift of avian origin, and more recently the swine reassortant 2009 pandemic H1N1.[45-48] The total death toll of these four pandemics was estimated around 50-100 million, with the 1918 pandemic causing the most mortality. Virulence of the aforementioned pandemics was eventually attenuated in humans, and today circulating variants of H1N1 (2009 origin) and H3N2 are responsible for seasonal epidemics. However, the likelihood of another pandemic is illustrated by the highly pathogenic avian influenza virus (HPAIV) H5 isolate and relatively less pathogenic H7, H9 and H10 isolates, which cause fowl plaque in poultry, and occasionally spill into the human population. Fortunately, human to human transmission is exceptionally rare.[49-51]

During the course of viral evolution, influenza naturally undergoes antigenic drift contributing to the diversification of the genome. The error prone viral polymerase causes rapid evolution of the viral genome with an estimated mutation rate $\geq 1 \times 10^{-3}$ substitutions per site, per year. Although every genome segment is impacted, positive selection of drift variants is highly dependent on maintaining a functional HA.[52] Viral tropism and spread are hypothesized to be major factors impacting the adaptation of receptor binding specificity and HA activation pH-threshold. Mutations that prevent viral attachment typically do not persist in the population and the amino acid composition of the RBS is highly conserved between viral types (discussed in detail below). Furthermore, mammalian strains have been shown to induce membrane fusion at a later pH (~5.5-5.0) than that observed for avian strains (~6.0-5.3), and as such avian HAs are typically less acid stable than mammalian isolates.[53-61] Overall, the comparison of structural contributions from naturally occurring and laboratory induced antigenic drift and antigenic shift mutants and divergent isolates can provide insight into the mechanism of HA activation and epitope presentation.

HA Structure, Activation and Role in Membrane Fusion

HA is the prototypical class-I membrane fusion protein, and was the first viral antigen structure to be elucidated. Reported by Wilson, Skehel and Wiley in 1981, the soluble pre-fusion HA ectodomain was liberated from the viral surface by bromelain digestion (BHA) and crystallized at neutral pH.[18] Each protomer within the glycosylated homotrimer consists of two functional subunits, HA1 and HA2, which are connected by a dense network of non-covalent interactions, and a single covalent disulfide (Figure 1.2 A).

During biogenesis, HA is synthesized as the fusion inactive precursor polypeptide, HA0, and proteolysis primes the trimer for fusion by liberating the HA1 C-terminus and the HA2 N-terminal hydrophobic fusion peptide, which is stabilized in a pocket within the base of the long helix formed from highly conserved residues (Figure 1.2 A).[62,63] A recent comprehensive study by the Steinhauer group suggests that HA0 cleavage efficiency is subtype specific, and amino acids flanking the cleavage site may alter the local structure of the cleavage loop, which may impact accessibility and specificity by a number of proteases.[55] Furthermore, tissue expression of proteases can also influence cleavage specificity and species tropism such that proteases expressed in the trans-golgi network are more likely to cleave HA0 with polybasic (RRRR) cleavage sites prevalent in HPAIV isolates, while less pathogenic avian and human HA0s containing monobasic sites (R/K) are shuttled to the surface unprimed and require priming by less abundant extracellular proteases, possibly explaining the differences in virulence between isolates. Nonetheless, comparison of HA0 and pre-fusion HA structures indicates that both share an identical conformation with the exception of the cleavage loop (Figure 1.2 A). However, the unique ability of pre-fusion HA to undergo pH-dependent membrane fusion suggests that at neutral pH, HA0 is ground state and upon proteolysis, the pre-fusion cleaved state becomes metastable, ready to facilitate membrane fusion.[62,63]

HA1: The Globular Receptor Binding Head

The membrane distal head (Figure 1.2 B) is formed by three identical copies of HA1 that comprise the HA1-HA1 trimeric interface formed by electrostatic pairs, which are hypothesized to stabilize pre-fusion conformation.[18,64-69] The receptor binding site (RBS) is a shallow groove formed by the highly conserved residues at the apex of each HA1 subunit.[13,70,71] Sequence alignments of avian and mammalian RBS show high conservation of Y98, W153, H183, Y195 and R220 in all subtypes, and mutagenesis of these residues can change sialic acid binding affinity and specificity.

The HA sialic acid preference is postulated to confer species tropism and may be an additional factor for why HPAIV infection is sporadic in humans. Using a panel of avian and mammalian viruses, Rogers and Paulson were the first to comprehensively show that avian viruses preferentially bind sialic acids containing an α2,3 glycosidic linkage to the penultimate galactose (SAα2,3Gal), while all human and swine strains they examined bound SAα2,6Gal with very minor SAα2,3Gal cross-over.[15,72] More current studies implementing glycomics, lectin- and immuno-histochemistry suggest that the respiratory tract of humans, swine and poultry contain a mixture of both α2,6 and α2,3 ligands, and the presence of both types may serve as a mixing vessel for both types of viruses, while the commonly used human-like ferret model only contains α2,6 type glycans in the respiratory tract. Yet, the relative abundance of the different glycans is less understood and may be a larger factor for HA specificity in subtypes that can only bind a single type.[73-78]

Mutatgenesis of HPAIV H5N1 viruses incapable of human to human transmission showed that as little as one mutation (N182K, Q222L/G224S,or N182K/Q222L/G224S) within HA1 was sufficient to switch the receptor specificity from avian towards human-like sialic acid. Furthermore, this mutant was also capable of adhering to human and ferret respiratory epithelial cells, and a similar study identified a similar H5N1 phenotype with mutations in N186K, S227N and Q226L (H5 numbering).[79,80] In a concurrent H5N1 study, viruses containing the HA1 mutations Q222L/G224S and E627K mutation in the PB1 RNA polymerase subunit were serially passaged in ferrets and acquired two additional HA1 mutations near the HA1-HA1 trimeric interface (H103Y and T156A) that allowed airborne transmission suggesting that changes in HA1 stability may be linked to species tropism and controlled pH-dependent HA1 dissociation.[81]

HA2: The Helical Fusion Hairpin

Electron micrographs depict HA projecting ~14 nm from the viral surface, where the HA2 fusion machinery is anchored in the viral membrane.[82] Folded in an elongated coiled-coil trimer of antiparallel helices and connected by a linear linker known as the B-loop, HA2 is a highly helical stalk-like structure (Figure 1.2 A).[18] Following HA0 priming, the fusion peptide is stabilized within a negatively charged cavity formed by the long helix, short helix and HA1 N-terminus[62,63](Figure 1.2 C). Mutagenesis of these regions has been shown to alter the pH-threshold of fusion, which impacts the overall stability of the trimer, presumably focused at the fusion peptide pocket.[61,83-86] Furthermore, the group-specific sequence conservation within the fusion peptide pocket suggests that alteration within the ionization of this cavity also has an overall impact on trimer stability, which is tied to the precision of HA triggering (discussed in more detail below). In the neutral conformation, the B-loop and base of the HA1 globular head are associated through attractive electrostatic interactions that form the HA1-HA2 intra-monomer interface (Figure 1.2 C).[67-69,87]

The High Resolution Transition from Pre-fusion HA to Post-fusion HA

Kim and Carr first postulated that the pre-fusion to post-fusion transition was carried out by a "spring-loaded" mechanism where the B-loop becomes helical at low pH, which extends the fusion peptide and short helix away from the virus towards the target membrane.[88,89] Crystallographic evidence of the post-fusion structure was first observed for a soluble HA2 fragment (TBHA2) that was treated with low pH and proteolyzed to remove HA1 and the fusion peptide for crystallization.[19] TBHA2 showed that at low pH, the B-loop indeed adopts a helical conformation that extends and repositions the short helix approximately 100 Å away from the viral membrane, presumably exposing the fusion peptide towards the target membrane.[18,19,90] In response to low pH, HA2 also undergoes a helix to loop transition within the long helix to form a hinge that allows the HA2 C-terminus to pack along the axis of the newly elongated coiled-coil, which brings the viral membrane anchor within the same plane as the endosomal membrane for fusion, while the C-terminus forms a helical cap with the N-terminus of the extended helix.[19,90-92]

High resolution structural characterization of post-fusion HA is limited to the HA2 ectodomain and does not provide information about the post-fusion HA1 conformation. HA1 monomers proteolyzed from acid-treated viral HA, complexed with an HA1 targeting antibody and crystallized at pH 6.0 suggests that the overall morphology of HA1 remains similar to that seen in the pre-fusion trimer, and during HA-activation, the HA1 clamp may dissociate from HA2 as a rigid body; however, the crystallization conditions are at a higher pH than required for fusion.[93] Differential scanning calorimetry of pre-fusion HA compared to detergent soluble post-fusion HA reinforces the hypothesis that pre-fusion HA is kinetically trapped in a metastable state, which is irreversibly triggered by low pH, or at neutral pH by heat and chaotropes (e.g. urea).[89,94-98] The spontaneous refolding of HA2 in absence of HA1 also argues that the globular head acts as clamp to stabilize the metastable pre-fusion conformation of HA2.[90,99]

Since low pH is the sole trigger for HA activation, the structural changes during HA mediated membrane fusion must be driven by an overall change in the charge of the protein.[67] HA activation is hypothesized to be controlled by the histidine switch mechanism (pK_a ~6 for free His side chain), which has been demonstrated to control other pH-dependent fusion proteins.[100] This mechanism is usually inferred to involve repulsive electrostatic interactions resulting from protonation of key residues (e.g. His) that drive the destabilization and opening of the pre-fusion trimer assembly, as well as the formation of new, favorable ionic interactions in the post-fusion conformation.[67,100-102] The histidine switch mechanism likely impacts various sub-domains within the HA structure and may not be as simple as a change in ionization for a single residue.

For example, HA2 residues D112 and K58 encompassing the fusion peptide cavity have been extensively characterized in H3 isolates through point mutations, and were found to destabilize or stabilize the trimer as observed by an increase or decrease in the pH threshold, respectively.[61,83-85,103] A new study published by the Steinhauer group investigated the impact of a single mutant D112G or K58I on HA stability across the phylogenetic spectrum by investigating 16 HA subtypes investigating both avian and human HAs.[104] They found D112 G destabilizes all mutants irrespective of decreased protein expression, while K58I stabilized all mutants with the exception of H11, which was attributed to a naturally occurring arginine at position 58. Furthermore, the conformation of D112 is fixed between groups while the structure K58 is different between groups, which may play a role in the additional steps during fusion and further structural characterization of these various mutants is needed.[105,106]

Additionally, Xu et al. characterized an H2 group specific swapped mutant R106H located in the HA2 long helix, which increased the stability of the pre-fusion trimer and was able to be crystalized at lower pH (~pH 6.0). Structural analysis of this early activation mutant showed moderate deformations in the HA1-HA2 interface, including rotamer changes within the fusion peptide pocket R106H but no changes in the fusion peptide structure. They hypothesize that this mutation changes the charge balance of the fusion peptide pocket and may stabilize the fusion peptide to be more acid-tolerant.[92]

Incorporation of residues enhancing the stability of the HA1-HA1 interface both covalently and non-covalently have also been shown to maintain the pre-fusion conformation when exposed to low pH.[87,102,107,108] The K-H charge pair located at residues HA1 205 and HA2 72 in the interface is hypothesized to regulate HA activation of 2009 pandemic H1N1 strains, which due to the histidine-switch hypothesis may result in an overall destabilized trimer. Mutations enhancing the ionic interaction within these sites (e.g., K-E pairs and K-Q pairs) were shown to reduce infectivity of three chimeric H1N1 strains, implicating H72 as a potential fusion trigger.[109] A recent investigation from the Herrmann group also identified a potential histidine trigger H184 located at the HA1-HA1 trimeric interface of the Vietnam H5 isolate.[102] Mutation of H184 destabilized the trimer by either abolishing fusion or increasing the pH threshold, and computational modeling suggested that the doubly protonated state competes with the adjacent R220 for stabilizing hydrogen bonds, which may result in HA1 unclamping. Furthermore, pK_a estimates of H184 were shown to be depressed, which is not surprising as local environment has been known to shift relative pK_a's.

Deciphering the Mechanism of HA Activation

Decades of studies implementing conformational epitope mapping, proteolytic sensitivity succeeding acid-treatment, acid-inactivation followed by re-neutralization, time resolved spectroscopy, membrane fusion fluorescence assays, and a number of mutagenesis analyses taken together suggest the conformational transition from pre-fusion to post-fusion may involve early structural intermediates that commence prior to the committed irreversible post-fusion conformation.[62,83,84,88,103,107,108,110-116] These findings may explain why, under certain conditions, early HA activation appears reversible.[21,92,96,117-121] Initial investigations characterizing HA activation intermediates by White and Wilson utilized conformational antibodies and showed that the fusion peptide release from the fusion peptide pocket precedes exposure of epitopes occluded in the pre-fusion structure, and in a follow-up study by Kemble et al., it was reported that fusion peptide exposure was concurrent with minor changes in the membrane distal apex of the trimer that occurred prior to HA1 dissociation[108,110] (Figure 1.2 B and C). However, these conformational mapping studies required re-neutralization of the activated species before immunoprecipitation, and detection of early reversible intermediates may thus have been masked. Recent cryo-electron tomograms of acidified virus displayed limited density at the base of the stem proximal to the membrane yet density for the globular head was still observed suggesting HA1 remains intact during early activation.[117]

These recent findings indicate that fusion peptide release may be the major mechanism of pH-dependent activation of HA. However, the fusion kinetics of three distinct viral subtypes showed substantial differences in the rate of fusion and inactivation.[122] A more recent investigation using single particle tracking also identified considerable differences between the fusion kinetics of lab adapted and clinically relevant isolates from the same subtype.[56] In addition to the known subtype specific structural changes (Figure 1.2 D); subtle differences within isolates may have a large impact on the overall activation profile of HA.[55,61,104-106] Thus, it is very likely that different HAs have different activation mechanisms as a result of differences in amino acid composition, which may manifest as changes in stability of the pre-fusion trimer.

Preventing Influenza Infection: Mechanisms of HA Neutralization

Currently, influenza prevention by antivirals are limited to the M2 proton channel inhibitors (amantadine and rimantadine), and NA inhibitors (oseltamivir, zanamivir and permavir), which can ameliorate the onset of infection by inhibiting viral uncoating and budding, respectively (Figure 1.1). Unfortunately, due to an increase in M2 inhibitor resistance in circulating seasonal strains, the CDC recommends only using NA inhibitors to treat influenza in the U.S. (http://www.cdc.gov/flu/about/qa/antiviralresistance.htm). While NA inhibitors can prevent infection if given prophylactically, they must be administered early during the course of infection to be most effective. Resistance has been observed in some strains, though the majority of resistant strains specifically evade oseltamivir.[123] Vaccination is still the most effective means of preventing influenza infection. Vaccines work by stimulating an adaptive immune response targeting viruses selected for the upcoming season. However, current vaccine formulations are highly specific and cannot prevent against antigenically disparate strains. Furthermore, issues with antigen stability may hinder the development and effectiveness of seasonal vaccines. Understanding the structural factors that impact HA antigenicity is essential for the development of more robust vaccines, and HA specific antivirals.

HA1 Elicits a Dominant but Variable Immune Response

Traditionally, the HA1 subunit is the immunodominant target for neutralizing antibodies (nabs) against influenza, and the antigenic sites have been mapped for both seasonal strains by natural and laboratory selection.[64,65] In H3 the sites are termed A,B,C,D and E, while H1 sites are termed Sa,Sb, Ca and Cb (Figure 1.3 A), and the majority of these sites are located near the RBS. The hypervariation of HA1 suggests that mutations within these regions are structurally tolerated in an active virus as long as receptor binding function and fusogenicity are retained. Furthermore, incorporation of N-linked glycans at the major antigenic sites has also been shown to shield HA from neutralization while still maintaining receptor binding function, as long as the residues required for binding sialic acid are conserved.[124-127] The HA inhibition assay is a diagnostic technique commonly used for identifying HA1 directed nabs. Many crystal structures of HA1 directed nabs fab fragments complexed with HA indicate that neutralization is largely mediated by indirectly occluding the RBS from sialic acid binding, typically by interactions from both the heavy and light chain.[93,128,129] However, recent identification of HA1-targeting broadly neutralizing antibodies (bnabs) and high resolution crystal structures of HA fab bnAb complexes suggest a common mechanism of HA1 directed heterosubtypic neutralization involving the insertion of hydrophobic and/or aromatic side chains from a single antibody loop into the highly conserved pocket of the RBS, which directly prevents binding; additionally the bivalency of the antibody-antigen complex has been shown to optimize neutralization versus fab fragments.[130,131] Laboratory escape mutants dramatically alter the receptor binding function suggesting that naturally occurring escape isolates would be rare due to the cost in viral fitness as postulated by Wilson and colleagues.[130] These studies suggest that the highly conserved RBS epitope may be a good target for rationally designed small molecules, peptides or proteins.[132] It should be noted that the natural HA interaction with sialic acid is low affinity, and viral attachment is likely mediated through avidity due to the dense copy number of HA on the surface of the virus and abundance of sialic acid presented by the extracellular glycocalyx. The synthesis of multivalent sialic acid-containing polymers may circumvent the low affinity for the RBS and have been shown to effectively inhibit infection.[70,71,133]

HA2 Fusion Stem Directed Antibodies are Broadly Neutralizing

The first influenza specific bnabs C179 was reported in 1993 after immunizing mice with A/Okuda/57 (H2N2) strain.[134] C179 did not prevent viral agglutination in HA inhibition assays but was shown to inhibit infection of multiple group 1 subtypes. Laboratory escape variants were found to include substitutions in the solvent accessible short helix of HA2 and C-terminal stem of HA1 (Figure 1.3 A). This was the first example of a stem directed nab and bnab, which suggested an alternative mechanism of virus neutralization can be achieved by recognition of highly conserved residues that are essential for membrane fusion. Over 15 years later, the first stem directed group 1 heterosubtypic bnabs such as CR6261, was identified by phage display libraries of IgM memory B cell libraries from H5N1 survivors, and high resolution crystal structures of the fab fragments complexed with HAs from different strains showed that the speculated C179 epitope was shared.[135,136] A year following, the bnAb F10 and other similar stem-directed bnabs were isolated from phage display libraries, and F10 fab HA interaction was nearly identical to CR6261.[137] Genetic analysis of CR6261 and F10 showed that they share the VH1-69 gene and both binding interfaces are formed only by residues from the germline encoded heavy chain complementary determining regions 1 and 2.[136,137]

The difference in sequence conservation between the two viral groups is hypothesized to subtly alter the local environment of the epitope enough to prevent CR6261 and F10 binding to group 2 isolates, and it is possible that the glycosylation pattern of the two groups may impact bnab breadth. However, more recently, the identification of group 2 bnab CR8020 isolated from recently vaccinated human blood donors was capable of binding and neutralizing H3 and H7 isolates.[138] Although crystal structures indicated that the epitope is also focused at the stem of the trimer near the short helix of HA2, the overall location is more proximal to the viral membrane, and contacts with C-terminal portion of the fusion peptide and downstream residues are part of the epitope (Figure1.3 A). Additionally, CR8020 binds the trimer with both the heavy and light chain, which is a distinct mechanism from the aforementioned group 1 stem directed bnabs, and the epitope may be sterically occluded by an HA1 N-linked glycan at N21 present in group 1 isolates possibly preventing the heavy-chain complementary determining region (HCDR)1 from binding. Similarly, it was also hypothesized that the HA1 N-linked glycan N38 in group 2 isolates prevents the heavy chains in CR6261 and F10 from binding.[136,137]

The bnab FI6 was meticulously mined from single cell cultures derived from the plasma of donors 1 week after vaccination, and found to bind and neutralize isolates from both groups.[139] Structures of FI6 with HAs from both groups indicated that the stem epitope has some sequence overlap with all the other stem directed bnabs and the long flexible loop from the HDCR3 targets the short helix in one monomer while the light chain CDR1 targets the fusion peptide from an adjacent monomer. Furthermore, FI6 with H3 showed that the clashes with the N38 glycan were ameliorated by the ability of the long flexible HCDR2 loop to reposition the base of the glycan and access the short helix, which may also be possible for CR6261. It was also shown that FI6 can prevent HA0 priming, providing another possible mechanism of neutralization against progeny viruses that rely on cell surface proteolysis for priming.[139,140]

It was also shown that passive immunization of these bnabs could provide heterosubtypic protection from group 1 and group 2 specific isolates suggesting a therapeutic role for these monoclonal antibodies, and if used in combination may be pan-protective. It appears that the neutralization with the seasonal vaccine is capable of eliciting a broadly neutralizing antibody response with significant breadth, and while group 1 type bnabs appear easier to elicit, the potential to stimulate an immune response that targets an immuno-subdominant region, such as the highly conserved HA2 stem may be highly dependent on the type of immunogen and method of vaccination.

New Immunization Techniques and Immunogens to Stimulate a Broad Immune Response

New efforts at enhancing a heterosubtypic immune response have been directed towards modifying various regions of the HA trimer. For example, studies from the Wong group have shown that enzymatically clipping the glycans from H5N1 HA bolstered antibody production and immune response by exposing epitopes that were shielded by glycans (Figure 1.3 B).[141] In a follow up study by the same group, these monoglycosylated HAs were shown to exhibit some cross-strain neutralization. The enhanced immune recognition was likely predominately targeting regions of HA1 that were previously shielded by the glycan sheath as improvement of the binding via the HA inhibition assay was observed.[142] Independent studies from both the Palese group and Wu group, hypothesized that hyperglycosylation of HA1 switched the immune recognition from the immunodominant head towards the more conserved residues in the HA2 stem.[143,144] The Palese group demonstrated that immunization of mice with the hyperglycosylated HA protein induced both heterologous and heterosubtypic protein, while the HPIAV H5N1 hyperglycosylated DNA vaccine and protein elicited cross-class reactive antibodies, some of which overlapped with the CR6261 epitope suggesting they may have broad group-1 reactivity[143-145] (Figure 1.3 B and C). The protein construct abolished HA1 antigenic site antibody binding but retained stem directed epitopes, and taken together, these data suggest that further masking of the hypervariable regions in HA1 may redirect the immune system to target the less immunogenic, but more immuno-productive HA2 stem.[143]

The Palese group has also engineered a library of stable chimeric HA trimers and infectious chimeric HA viruses, in which the HA1 sequence encoded between the highly conserved intersubunit disulfide linker can be swapped with HA1 sequences from other subtypes (Figure 1.3 B).[146] A novel prime boost immunization method using this chimeric HA library continually exposed mice a constant

HA2 stem from H1N1 while varying the presentation of the immunodominant HA1 head.[147] This vaccination method appeared to elicit a robust immune response in mice that was capable of neutralizing heterologous and heterosubtypic viruses, such as H5N1. IgGs purified from sera of vaccinated mice did not inhibit HA binding to antibodies in HAI assays and the purified IgGs were protective in passive transfer experiments suggesting that neutralization is predominately mediated by stem directed antibodies. In a follow up study in ferrets whole virus chimeric HAs appeared to be just as effective at stimulating a heterosubtypic immune response as seen earlier, and passive antibody transfer was also protective in ferrets.[148] However, these methods have yet to be tested in group 2 subtypes, and as mentioned earlier, although it is likely that using this immunization strategy with a combination of group 1 and group 2 chimeric HAs may be pan-protective. The Palese group has also shown that mice immunized with chimeric HA proteins in combination with different adjuvants were capable of eliciting both heterologous and heterosubtypic stem-directed antibodies when administered intranasally and intramuscularly suggesting that alterations in vaccine formulation can elicit a broadly reactive humoral immune response.[149] It would be interesting to see how improvements in immunization changes to better improve cross-reactivity, one combination may be to use hyperglycosylated HAs in combination with the novel chimeric HAs immunization strategy in order to initially prime the immune system with an immunosilent HA1 then boost with different alterations of hyperglycosylated HAs.

Other strategies for stimulating an HA2 focused response more recently includes expression of HA2 constructs in the absence of HA1. However, in order to elicit a robust neutralizing response, HA2 must maintain its pre-fusion conformation, which in the absence of HA1 would require extensive modifications in the HA2 structure.[90,99] Early *E. coli* expressed HA2 immunogens were designed and optimized to contain portions of the N- and C-termini of HA1 linked to the HA2 antiparallel hairpin that comprises the majority of the HA2 ectodomain. Mutagenesis of the short helix and B-loop prevented spontaneous helix formation, and cysteine mutagenesis at the HA1 C-terminus prevented intermolecular disulfides. The downstream incorporation of a trimerization motif assisted in productive trimer formation.

These constructs were shown to elicit a protective and broadly neutralizing immune response, suggesting that these immunogens may be clinically relevant immunogens.[150-153]

More recently, trimeric mini-HA constructs that also lacked the immunodominant HA1 head (Figure 1.3 C). These mini-HAs were sequentially designed in an attempt to retain more native like contacts within the trimeric construct: mutagenesis of B-loop and preservation of the HA0 cleavage site and HA1 termini were necessary generate to a trimeric mini-HA with comparable dynamics to full-length pre-fusion HA. The trimeric mini-HA appeared to elicit high titers of antibodies against full-length homologous HA and other strains such as H5 and H9 subtypes. Additionally, trimeric mini-HA appeared to be heterosubtypically protective against infection in both mice and cynomologous monkeys in both immunization and passive transfer of serum.[154]

A similar study by the Nable group attempted to concentrate the immune response to the HA2 stem by presentation of HA2 constructs tethered to ferritin from *H. pylori*, which multimerizes into nanoparticles mimicking the dense presentation of HA2 on the surface of a virion, or virus-like particle (VLP) (Figure 1.3 C).[155,156] Introduction of a stabilizing salt bridge pair at the HA2 core and HA1 terminal disulfide appeared to stabilize the native HA2 conformation for binding of C6261. Immunization of the HA2 ferritin nanoparticle in mice and ferrets showed protection against homologous H1N1 and divergent strains, as well as an antibody mediated response against H5N1.

Dissertation Goals

The studies mentioned above have established and identified important regions contributing to the stability (e.g. pH-dependent activation) and antigenicity (e.g. HA evolution and sequence conservation) of influenza HA. However, many of these experiments provide a static understanding of the structural and energetic components associated with pH dependent activation and pre-fusion stabilization. Due to the transient and reversible nature of HA mediated membrane fusion, characterization of HA-activation intermediates remain refractory to high resolution structural techniques, and the detailed biophysical characterization of HA neutralization is still in its infancy. This dissertation will aim to characterize the protein dynamics of HA during pH-dependent activation, in complex with neutralizing antibodies and rationally-designed protein inhibitors by implementing solution-based approaches such as hydrogen-deuterium exchange (HDX-MS), small angle X-ray scattering and other light scattering methodologies.

CHAPTER I FIGURES

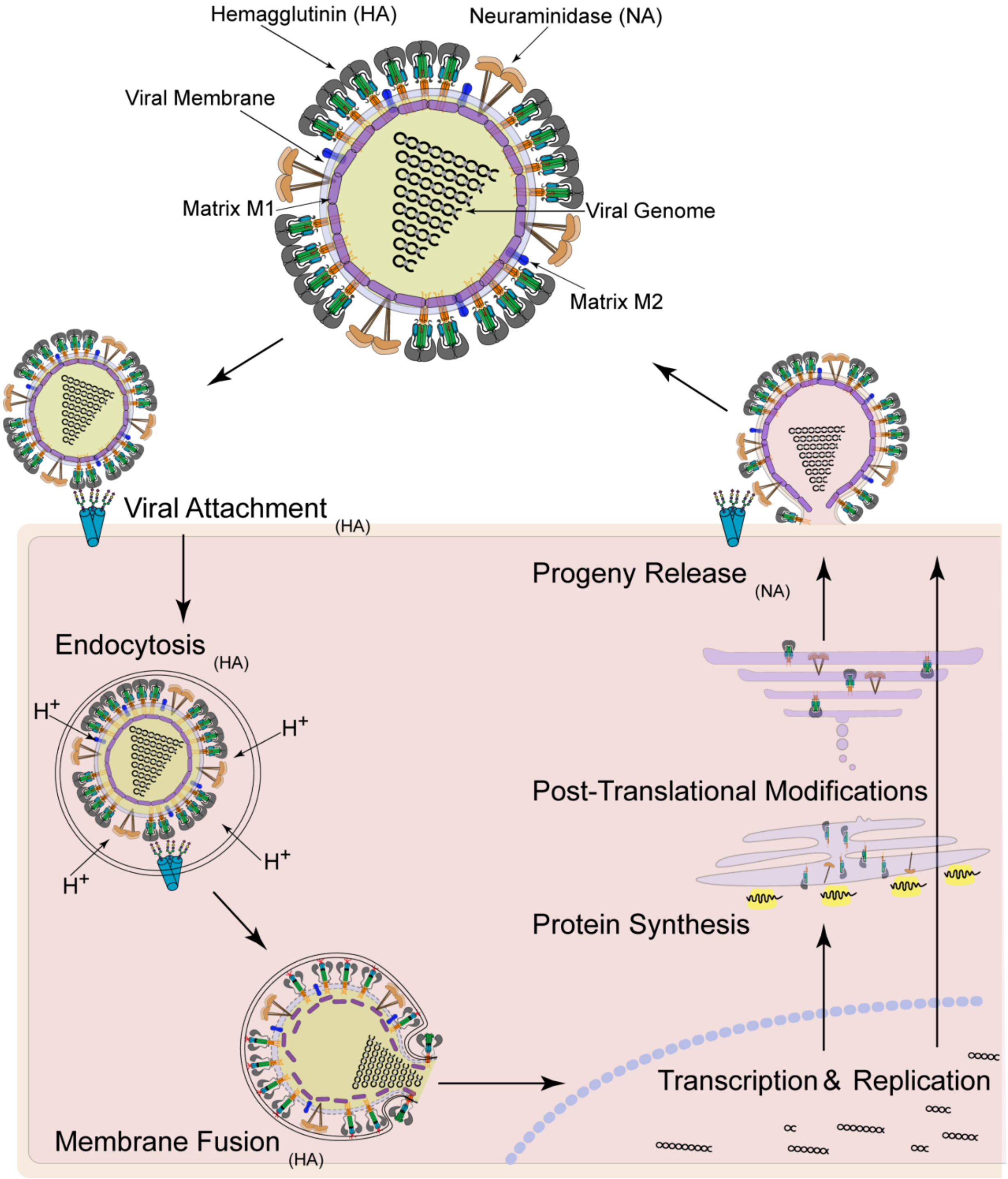

Figure 1.1 The Influenza Virus Structure and Lifecycle. The virus surface dense with hundreds of HA copies covering essentially the entire exterior of the particle, and interspersed with the less-abundant NA tetramer. Viral attachment is mediated by Hemagglutinin (HA) upon binding to host cell surface glycans,

which triggers endocytosis of the virion. Following acidification of the endosome, HA undergoes large structural change to facilitate membrane fusion and releases the genetic information into the cytosol, which is transported to the nucleus for genome transcription and replication. Viral proteins are synthesized and post-translationally modified via the endoplasmic reticulum and trans-golgi network. Progeny viruses are assembled at the cell surface, where Neuraminidase (NA) cleaves neighboring sialic acid for release of newly formed virus into the extracellular milieu.

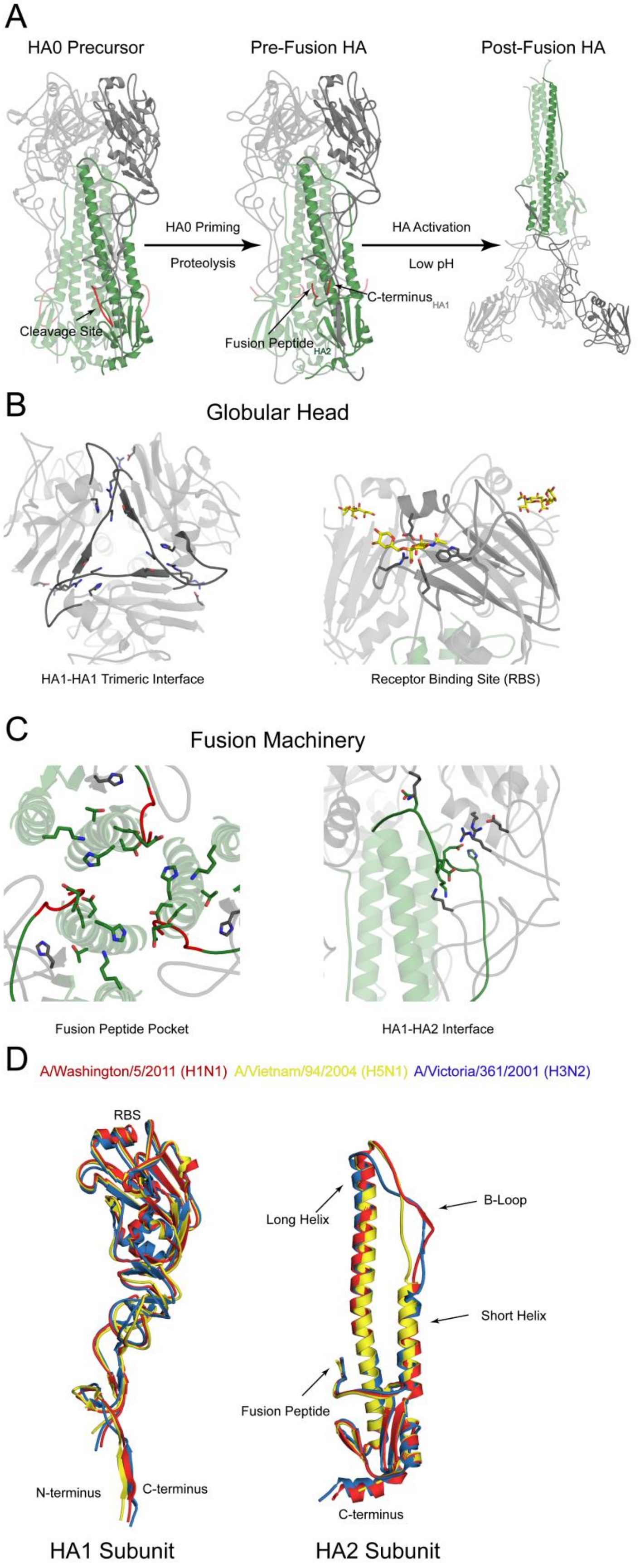
A
HA0 Precursor
Pre-Fusion HA
Post-Fusion HA
HA0 Priming
Proteolysis
HA Activation
Low pH
Cleavage Site
C-terminus$_{HA1}$
Fusion Peptide$_{HA2}$
B
Globular Head
HA1-HA1 Trimeric Interface
Receptor Binding Site (RBS)
C
Fusion Machinery
Fusion Peptide Pocket
HA1-HA2 Interface
D
A/Washington/5/2011 (H1N1) A/Vietnam/94/2004 (H5N1) A/Victoria/361/2001 (H3N2)
RBS
N-terminus
C-terminus
Long Helix
B-Loop
Short Helix
Fusion Peptide
C-terminus
HA1 Subunit
HA2 Subunit

Figure 1.2 Hemagglutinin Structural Architecture. A) HA0 priming and activation of pre-fusion HA to post-fusion HA. The HA1 globular head is in grey and the fusion stem is in green. The HA0 cleavage loop is in red, which following cleavage becomes the N-terminal fusion peptide in HA2 and the C-terminus in HA1. **B)** Important stabilizing contacts in the globular head. Left panel shows electrostatic interactions that are required for HA1 de-trimerization upon activation. Right panel shows important residues for sialic acid binding. **C)** Highly conserved features in in the fusion peptide pocket (left) located in the coiled-coil pre-fusion core, and HA1-HA2 interface. Both show stabilizing contacts, where the first 12 residues of the fusion peptide are red. **D)** Subtle structural changes between H1 (red), H5(yellow) and H3(blue) isolates. HA2 contains an extra half turn in the short helix in the group 1 isolates (H1 and H5) that extend the N-terminal portion of the long helix, altering the position of the HA1-HA2 interface between subtypes. All structures depict H3 isolate from 3HMG.pdb for clarity unless otherwise noted, structures were generated using PyMOL.

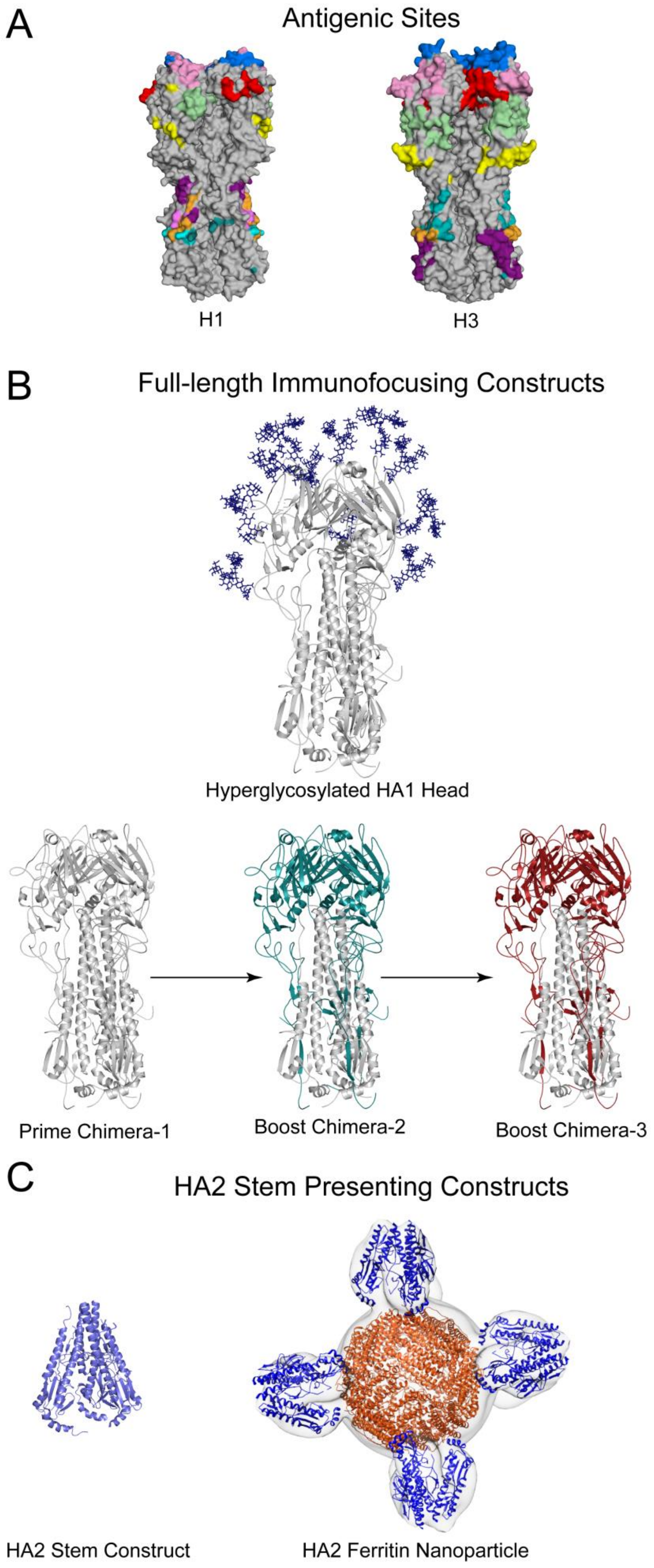
A
Antigenic Sites
H1
H3
B
Full-length Immunofocusing Constructs
Hyperglycosylated HA1 Head
Prime Chimera-1
Boost Chimera-2
Boost Chimera-3
C
HA2 Stem Presenting Constructs
HA2 Stem Construct
HA2 Ferritin Nanoparticle

Figure 1.3 Hemagglutinin Antigenicity and Immunogen Design. A) HA Antigenic Sites Mapped onto Trimer. H1 antigenic sites for Head-directed antibodies (Sb is blue, Sa is pink, Ca1 is pale green, Ca2 is red, Cb is yellow) and Stem-directed antibodies (Unique FI6 epitope is teal, unique CR6261 epitope is purple, epitopes shared between all three is orange, epitopes shared between F10 and CR6261 is light purple and epitopes shared between F10 and FI6 is cyan). H3 antigenic sites for Head-directed antibodies (Site A is pink, Site B is blue, Site C is yellow, Site D is red, Site E is pale green) and Stem-directed antibodies (Unique CR8020 epitope is purple, unique FI6 epitope is teal, and epitopes shared between both antibodies is tan). **B)** Full-length Immunofocusing Constructs. HA trimers containing extra glycans (hyperglycosylated HA top panel) on HA1 mask the immune response and direct affinity maturation towards the more conserved HA2 stem. A novel immunization technique also directs affinity maturation towards HA2 by priming the immune system using trimeric HA, then boosting the immune response with another chimeric HA containing a novel HA1 head(chimera-2 teal), which is then repeated a second time using an additional chimeric HA (chimera-3 red). **C)** HA2 Stem Presenting Constructs Immunogens only displaying the highly conserved pre-fusion HA2 sequence are used to enhance production of stem-directed antibodies. Soluble constructs (left panel) or multivalent presentation using ferritin nanoparticles (right panel) have been utilized with some efficacy.

CHAPTER I REFERENCES

1. Munster, V.J., Baas, C., Lexmond, P. & Waldenstrom, J. Spatial, temporal, and species variation in prevalence of influenza A viruses in wild migratory birds. *PLoS Pathog* (2007).
2. Olsen, B. Global Patterns of Influenza A Virus in Wild Birds. *Science* **312**, 384-388 (2006).
3. Graham-Rowe, D. Epidemiology: Racing against the flu. *Nature* **480**, 3 (2011).
4. Andrewes, C.H., Bang, F.B. & Burnet, F.M. A short description of the Myxovirus group (influenza and related viruses). *Virology* (1955).
5. Pons, M.W. A reexamination of influenza single-and double-stranded RNAs by gel electrophoresis. *Virology* (1976).
6. Inglis, S.C., Carroll, A.R., Lamb, R.A. & Mahy, B.W. Polypeptides specified by the influenza virus genome I. Evidence for eight distinct gene products specified by fowl plague virus. *Virology* **74**, 489-503 (1976).
7. Palese, P. & Schulman, J.L. Mapping of the influenza virus genome: identification of the hemagglutinin and the neuraminidase genes. *PNAS* **73,** 2142-2146 *(*1976).
8. Gregoriades, A. Interaction of influenza M protein with viral lipid and phosphatidylcholine vesicles. *J Virol* **36,** 470-479 (1980).
9. Harris, A. et al. Influenza virus pleiomorphy characterized by cryoelectron tomography. *PNAS* **103**, 19123-7 (2006).
10. Schulze, I.T. Structure of the influenza virion. *Adv. Virus Res* (1973).
11. Laver, W.G. The polypeptides of influenza viruses. *Adv. Virus Res* (1973).
12. Lamb, R.A., Zebedee, S.L. & Richardson, C.D. Influenza virus M 2 protein is an integral membrane protein expressed on the infected-cell surface. *Cell* **40**, 627-633 (1985).
13. Skehel, J.J. & Wiley, D.C. Receptor binding and membrane fusion in virus entry: the influenza hemagglutinin. *Annu Rev Biochem* **69**, 531-69 (2000).

14. Wiley, D.C. & Skehel, J.J. The structure and function of the hemagglutinin membrane glycoprotein of influenza virus. *Annu Rev Biochem* **56**, 365-94 (1987).

15. Paulson, J.C., Sadler, J.E. & Hill, R.L. Restoration of specific myxovirus receptors to asialoerythrocytes by incorporation of sialic acid with pure sialyltransferases. *J Biol Chem* **254**, 2120-2124 (1979).

16. Matlin, K.S., Reggio, H., Helenius, A. & Simons, K. Infectious entry pathway of influenza virus in a canine kidney cell line. *J Cell Biol* **91**, 601-13 (1981).

17. Ruigrok, R.W. et al. Studies on the structure of the influenza virus haemagglutinin at the pH of membrane fusion. *J Gen Virol* **69,** 2785-95 (1988).

18. Wilson, I.A., Skehel, J.J. & Wiley, D.C. Structure of the haemagglutinin membrane glycoprotein of influenza virus at 3 A resolution. *Nature* **289**, 366-73 (1981).

19. Bullough, P.A., Hughson, F.M., Skehel, J.J. & Wiley, D.C. Structure of influenza haemagglutinin at the pH of membrane fusion. *Nature* **371**, 37-43 (1994).

20. Rust, M.J., Lakadamyali, M. & Zhang, F. Assembly of endocytic machinery around individual influenza viruses during viral entry. *NSMB* **11,**567-573 (2004).

21. Stegmann, T., White, J.M. & Helenius, A. Intermediates in influenza induced membrane fusion. *EMBO J* **9**, 4231-41 (1990).

22. Lakadamyali, M. & Rust, M.J. Visualizing infection of individual influenza viruses. *PNAS* **100,** 9280-9285 (2003).

23. Martin, K. & Helenius, A. Transport of incoming influenza virus nucleocapsids into the nucleus. *J Virol* **65,** 232-244 (1991).

24. Schnell, J.R. & Chou, J.J. Structure and mechanism of the M2 proton channel of influenza A virus. *Nature* **451**, 591-595 (2008).

25. Pinto, L.H., Holsinger, L.J. & Lamb, R.A. Influenza virus M 2 protein has ion channel activity. *Cell* **69,** 517-528 (1992).

26. Harris, A., Forouhar, F., Qiu, S., Sha, B. & Luo, M. The crystal structure of the influenza matrix protein M1 at neutral pH: M1-M1 protein interfaces can rotate in the oligomeric structures of M1. *International Congress Series* **1219,** 405-410 (2001).

27. Fontana, J. & Steven, A.C. At low pH, influenza virus matrix protein M1 undergoes a conformational change prior to dissociating from the membrane. *J Virol* **87**, 5621-8 (2013).

28. Copeland, C.S., Zimmer, K.P., Wagner, K.R. & Healey, G.A. Folding, trimerization, and transport are sequential events in the biogenesis of influenza virus hemagglutinin. *Cell* **53,** 197-209 (1988).

29. Boulay, F., Doms, R.W. & Webster, R.G. Posttranslational oligomerization and cooperative acid activation of mixed influenza hemagglutinin trimers. *JCB* **106,** 629-639 (1988).

30. Veit, M., Kretzschmar, E., Kuroda, K. & Garten, W. Site-specific mutagenesis identifies three cysteine residues in the cytoplasmic tail as acylation sites of influenza virus hemagglutinin. *J Virol* **65,** 2491-2500 (1991).

31. Schuy, W., Will, C., Kuroda, K. & Scholtissek, C. Mutations blocking the transport of the influenza virus hemagglutinin between the rough endoplasmic reticulum and the Golgi apparatus. *EMBO J* **5,** 2831-2836 (1986).

32. Scheiffele, P., Rietveld, A., Wilk, T. & Simons, K. Influenza viruses select ordered lipid domains during budding from the plasma membrane. *JBC* **274**, 2038-2044 (1999).

33. Takeda, M., Leser, G.P., Russell, C.J. & Lamb, R.A. Influenza virus hemagglutinin concentrates in lipid raft microdomains for efficient viral fusion. *PNAS* **100**, 14610-7 (2003).

34. Zhang, J., Pekosz, A. & Lamb, R.A. Influenza virus assembly and lipid raft microdomains: a role for the cytoplasmic tails of the spike glycoproteins. *J Virol* **74**, 4634-44 (2000).

35. Barman, S., Adhikary, L. & Chakrabarti, A.K. Role of transmembrane domain and cytoplasmic tail amino acid sequences of influenza a virus neuraminidase in raft association and virus budding. *J Virol* **78,** 5258-5269 (2004).

36. Eichelberger, M.C., Compans, R.W. & Air, G.M. Influenza type A virus neuraminidase does not play a role in viral entry, replication, assembly, or budding. *J Virol* **69,** 1099-1106 (1995).

37. Palese, P. & Compans, R.W. Inhibition of influenza virus replication in tissue culture by 2-deoxy-2, 3-dehydro-N-trifluoroacetylneuraminic acid (FANA): mechanism of action. *J Gen. Virol.* **33,** 159-163 (1976).

38. Matrosovich, M.N., Matrosovich, T.Y. & Gray, T. Neuraminidase is important for the initiation of influenza virus infection in human airway epithelium. *J Virol.* **78,** 12665-12667 (2004).

39. Duez, J.M., Sixt, N. & Péchinot, A. Influenza virus infection: don't forget the role of the mucociliary system! *J Antimicro.Chemo.*421-422 (2009).

40. Cohen, M., Zhang, X.Q., Senaati, H.P., Chen, H.W. & Varki, N.M. Influenza A penetrates host mucus by cleaving sialic acids with neuraminidase. *Virol. J* **10,** 1-13 (2013).

41. Memorandum. A revision of the system of nomenclature for influenza viruses: a WHO memorandum. *Bulletin of the WHO* **58,** 585-591 (1980).

42. Tong, S., Li, Y., Rivailler, P. & Conrardy, C. A distinct lineage of influenza A virus from bats. *PNAS* **109,** 4269-4274 (2012).

43. Tong, S. et al. New world bats harbor diverse influenza A viruses. *PLoS Path.* **9,** e1003657 (2013).

44. Ma, W., García-Sastre, A. & Schwemmle, M. Expected and unexpected features of the newly discovered bat influenza A-like viruses. *PLoS Path.* **11,** e1004819 (2015).

45. Johnson, N. & Mueller, J. Updating the accounts: global mortality of the 1918-1920" Spanish" influenza pandemic. *Bulletin of the History of Medicine.* **76,** 105-115 (2002).

46. Scholtissek, C., Rohde, W., Hoyningen, V.V. & Rott, R. On the origin of the human influenza virus subtypes H2N2 and H3N2. *Virology* **87,** 13-20 (1978).

47. Garten, R.J., Davis, C.T., Russell, C.A., Shu, B. & Lindstrom, S. Antigenic and genetic characteristics of swine-origin 2009 A (H1N1) influenza viruses circulating in humans. *Science* (2009).

48. Dawood, F.S., Iuliano, A.D., Reed, C. & Meltzer, M.I. Estimated global mortality associated with the first 12 months of 2009 pandemic influenza A H1N1 virus circulation: a modelling study. *Lancet Infect. Dis.* **12,** 687-695 (2012).

49. Writing Committee of the Second World Health Organization Consultation on Clinical Aspects of Human Infection with Avian Influenza, A.V. et al. Update on avian influenza A (H5N1) virus infection in humans. *NEJM* **358**, 261-273 (2008).

50. Abdelwhab, E.M. & Veits, J. Prevalence and control of H7 avian influenza viruses in birds and humans. *Epidemiol. Infect.* **142,** 896-920 (2014).

51. Trombetta, C., Piccirella, S., Perini, D. & Kistner, O. Emerging Influenza Strains in the Last Two Decades: A Threat of a New Pandemic? *Vaccines* **3,** 172-185 (2015).

52. Chen, R. & Holmes, E.C. Avian influenza virus exhibits rapid evolutionary dynamics. *Mol. Biol. Evol.* **23,** 2336-2341 (2006).

53. Lin, Y.P. et al. Adaptation of egg-grown and transfectant influenza viruses for growth in mammalian cells: selection of hemagglutinin mutants with elevated pH of membrane fusion. *Virology* **233**, 402-10 (1997).

54. Brown, J.D., Swayne, D.E., Cooper, R.J., Burns, R.E. & Stallknecht, D.E. Persistence of H5 and H7 avian influenza viruses in water. *Avian Dis* **51**, 285-9 (2007).

55. Galloway, S.E., Reed, M.L., Russell, C.J. & Steinhauer, D.A. Influenza HA subtypes demonstrate divergent phenotypes for cleavage activation and pH of fusion: implications for host range and adaptation. *PLoS Path.* **9,** e1003151 (2013).

56. Costello, D.A., Whittaker, G.R. & Daniel, S. Variations in pH sensitivity, acid stability, and fusogenicity of three influenza virus H3 subtypes. *J Virol* **89**, 350-360 (2015).

57. Cotter, C.R., Jin, H. & Chen, Z. A single amino acid in the stalk region of the H1N1pdm influenza virus HA protein affects viral fusion, stability and infectivity. *PLoS Pathog* **10**, e1003831 (2014).

58. Daidoji, T., Watanabe, Y., Ibrahim, M.S. & Yasugi, M. Avian Influenza Virus Infection of Immortalized Human Respiratory Epithelial Cells Depends upon a Delicate Balance between Hemagglutinin Acid Stability and Endosomal pH. *JBC* **290,** 10627-10642 (2015).

59. DuBois, R.M. et al. Acid stability of the hemagglutinin protein regulates H5N1 influenza virus pathogenicity. *PLoS Pathog* **7**, e1002398 (2011).

60. Reed, M.L. et al. The pH of activation of the hemagglutinin protein regulates H5N1 influenza virus pathogenicity and transmissibility in ducks. *J Virol* **84**, 1527-35 (2010).

61. Reed, M.L. et al. Amino acid residues in the fusion peptide pocket regulate the pH of activation of the H5N1 influenza virus hemagglutinin protein. *J Virol* **83**, 3568-80 (2009).

62. Steinhauer, D.A., Wharton, S.A., Skehel, J.J. & Wiley, D.C. Studies of the membrane fusion activities of fusion peptide mutants of influenza virus hemagglutinin. *J Virol* **69**, 6643-51 (1995).

63. Chen, J. et al. Structure of the hemagglutinin precursor cleavage site, a determinant of influenza pathogenicity and the origin of the labile conformation. *Cell* **95**, 409-17 (1998).

64. Wiley, D.C., Wilson, I.A. & Skehel, J.J. Structural identification of the antibody-binding sites of Hong Kong influenza haemagglutinin and their involvement in antigenic variation. *Nature* **289**, 373-8 (1981).

65. Gerhard, W., Yewdell, J., Frankel, M.E. & Webster, R. Antigenic structure of influenza virus haemagglutinin defined by hybridoma antibodies. *Nature* **290,** 713-717 (1981).

66. Bottcher, C., Ludwig, K., Herrmann, A., van Heel, M. & Stark, H. Structure of influenza haemagglutinin at neutral and at fusogenic pH by electron cryo-microscopy. in *FEBS Lett*, Vol. 463 255-9 (1999).

67. Huang, Q., Opitz, R., Knapp, E.W. & Herrmann, A. Protonation and stability of the globular domain of influenza virus hemagglutinin. *Biophys J* **82**, 1050-8 (2002).

68. Huang, Q. et al. Early steps of the conformational change of influenza virus hemagglutinin to a fusion active state: stability and energetics of the hemagglutinin. *Biochim Biophys Acta* **1614**, 3-13 (2003).

69. Korte, T., Ludwig, K., Huang, Q., Rachakonda, P.S. & Herrmann, A. Conformational change of influenza virus hemagglutinin is sensitive to ionic concentration. *Eur Biophys J* **36**, 327-35 (2007).

70. Sauter, N.K. et al. Binding of influenza virus hemagglutinin to analogs of its cell-surface receptor, sialic acid: analysis by proton nuclear magnetic resonance spectroscopy and X-ray crystallography. *Biochemistry* **31**, 9609-21 (1992).

71. Sauter, N.K. et al. Hemagglutinins from two influenza virus variants bind to sialic acid derivatives with millimolar dissociation constants: a 500-MHz proton nuclear magnetic resonance study. *Biochemistry* **28**, 8388-96 (1989).

72. Rogers, G.N. & Paulson, J.C. Receptor determinants of human and animal influenza virus isolates: differences in receptor specificity of the H3 hemagglutinin based on species of origin. *Virology* **127**, 361-373 (1983).

73. Trevenan, W. et al. Glycomic Analysis of Human Respiratory Tract Tissues and Correlation with Influenza Virus Infection. *PLoS Path.* **9,** e1003223 (2013).

74. Shinya, K. et al. Avian flu: influenza virus receptors in the human airway. *Nature* **440**, 435-436 (2006).

75. Nicholls, J.M., Bourne, A.J., Chen, H., Guan, Y. & Peiris, J.S. Sialic acid receptor detection in the human respiratory tract: evidence for widespread distribution of potential binding sites for human and avian influenza viruses. *Respiratory research* **8**, 73 (2007).

76. Bateman, A.C. et al. Glycan Analysis and Influenza A Virus Infection of Primary Swine Respiratory Epithelial Cells: The Importance of NeuAc 2-6 Glycans. *JBC* **285**, 34016-34026 (2010).

77. Taiana, C. et al. Distribution patterns of influenza virus receptors and viral attachment patterns in the respiratory and intestinal tracts of seven avian species. *Veterinary Research* **43**, 28 (2012).

78. Jayaraman, A., Chandrasekaran, A. & Viswanathan, K. Decoding the distribution of glycan receptors for human-adapted influenza A viruses in ferret respiratory tract. *PLoS One* **7,** e27517 (2012).

79. Chutinimitkul, S., van Riel, D. & Munster, V.J. In vitro assessment of attachment pattern and replication efficiency of H5N1 influenza A viruses with altered receptor specificity. *J Virol.* **84,** 6825-6833 (2010).

80. Imai, M. et al. Experimental adaptation of an influenza H5 HA confers respiratory droplet transmission to a reassortant H5 HA/H1N1 virus in ferrets. *Nature* **486,** 420-430 (2012).

81. Herfst, S. et al. Airborne Transmission of Influenza A/H5N1 Virus Between Ferrets. *Science* **336**, 1534-1541 (2012).

82. Harris, A., Cardone, G. & Winkler, D.C. Influenza virus pleiomorphy characterized by cryoelectron tomography. *PNAS* **103,** 19123-19127 (2006).

83. Daniels, R.S. et al. Fusion mutants of the influenza virus hemagglutinin glycoprotein. *Cell* **40**, 431-439 (1985).

84. Weis, W.I. et al. The structure of a membrane fusion mutant of the influenza virus haemagglutinin. *EMBO J* **9**, 17-24 (1990).

85. Thoennes, S. et al. Analysis of residues near the fusion peptide in the influenza hemagglutinin structure for roles in triggering membrane fusion. *Virology* **370**, 403-14 (2008).

86. Cross, K.J., Wharton, S.A., Skehel, J.J. & Wiley, D.C. Studies on influenza haemagglutinin fusion peptide mutants generated by reverse genetics. *EMBO J* **20,** 4432-4442 (2001).

87. Rachakonda, P.S. et al. The relevance of salt bridges for the stability of the influenza virus hemagglutinin. *FASEB J* **21**, 995-1002 (2007).

88. Skehel, J.J. et al. Changes in the conformation of influenza virus hemagglutinin at the pH optimum of virus-mediated membrane fusion. *PNAS* **79**, 968-72 (1982).

89. Carr, C.M. & Kim, P.S. A spring-loaded mechanism for the conformational change of influenza hemagglutinin. *Cell* **73**, 823-32 (1993).

90. Chen, J., Skehel, J.J. & Wiley, D.C. N- and C-terminal residues combine in the fusion-pH influenza hemagglutinin HA(2) subunit to form an N cap that terminates the triple-stranded coiled coil. *PNAS* **96**, 8967-72 (1999).

91. Park, H.E., Gruenke, J.A. & White, J.M. Leash in the groove mechanism of membrane fusion. *NSMB* **10**, 1048-53 (2003).

92. Xu, R. & Wilson, I.A. Structural characterization of an early fusion intermediate of influenza virus hemagglutinin. *J Virol* **85**, 5172-82 (2011).

93. Bizebard, T. et al. Structure of influenza virus haemagglutinin complexed with a neutralizing antibody. *Nature* **376**, 92-4 (1995).

94. Baker, D. & Agard, D.A. Influenza hemagglutinin: kinetic control of protein function. *Structure* **2**, 907-10 (1994).

95. Carr, C.M., Chaudhry, C. & Kim, P.S. Influenza hemagglutinin is spring-loaded by a metastable native conformation. *Proc Natl Acad Sci U S A* **94**, 14306-13 (1997).

96. Remeta, D.P. et al. Acid-induced changes in thermal stability and fusion activity of influenza hemagglutinin. *Biochemistry* **41**, 2044-54 (2002).

97. Ruigrok, R.W. et al. Conformational changes in the hemagglutinin of influenza virus which accompany heat-induced fusion of virus with liposomes. *Virology* **155**, 484-97 (1986).

98. Ruigrok, R.W. et al. Electron microscopy of the low pH structure of influenza virus haemagglutinin. *EMBO J* **5**, 41-9 (1986).

99. Chen, J. et al. A soluble domain of the membrane-anchoring chain of influenza virus hemagglutinin (HA2) folds in Escherichia coli into the low-pH-induced conformation. *PNAS* **92**, 12205-9 (1995).

100. Kampmann, T., Mueller, D.S., Mark, A.E., Young, P.R. & Kobe, B. The Role of histidine residues in low-pH-mediated viral membrane fusion. *Structure* **14**, 1481-7 (2006).

101. Kalani, M.R., Moradi, A., Moradi, M. & Tajkhorshid, E. Characterizing a histidine switch controlling pH-dependent conformational changes of the influenza virus hemagglutinin. *Biophys J* **105**, 993-1003 (2013).

102. Mair, C.M., Meyer, T., Schneider, K. & Huang, Q. A histidine residue of the influenza virus hemagglutinin controls the pH dependence of the conformational change mediating membrane fusion. *J Virol.* **88,** 13189-13200 (2014).

103. Steinhauer, D.A. & Wharton, S.A. Amantadine selection of a mutant influenza virus containing an acid-stable hemagglutinin glycoprotein: evidence for virus-specific regulation of the pH of glycoprotein. *PNAS* **88,** 11525-11529 (1991).

104. Byrd-Leotis, L., Galloway, S.E. & Agbogu, E. Influenza Hemagglutinin (HA) Stem Region Mutations That Stabilize or Destabilize the Structure of Multiple HA Subtypes. *J Virol.* **89,** 4504-4516 (2015).

105. Ha, Y., Stevens, D.J., Skehel, J.J. & Wiley, D.C. H5 avian and H9 swine influenza virus haemagglutinin structures: possible origin of influenza subtypes. *EMBO J* **21**, 865-75 (2002).

106. Russell, R.J. et al. H1 and H7 influenza haemagglutinin structures extend a structural classification of haemagglutinin subtypes. *Virology* **325**, 287-96 (2004).

107. Godley, L. et al. Introduction of intersubunit disulfide bonds in the membrane-distal region of the influenza hemagglutinin abolishes membrane fusion activity. *Cell* **68**, 635-45 (1992).

108. Kemble, G.W., Bodian, D.L., Rose, J., Wilson, I.A. & White, J.M. Intermonomer disulfide bonds impair the fusion activity of influenza virus hemagglutinin. *J Virol* **66**, 4940-50 (1992).

109. Wang, W., DeFeo, C.J., Alvarado, E. & Vassell, R. Intermonomer Interactions in Hemagglutinin subunits HA1 and HA2 Affecting Hemagglutinin Stability and Influenza Virus Infectivity. *J Virol.* **doi:10.1128/JVI.00939-15** (2015).

110. White, J.M. & Wilson, I.A. Anti-peptide antibodies detect steps in a protein conformational change: low-pH activation of the influenza virus hemagglutinin. *J Cell Biol* **105**, 2887-96 (1987).

111. Pak, C.C., Krumbiegel, M. & Blumenthal, R. Intermediates in influenza virus PR/8 haemagglutinin-induced membrane fusion. *J Gen Virol* **75,** 395-9 (1994).

112. Daniels, R.S., Douglas, A.R., Skehel, J.J. & Wiley, D.C. Analysis of the Antigenicity of Influenza Haemagglutinin at the pH Optimum for Virus-mediated Membrane Fusion. *Journal of General Virology* **64**, 1657-1662 (1983).

113. Skehel, J.J. et al. Structural changes in influenza virus haemagglutinin at the pH of membrane fusion. *Biochem Soc Trans* **14**, 252-3 (1986).

114. Wharton, S.A. et al. Electron microscopy of antibody complexes of influenza virus haemagglutinin in the fusion pH conformation. *EMBO J* **14**, 240-6 (1995).

115. Steinhauer, D.A. et al. Studies using double mutants of the conformational transitions in influenza hemagglutinin required for its membrane fusion activity. *PNAS* **93**, 12873-8 (1996).

116. Gething, M.J., Doms, R.W., York, D. & White, J. Studies on the mechanism of membrane fusion: site-specific mutagenesis of the hemagglutinin of influenza virus. *J Cell Biol* **102**, 11-23 (1986).

117. Fontana, J., Cardone, G., Heymann, J.B., Winkler, D.C. & Steven, A.C. Structural changes in Influenza virus at low pH characterized by cryo-electron tomography. in *J Virol*, Vol. 86 2919-29 (United States, 2012).

118. Leikina, E., Ramos, C., Markovic, I., Zimmerberg, J. & Chernomordik, L.V. Reversible stages of the low-pH-triggered conformational change in influenza virus hemagglutinin. *EMBO J* **21**, 5701-10 (2002).

119. Korte, T. et al. Transient changes of the conformation of hemagglutinin of influenza virus at low pH detected by time-resolved circular dichroism spectroscopy. *J Biol Chem* **272**, 9764-70 (1997).

120. Krumbiegel, M., Herrmann, A. & Blumenthal, R. Kinetics of the low pH-induced conformational changes and fusogenic activity of influenza hemagglutinin. *Biophys J* **67**, 2355-60 (1994).

121. Korte, T., Ludwig, K., Booy, F.P., Blumenthal, R. & Herrmann, A. Conformational intermediates and fusion activity of influenza virus hemagglutinin. *J Virol* **73**, 4567-74 (1999).

122. Puri, A., Booy, F.P., Doms, R.W., White, J.M. & Blumenthal, R. Conformational changes and fusion activity of influenza virus hemagglutinin of the H2 and H3 subtypes: effects of acid pretreatment. *J Virol* **64**, 3824-32 (1990).

123. Kamali, A. & Holodniy, M. Influenza treatment and prophylaxis with neuraminidase inhibitors: a review. *Infection and Drug Resistance* **6,** 187-198 (2013).

124. Vigerust, D.J., Ulett, K.B., Boyd, K.L. & Madsen, J. N-linked glycosylation attenuates H3N2 influenza viruses. *J Virol.* **81,** 8593-8600 (2007).

125. Medina, R.A. et al. Glycosylations in the globular head of the hemagglutinin protein modulate the virulence and antigenic properties of the H1N1 influenza viruses. *Sci. Trans. Med.* **5,** (2013).

126. Wei, C.J., Boyington, J.C., Dai, K. & Houser, K.V. Cross-neutralization of 1918 and 2009 influenza viruses: role of glycans in viral evolution and vaccine design. *Sci. Trans. Med.* (2010).

127. Das, S.R., Puigbò, P., Hensley, S.E., Hurt, D.E. & Bennink, J.R. Glycosylation focuses sequence variation in the influenza A virus H1 hemagglutinin globular domain. *PLOS Path.* **6,** e1001211 (2010).

128. Fleury, D. et al. A complex of influenza hemagglutinin with a neutralizing antibody that binds outside the virus receptor binding site. *Nat Struct Biol* **6**, 530-4 (1999).

129. Knossow, M. et al. Mechanism of Neutralization of Influenza Virus Infectivity by Antibodies. *Virology* **302**, 294-298 (2002).

130. Xu, R. et al. A recurring motif for antibody recognition of the receptor-binding site of influenza hemagglutinin. *Nat Struct Mol Biol* **20**, 363-70 (2013).

131. Lee, P.S. et al. Receptor mimicry by antibody F045-092 facilitates universal binding to the H3 subtype of influenza virus. *Nat. Comm.* **5** (2014).

132. Matsubara, T., Onishi, A., Saito, T. & Shimada, A. Sialic acid-mimic peptides as hemagglutinin inhibitors for anti-influenza therapy. *J Med. Chem* **53,** 4441-4449 (2010).

133. Lees, W.J., Spaltenstein, A., Kingery-Wood, J.E. & Whitesides, G.M. Polyacrylamides bearing pendant alpha-sialoside groups strongly inhibit agglutination of erythrocytes by influenza A

virus: multivalency and steric stabilization of particulate biological systems. *Journal of medicinal chemistry* **37**, 3419-3433 (1994).

134. Okuno, Y., Isegawa, Y., Sasao, F. & Ueda, S. A common neutralizing epitope conserved between the hemagglutinins of influenza A virus H1 and H2 strains. *J Virol* **67,** 2552-2558 (1993).

135. Throsby, M. et al. Heterosubtypic neutralizing monoclonal antibodies cross-protective against H5N1 and H1N1 recovered from human IgM+ memory B cells. *PLoS One* **3,** e3942 (2008).

136. Ekiert, D.C. et al. Antibody recognition of a highly conserved influenza virus epitope. *Science* **324**, 246-51 (2009).

137. Sui, J. et al. Structural and functional bases for broad-spectrum neutralization of avian and human influenza A viruses. *NSMB* **16**, 265-73 (2009).

138. Ekiert, D.C. et al. A highly conserved neutralizing epitope on group 2 influenza A viruses. *Science* **333**, 843-50 (2011).

139. Corti, D. et al. A neutralizing antibody selected from plasma cells that binds to group 1 and group 2 influenza A hemagglutinins. *Science* **333**, 850-6 (2011).

140. Russell, E.S. et al. The genetic bottleneck in vertical transmission of subtype C HIV-1 is not driven by selection of especially neutralization-resistant virus from the maternal viral population. *J Virol* **85**, 8253-62 (2011).

141. Wang, C.C., Chen, J.R. & Tseng, Y.C. Glycans on influenza hemagglutinin affect receptor binding and immune response. *PNAS* **106,** 18137-18142 (2009).

142. Chen, J.-R.R. et al. Vaccination of monoglycosylated hemagglutinin induces cross-strain protection against influenza virus infections. *PNAS* **111**, 2476-2481 (2014).

143. Eggink, D., Goff, P.H. & Palese, P. Guiding the immune response against influenza virus hemagglutinin toward the conserved stalk domain by hyperglycosylation of the globular head domain. *J Virol* **88**, 699-704 (2014).

144. Lin, S.C., Lin, Y.F., Chong, P. & Wu, S.C. Broader Neutralizing Antibodies against H5N1 Viruses Using Prime-Boost Immunization of Hyperglycosylated Hemagglutinin DNA and Virus-Like Particles. *Plos One* **7,** e39075 (2012).

145. Lin, S.C., Liu, W.C., Jan, J.T. & Wu, S.C. Glycan Masking of Hemagglutinin for Adenovirus Vector and Recombinant Protein Immunizations Elicits Broadly Neutralizing Antibodies against H5N1 Avian Influenza Viruses. *Plos One* **9,** 92822 (2014).

146. Hai, R. et al. Influenza viruses expressing chimeric hemagglutinins: globular head and stalk domains derived from different subtypes. *J Virol* **86**, 5774-5781 (2012).

147. Krammer, F., Pica, N., Hai, R. & Margine, I. Chimeric hemagglutinin influenza virus vaccine constructs elicit broadly protective stalk-specific antibodies. *J Virol* **87,** 6542-6550 (2013).

148. Krammer, F. et al. Assessment of Influenza Virus Hemagglutinin Stalk-Based Immunity in Ferrets. *J Virol* **88**, 3432-3442 (2014).

149. Goff, P.H. et al. Adjuvants and immunization strategies to induce influenza virus hemagglutinin stalk antibodies. *PLoS One* **8**, e79194 (2013).

150. Bommakanti, G., Lu, X., Citron, M.P. & Najar, T.A. Design of Escherichia coli-expressed stalk domain immunogens of H1N1 hemagglutinin that protect mice from lethal challenge. *J Virol* **86,** 13434-13444 (2012).

151. Bommakanti, G., Citron, M.P. & Hepler, R.W. Design of an HA2-based Escherichia coli expressed influenza immunogen that protects mice from pathogenic challenge. *PNAS* **107,** 13701-13706 (2010).

152. Mallajosyula, V.V. et al. Hemagglutinin Sequence Conservation Guided Stem Immunogen Design from Influenza A H3 Subtype. *Frontiers in immunology* **6**, 329 (2015).

153. Mallajosyula, V.V.A., Citron, M. & Ferrara, F. Influenza hemagglutinin stem-fragment immunogen elicits broadly neutralizing antibodies and confers heterologous protection. *PNAS* **E2514-E2523** (2014).

154. Impagliazzo, A. et al. A stable trimeric influenza hemagglutinin stem as a broadly protective immunogen. *Science* **349,** 1301-1306 (2015).

155. Kanekiyo, M., Wei, C.J., Yassine, H.M. & McTamney, P.M. Self-assembling influenza nanoparticle vaccines elicit broadly neutralizing H1N1 antibodies. *Nature **499,*** 102-106 (2013).

156. Yassine, H.M. et al. Hemagglutinin-stem nanoparticles generate heterosubtypic influenza protection. *Nature Medicine* **21**, 1065-1070 (2015).

CHAPTER II: Dynamic Changes During Acid-induced Activation of Influenza Hemagglutinin

[Reproduced in part with permission from © Cell Press, Structure, Vol. 23(4), 2015 p666-676. doi: http://dx.doi.org/10.1016/j.str.2015.02.006]

INTRODUCTION

For influenza hemagglutinin (HA) the pH-dependent membrane fusion and activation is a highly dynamic process that requires large structural changes, which are often transient and difficult to characterize by classical techniques such as X-ray crystallography. The crystal structures of the pre-fusion bromelain-released ectodomain (BHA)[1] and HA2 subunit either following exposure to low pH and proteolysis (TBHA2) or expression of HA2 in *E. coli* (EHA2)[2,3] revealed the extent of the HA2 reorganization required for membrane fusion (Figure 2.1), and in chapter I, the wealth of molecular and structural characterization for HA activation was described in detail. Still, it is unclear how low pH initiates this molecular machine to carry out membrane fusion and it has been proposed that HA, when exposed to the low pH of the maturing endosome, activation progresses through the pathways depicted in Figure 2.1 B. Analytical approaches that can directly monitor the structural transitions and conformational dynamics of short-lived protein states in the native state are required to effectively characterize how HA becomes membrane active during the initial events that promote fusion.

Solution-phase protein labeling experiments is a growing field in structural biology that provides sequence-specific information about native protein conformational dynamics and structural organization (Figure 2.2). Hydrogen/deuterium-exchange mass spectrometry (HDX-MS) (Figure 2.2 A) can be applied to a broad range of proteins, glycoproteins, membrane-bound proteins and even proteins in the context of whole virus particles.[4-10] Protein size is less of a limiting factor for such techniques, than for example with NMR, which also can be used to probe structural dynamics of smaller macromolecules but is less suitable for analysis of objects in the size range of viral glycoproteins. With the advent of more advanced mass spectrometers such as those employing ion mobility for enhanced separation of peptide fragments, it is becoming possible to analyze even more complex targets.[11] The mass spectrometry-based methods are particularly powerful for comparative studies looking at the difference between two related states or variants such as mutant and wild-type, ligand-bound and free states, or across a range of solution conditions (e.g. pH), and can even prove useful for mapping of both linear and conformational epitopes within an antibody-antigen complexes.[12-15]

HDX-MS (Figure 2.2 A) probes local structural dynamics in native proteins yielding a “fingerprint” of structural dynamics with the resolution necessary to identify isolate-specific differences in structure and the ability to identify ligand-induced structural changes.[16-19] By itself this approach does not provide 3-dimensional structural information; rather one obtains a measurement of structural dynamics or flexibility of segments of the protein as they exist under native conditions in the folded protein. In combination with other available structural information, HDX-MS can be a powerful method for mapping conformational changes and characterizing structures that may be too dynamic and flexible to characterize by crystallography or electron microscopy (EM).

HDX-MS measures the rate of deuterium incorporation at the backbone amides, which is dependent on local structural order. The apparent deuterium exchange rates of each amide in the protein polypeptide backbone are predominately influenced by hydrogen bonding, such as in secondary structure formation. The temperature and pH of the solution also plays a factor in deuterium incorporation and must be precisely controlled during the experiment.[12,19] In a typically experiment, a protein is incubated in D_2O-based buffer typically under native conditions for a range of times, after which, the solution is acidified to pH 2.5 to slow deuterium exchange at the amides. Structural analysis of the protein requires proteolytically digesting the partially deuterated protein under quench conditions using acid-active proteases such as pepsin. Pepsin reproducibly cleaves polypeptides into a range of segments of varying length, and as a result, peptides can range from a few to tens of residues in length.[20] The peptic fragments are resolved chromatographically and analyzed by mass spectrometry. The extent of deuterium up-take for each peptide is interpreted by the mass shift as a function of deuteration time. The reliance upon the acid-active protease, pepsin, imposes one major limitation in HDX-MS analysis as it results in non-uniform sequence resolution.

For glycoproteins, such as HA, resistance to proteolysis and poor signal for glycopeptides can complicate analysis, and hyperglycosylated regions can generate large peptic fragments that may contain multiple glycans per peptide.[21,22] In some cases the highly glycosylated peptides bind poorly to the reverse-phase columns implemented during liquid chromatography. Each glycosylation site within a glycopeptide can also exhibit a high degree of variation known as "microheterogeneity", which results in the signal for the glycopeptide to be distributed among several glycoforms, and in the case of poorly ionizable peptides, can significantly hamper detection.[23] Nonetheless, continual improvement in liquid chromatography and mass spectrometry instruments, sample handling, and downstream HDX software has improved the resolution, sensitivity, and analysis of intrinsically complex samples such as the highly glycosylated HA viral protein.[24]

For a homogenous protein conformation, amide deuterium uptake is typically gradual due to rapid, uncorrelated, local unfolding events, which is reflected by a unimodal isotopic envelope distribution for each resolved peptide, known as "EX2" kinetics. However, the ability to detect bimodal distributions within a dataset is indicative of protein states where a region is undergoing large-scale, correlated motions (e.g. global unfolding) or in other cases can reflect heterogeneous protein samples, in which multiple conformations are present (e.g. aggregate versus properly folded species), thus illustrating strengths of such an analytical tool.[25]

Similar to HDX-MS, small angle X-ray scattering (SAXS) (Figure 2.2 B) is a technique that can be used to characterize the solution-state of a protein. SAXS involves the measurement of elastic X-ray scattering from macromolecules and the SAXS pattern obtained is directly related to the average 3-dimensional organization of atoms in the scattering object.[26,27] In the most elemental but rigorous application, SAXS can be used to determine accurate protein and glycoprotein molecular masses, radii of gyration (R_G) and maximum point-to-point dimensions of the object (D_{Max}) using the interatomic distance distribution function, P(r).[16,28-34] With the aid of *ab initio* shape reconstruction programs, the scattering pattern can yield low-resolution morphological information about proteins and protein complexes in solution.[27,35-37]

A particularly powerful SAXS analytical approach has come into use more recently, in which one builds upon sometimes fragmentary high-resolution structural information by modeling in missing features and iteratively changing and selecting models that produce optimal agreement with experimentally measured SAXS data.[38-42] However, it is important to note that the solution scattering profile results from the entirety of scattering correlations of atoms in the object of interest hence it is essential to model in not just missing protein loops but to include glycans and other post-translational modifications as well.[31,34] With the experimental SAXS pattern as a constraint, in simpler cases, it is possible to identify ensembles of models with glycan orientations that show a better agreement with the measured data, allowing the spatial occupancy of the glycans to be estimated.[31] In *ab initio* modeling, due to averaging effects and limitations on resolution, glycans tend to not be resolved as distinct features.[31,33]

The use of hybrid technologies such as those mentioned above, are imperative for the detailed characterization of complex, heterogeneous and dynamic influenza HA glycoprotein when approaching the low pH of membrane activation. Here HDX-MS and SAXS are used to investigate the structural and dynamic changes in HA and to identify specific regions involved in native fusion activation. We find that as the pH of activation is approached, an increase in flexibility of the fusion subunit, centered on the fusion peptide and HA1-HA2 interface, occurs concomitant with stabilization of the HA1-HA1 interface, suggesting that fusion peptide release may be the initiating step in HA activation, prior to unclasping of the HA1 cage.

RESULTS

BHA and full-length HA on virus show similar HDX-kinetics

To determine whether the soluble, bromelain-released HA ectodomain (BHA) retains its native HA structure when liberated from the HA2 transmembrane domain anchor and crowded viral surface, BHA was analyzed by HDX-MS and compared to intact HA on whole virions (X-31 H3N2). 90%

sequence coverage of BHA was obtained from 58 and 27 unique peptides for HA1 and HA2, respectively (Figure S2.1). In whole influenza samples, HA1 coverage remained similar to BHA coverage while approximately half of HA2 sequence coverage was lost due to spectral overlap from additional viral proteins (Figure 2.2 A,B). Western blots comparing supernatant and virus pellet were used to verify that no free HA was present in the viral samples under HDX conditions and that only intact trimeric HA anchored in the viral membrane was being observed (Figure S2.2). The exchange kinetics for the peptides monitored from BHA and HA on the virus were identical within error, indicating they have very similar conformational dynamics and structures despite bromelain-cleavage of the ectodomain and release from contact with adjacent glycoproteins and membrane (Figure 2.3).

Reorganization in post-fusion BHA

In order to examine the large changes in conformation between pre- and post-fusion HA, HDX-MS was also performed on acid-triggered BHA. BHA was incubated at low pH allowing it to convert to the post-fusion state, followed by reneutralization to pH 7.5 to match the pre-fusion exchange conditions. After 3 hours of incubation at pH 4.9 at 22 ˚C, most of the population had adopted the post-fusion form, but a minor population of pre-fusion BHA persisted. This sub-population was detected by the presence of bimodal exchange behavior for several peptides, in contrast to the consistently unimodal pre-fusion BHA spectra (Figure S2.3). Bimodal deconvolution of the acid-triggered BHA spectra enabled us to extract the exchange kinetics for the post-fusion population alone (see experimental procedures).[43] Acid-triggering of BHA at pH lower than 4.9 and at 37 °C eliminated the residual non-triggered sub-population; but this treatment also appeared to induce global destabilization of HA1 (data not shown).

By HDX-MS, the peptides spanning the fusion peptide (HA2 1-21) in post-fusion BHA displayed significant envelope broadening that could not be unambiguously deconvoluted (Figure S2.4). This behavior in the post-fusion BHA was unique to the fusion peptide and is presumably due to the involvement of this specific segment in mediating aggregation such as in “rosettes”, where several triggered spikes are tethered together by their fusion peptides.[44] Due to this complication, HDX data for the fusion peptide in the post-fusion state was not analyzed further.

The HDX-MS analysis revealed many sites that show significant differences in structural organization between pre- and post-fusion BHA (Figure 2.4). The difference exchange butterfly plot shows all the changes throughout the data set for each peptide, regions that are more protected in the post-fusion state are plotted above the zero axis, and regions that are more flexible in the post-fusion state are plotted below the zero axis (Figure 2.4 B). The changes were largely consistent with available crystallographic structures for HA2.[1,2] Deuterium exchange profiles for the majority of the HA2 Helix-C core (HA2 88-91 and 92-99) were unchanged, suggesting that this region maintains helicity following the post-fusion transition, possibly serving as a fulcrum around which the rest of HA2 reorganizes. By contrast the B-loop in HA2 (HA2 53-69 and 70-87), which exhibits significant exchange in pre-fusion HA, showed substantial protection in post-fusion BHA, consistent with the formation of the stable, extended helix seen in TBHA2 (Figure 2.4 C). Helix-C peptides (HA2 102-109, 100-115 and 110-115) exhibited faster exchange kinetics in post-fusion BHA, consistent with the transition from an ordered helix in the pre-fusion structure to a less protected loop in the post-fusion HA state. C-terminal HA2 segments (139-148, 149-167 and 168-175) pack in an extended conformation along the central coiled-coil in post-fusion structures, and peptides spanning this region had elevated deuterium incorporation in post-fusion BHA, consistent with exposed amides.[3,45]

Crystallographic data representative of post-fusion HA1 is limited to a crystal structure of HA1 monomer complexed with the Fab domain of antibody HC19.[46] The HA1-HC19 structure suggests that HA1 may retain its structure, essentially unchanged, following acid-activation and release from the HA2 fusion domain. By HDX-MS, several regions in HA1 showed substantial increases in deuterium uptake between the pre- and post-fusion BHA states, reflecting local destabilization (Figure 2.4). Protein segments involved in the pre-fusion HA1-HA1 trimeric interface (HA1 195-228 and 212-228) lost protection in the post-fusion conformation, consistent with unclasping of the subunits at the trimer apex (Figure S2.5). Peptides spanning the 190-helix (HA1 175-194 and 178-194) of the receptor binding site, which are also adjacent to the HA1-HA1 interface, exhibited greater exchange in post-fusion BHA. A few regions exhibited uptake profiles that did not change between pre- and post-fusion HA. These invariant regions included peptides within the 8-stranded β-sheet in the globular head that are located distal from the HA1-HA1 interfaces in the pre-fusion crystal structure (HA1 148-161, 162-174 and 178-189).

All observable peptides in the HA1 F’ domain (HA1 1-13, 26-33, 33-42, 281-316 and 315-328), exhibited elevated deuterium exchange in the post-fusion conformation, likely due to the disruption of stabilizing contacts between the F’ domain and the HA2 subunit. Furthermore, the N- and C-termini did not retain secondary structure in the post-fusion conformation as reflected by their rapid exchange kinetics. Peptides in the E’ domain (HA1 79-86 and 269-277) at the base of the globular head, form a “hinge” between the globular head and F’ domain, which also form interactions with the HA2 B-loop in pre-fusion HA. In post-fusion BHA, this “hinge” and HA1 peptides that adjoin the B-loop prior to triggering (HA1 88-108 and 281-316) showed greater deuterium uptake relative to the pre-fusion state. Increased deuterium incorporation of the HA1 peptides involved in the HA1-HA2 interface suggested that interactions between HA1 and HA2 were disrupted in the post-fusion conformation.

Characterization of BHA at pH conditions approaching fusion activation

We sought to probe the underlying pH-dependent changes in the structural dynamics of BHA by investigating the HDX of BHA under pH conditions mimicking the maturing endosome. Liposome leakage assays, light scattering, native PAGE and small angle X-ray scattering (SAXS) were used to identify pH conditions that would be amenable to HDX-MS analysis at 22 °C (Figure 2.5 and 2.6). With the exception of native PAGE, the assays did not require reneutralization of the samples, hence their behavior was examined under the pH conditions where HA is functional.

BHA does not include the transmembrane domain and is not anchored in the viral membrane, thus the liposome leakage assays only report on membrane activity of the fusion peptide-bearing ectodomain and not fusion *per se*. Based on increases in fluorescence dequenching from the liposomeencapsulated sulforhodamine-B dye, BHA was observed to become increasingly membrane-active at pH<5.5, with its activity plateauing below pH 5.0 (Figure 2.5 A,B).

Dynamic light scattering (DLS) measures the radius of a particle in solution, and due to the large scattering signal of micelles present in detergent samples, DLS of BHA under various pH conditions was performed in the absence of detergent. The DLS measurements indicated that at pH 7.4, 6.0, and 5.5 the hydrodynamic radius of BHA did not change, but it increased dramatically at pH 5.0 (Figure 2.5 C). Hence at pH≥5.5, the BHA spike retains its overall organization and solubility in the absence of detergents, but at lower pH such as 5.0, the spikes aggregate, presumably through fusion peptide-mediated association. Native PAGE, also in the absence of detergent (Figure 2.5 D), likewise showed that when BHA was incubated for 30 min at pH 5.5, it remained well-behaved and soluble, while at pH 5.25 or 5.0 the material did not enter the gel, suggesting the hydrophobic fusion peptides may be more accessible and mediate aggregation at the lower pH conditions.

Interestingly, when BHA was examined by SAXS with in-line size exclusion chromatography in the presence of n-dodecyl maltoside (n-DDM) detergent at pH 5.2, it was observed to retain a similar overall structure to pre-fusion BHA at neutral pH, although the scattering of the detergent increased the background scattering, which unfortunately decreased the signal to noise (Figure 2.6 A). The P(r) plots (Figure 2.6 B) and *ab initio* shape reconstruction (Figure 2.6 C), showed that the mass distribution remained largely the same, indicative of the spike's main elements remaining in a similar organization, unlike, for example, what one would observe upon dissociation of the HA1 heads (Figure S2.6).

With these combined data, we concluded that BHA in the absence of detergent was well-behaved and non-aggregated if kept at pH 5.5 or above, while even at pH 5.2 it appears to retain an intact spike organization, although likely with fusion peptides exposed and capable of mediating membrane interactions and aggregation.

HDX-MS analysis of BHA at pH conditions approaching fusion activation

HDX-MS was next employed to monitor BHA structural dynamics as the activation pH threshold was approached. We focused on a pH range where the protein remained soluble without detergent (pH>5.5). In order to rigorously carry out a comparison of HDX under different pH conditions, it was necessary to adjust the deuterium incubation times to compensate for the pH-dependent differences in the intrinsic chemical exchange rate. Over the pH range where BHA was examined, pH* 7.5-5.6 (where pH* is the measured pH in D_2O), the chemical HDX mechanism is base catalyzed. As the solution becomes more acidic, the concentration of base decreases resulting in a slower rate of exchange. Studies by Bai et al. derived the activation energy of the base catalyzed HDX, making it possible to calculate the chemical rate for each mildly acidic condition (pH* 6.5, 5.9 and 5.6) relative to pH* 7.5.[47,48] By adjusting deuteration times the exchange rates at different pH* values could be compared. For more precise time scaling, we also included an internal standard (PPPI peptide) to directly compare the HDX profiles of BHA over pH* values 7.5 to 5.6 (see experimental procedures and Figure S2.7).[49]

Under these conditions, the fusion peptide and every other monitored peptide displayed unimodal spectra, indicating that a single conformational population was present and no population of post-fusion BHA was detected (Figure 2.7). All experiments were performed in duplicate and the errors from each measurement were narrow enough to reliably infer qualitative changes occurring throughout BHA leading up to the threshold of pH activation (Figures 2.8, S2.8). The significant dynamic differences exhibited a pH-dependent trend suggesting HA activation responds progressively to lowering the pH.

Many regions of both HA1 and HA2 remained unchanged by exposure to a pH* range approaching the activation threshold (~pH* 5.6), exhibiting deuterium uptake plots that were superimposable to within error. Regions in HA2 by contrast showed dynamic differences as a function of pH* (Figures 2.8 A, S2.8). The N-terminal fusion peptide (HA2 1-9; peptide 1, Figure 2.8A) displayed the greatest pH-dependent changes, becoming considerably more dynamic at lower pH*. A modest increase in dynamics was also seen at the C-terminal end of the fusion peptide (HA2 10-21; peptide 2, Figure 2.8 A) at pH* 5.6. Both Hairpin-1 (HA2 22-38; peptide 3, Figure 2.7 A) and Helix-A (HA2 39-52;

peptide 4, Figure 2.8 A) downstream from the fusion peptide were also measurably more dynamic at pH* 5.6, outside of calculated error. Peptides spanning the B-loop, (HA2 53-69; peptide 5, Figure 2.8 A), which sits directly beneath the E’ domain in HA1, became more dynamic at lower pH, while no pH-dependent changes were observed at HA2 70-87, spanning the top of the coiled-coil stalk (peptide 6, Figure 2.8 A). Additionally, peptides in HA2 covering the central coiled-coil stalk also maintained strong protection (HA2 92-99; peptide 7, Figure 2.8 A). By contrast, regions near the C-terminus of HA2, such as Hairpin-2 (119-138; peptide 8 in Figure 2.8 A), which form the base of the fusion peptide cavity in pre-fusion HA, located proximal to the base of the coiled-coil, showed increased dynamics at lower pH*.

Relatively subtle effects were observed within HA1 as a function of pH, with many peptides showing no changes at all. HA1 peptides that form the receptor binding pocket (HA1 175-194; peptide 3 in Figure 2.8 C) showed no pH-dependent changes nor did much of the β-sheet substructure of the globular head domain (HA1 244-258; peptide 5 in Figure 2.8 C). The HA1-HA2 interface exhibited a more complex pattern of pH-dependence such that some peptides including HA1 E’ domain peptides that make contacts with the HA2 B-loop (HA1 87-108 and 281-316; peptides 2 and 7 in Figure 2.8 C) showed minimal differences between pH* 7.5 and 5.6. Other HA1-HA2 interfacial peptides showed some of the largest increases in deuterium exchange within HA1. For example large changes were observed in two separate peptides that form the hinge at the base of the HA1 globular head (HA1 79-86 and 258-268, peptides 1 and 6 in Figure 2.8 C), which are adjacent to the internal portion of the B-loop. Likewise, the C-termini of HA1 (HA1 317-328; peptide 8, Figure 2.8 C) showed some of the largest pH-dependent increases in deuterium incorporation. These data suggest that flexibility of the HA1 hinge and regions that neighbor the HA2 fusion peptide and associated sites constitute the initial elements that respond to mildly acidic conditions during endosomal maturation (Figure 2.8 B,D). While most of the F’ domain and the peripheral E’ domain were more dynamic at lower pH, one peptide located between these two regions (HA1 269-277; Figure S2.8) was more ordered at pH* 5.6. Surprisingly, peptides spanning the entire HA1-HA1 trimeric interface (HA1 195-228; peptide 4 in Figure 2.8 C) also became *more* protected at pH* 5.6.

The current study made no correction for changes in the local intrinsic rate due to the protonation of histidine residues, which as a function of pH can increase the exchange rate by a factor of two.[47] Many of the major pH-dependent changes observed by HDX were in peptides (including the fusion peptide) that do not contain histidine residues, while some histidine containing peptides (HA1 175-194 and HA2 100-115) did not exhibit pH-dependent changes (Figure 2.8 B,D and Figure S2.8). Therefore, the effects on the intrinsic exchange rate from altered histidine protonation appear to have a marginal impact, if any, on the current comparisons within these experiments.

DISCUSSION

In order to carry out membrane fusion, viral fusion proteins undergo a series of conformational changes once activated by receptor binding or environmental triggers such as endosomal acidification.[50] While spectroscopy[51,52], limited proteolysis[44,53-55], and epitope exposure mapping studies[54,55] support the existence of HA intermediates populated under acidic pH conditions, these functionally important states have been refractory to structure determination methods such as crystallography. Characterization of HA intermediates is essential for understanding the process of protein-mediated membrane fusion as well as for developing therapeutics that could inhibit the transition that leads to the initial steps of viral replication. This study examined HA using HDX-MS to probe the structural dynamic changes in soluble, bromelain-released HA induced by acidification.

Post-fusion HA exhibits dramatic overall remodeling of HA1 and HA2

Post-fusion HA2 crystal structures have been crucial for understanding the end-state structure of the fusion subunit. However, due to the unconstrained nature of post-fusion HA1, structural insight of HA in the post-fusion state has been limited to fragmentary information for the HA2 subunit and a monomeric HA1-antibody complex.[2,3,46] Our HDX-MS data provides a detailed portrait of the large-scale reorganization in HA that occurs as a result of the conversion to the post-fusion form, including the full HA2 ectodomain with the HA1 subunits still covalently linked.

The data for the HA2 subunit in the post-fusion state are largely consistent with the available structural information of the isolated HA2 crystal structure (Figure 2.4).[2,3] The analysis also demonstrates that HA1-HA1 contacts are disrupted once the spike has transitioned to the post-fusion configuration (Figure 2.4), as reported by increased exchange at the trimeric interface and portions of the receptor binding site that line this interface (220-loop and 190-helix). The neighboring 130-loop and parts of the anti-parallel β-sheets away from the HA1-HA1 interface by contrast, are consistent with the findings of Bizebard et al., which revealed nearly identical structures of the monomeric receptor binding head domain (in complex with HC19 Fab) and in the context of the BHA trimer.[1,46] The differences in HA1 in post-fusion BHA observed by HDX-MS likely reflect the loss of quaternary contacts upon HA1 dissociation rather than a loss of tertiary structure throughout the HA1 head domain.

Our findings also indicate a loss of structural order at the HA1-HA2 interface in post-fusion BHA as observed by faster exchange kinetics for the E' and F' domains. Changes within the F' domain, specifically in regions adjacent to the fusion peptide pocket were among the largest within this dataset, indicating the importance of this region in forming a stabilizing "cage" that maintains the pre-fusion HA2 conformation.[56] This post-fusion BHA data serves as a valuable reference for comparisons with intermediate BHA conformations described below.

At the threshold for fusion activation, the fusion peptide gains dynamics while the "spring" remains caged by HA1

HDX-MS was also used to probe the structural changes in HA that occur as it approaches fusion under maturing endosomal pH (down to pH* 5.6) (Figure 2.9 A). Dissociation of the HA1 globular head domains does not appear to be involved in the initial activation given that the head and receptor binding site show largely identical exchange kinetics over this pH range (Figure 2.9 B). Peptides spanning the HA1-HA1 trimeric interface actually become more protected, opposite to what we observed in the post-fusion state, suggesting that this interface is strengthened at pH approaching the threshold for activation (Figure 2.9 B). In this transitional pH range, we considered the possibility that intermediate pH conditions might give rise to a mixture of species, for example sub-populations of pre- and post-fusion trimers. The peak width analysis of the HDX-MS spectra for conditions down to pH* 5.6 show that the BHA spike in these experiments populated a single state. SAXS data show that even at pH 5.2, the overall spike organization, at least at low resolution, was similar to the intact pre-fusion BHA structure at neutral pH. This suggests that the HDX-MS data report on localized dynamic changes in the context of a still well-formed, trimeric spike.

The new findings are in good agreement with previously published data from White and Wilson, which probed HA structure when exposed to a range of acidic pH.[54] Namely, antibodies could bind the fusion peptide and N- and C-termini of HA1 along the HA stalk at a pH higher than was required for an antibody to bind to a peptide buried at the HA1-HA1 interface. It was inferred that this reflected fusion peptide exposure without complete HA1 dissociation. In a follow-up study using additional conformation-specific antibodies against antigenic site B (approximately 154-160 and 188-198 spanning the 190-helix), it was reported that changes in fusion peptide exposure take place concomitant with epitopic changes in the apex of the spike.[55] The HA1-HA1 interface did not become accessible until later in the low pH transition. Kemble et al. interpreted the data to reflect a partial dissociation of HA1 head domains coupled to fusion peptide and associated changes in the stalk regions. We observed a small change in HDX-MS for the peptide spanning 152-161 in HA1 at pH* 5.6, while peptides spanning the 190-helix did not exhibit major changes (Figure 2.9 B, S2.8). The fusion peptide and peptides forming the HA1 hinge experienced some of the largest increases in deuterium incorporation (Figure 2.9 C, D). It is possible that at low pH, flexibility at these sites may influence epitope presentation as described by Kemble et al.[55] However, since the HA1-HA1 interface by HDX-MS appears to be moderately bolstered at pH* 5.6, we suggest that a subtle reorganization of HA1 domains occurs without requiring domain dissociation. It should also be noted that the HDX-MS data presented in this study probed dynamic differences in the HA ectodomain under the native fusion-activation conditions without necessitating reneutralization, which antibody binding assays required.

The sites that become more dynamic under low pH also coincide with regions that Fontana et al. infer to change in HA on the surface of virions as imaged by cryo-electron tomography.[57] Fontana et al. observed a modest narrowing of the HA stem with the preservation of the HA1 trimeric crown distal to the viral membrane upon acidification, suggesting that the HA2 N-terminal regions including the fusion peptide and associated segments leading up to the B-loop may have been released from the core of the stem, while the HA1 domains remain clasped together.

The regions in HA where we observe increased dynamics upon acidification are also in excellent agreement with regions where mutations have been shown to produce substantial shifts in the activation pH.[58] For instance, the fusion peptide pocket is lined by highly conserved ionizable residues from the F' Domain, Helix-A, and Helix-C (HA1 H17, HA2: K51, H106, D109, and D112); mutations of these residues have been shown to alter the protonation state of this pocket (specifically HA1 H17, and HA2 D109 and D112), which is hypothesized to regulate fusion peptide release.[58,59] While our data does not cover peptides containing HA1 H17, all other regions of this cavity can be monitored. Upon acidification, the fusion peptide and HA1 C-terminus exhibits a large increase in deuterium incorporation, consistent with an increase in dynamics and accessibility for greater solvent exchange (Figure 2.9 C).

Conserved group-specific ion pairs have been proposed to stabilize pre-fusion HA at the HA1-HA2 interface, which is composed of the E' domain and B-loop.[56,60] Crystallographic evidence of HA2 B-loop side chain repositioning and local reordering within the E' domain of two HA variants was obtained under moderately acidic conditions, both of which still maintained an overall pre-fusion configuration.[61,62] Our pH-dependent HDX-MS data covering the N-terminal portion of the B-loop shows increased dynamics at lower pH (Figure 2.9 D), supporting the aforementioned crystallographic observations. However, since HA1 E' peptides directly contacting the termini of the B-loop ("110-helix" in DuBois et al.) did not show any pH-dependent changes in deuterium exchange when approaching the threshold of activation, the B-loop may respond at a higher pH than the neighboring HA1 peptides, possibly mediating the reorganization of this interface. We surmise that movements within the B-loop in concert with the adjacent HA1 hinge play a role in HA activation, which ultimately results in the complete disruption of the HA1-HA2 interface at later stages of HA remodeling as adopted in the post-fusion state (Figure 2.4).

In contrast to the models proposed by Kembel et al.[55] and Fontana et al.[57], others have suggested that HA activation may be driven by protonation of key ionizable residues in HA1 leading to repulsive electrostatic interactions and dissociation of the HA1 head domains.[63] This particular model ("Uncaging" model, Figure 2.1 B) posits that HA1 dissociation allows solvent penetration into the core of the ectodomain, driving the refolding of HA2 to the coiled-coil, post-fusion state. While such changes may transpire at later stages of the conformational cascade, our findings support a mechanism ("FP release" in Figure 2.1 B) similar to that proposed by Kembel et al.[55] and Fontana et al.[57] where the fusion peptide and associated structural elements become highly dynamic, primed for fusion and accompanied by modest HA1 reorganization rather than the full uncaging of HA1. The HA1 head domains remained clasped together, preventing the spring-loaded refolding of HA2 to an extended helical bundle and post-fusion conformation.

The observed pH-dependent dynamic response exhibited by HA parallels the decrease in pH observed in endocytic vesicles during their maturation, and the elevated fusion peptide dynamics at intermediate acidic pH conditions may enable HA to bind a target membrane prior to HA1 uncaging and the "spring-loaded", large-scale refolding of HA2 that drives membrane apposition and fusion. These staged sequences would likely yield more efficient fusion of virus and host cell membranes possibly preventing premature HA inactivation as hypothesized in past studies.[64,65]

In this report we have primarily focused on the soluble HA ectodomain (BHA). Presentation of the HA on the exterior of the virus surface differs from BHA due to its anchoring to the membrane and likely interactions between the HA cytoplasmic tail and M1 matrix layer.[65,66] Although HDX-MS data has been used to characterize complex protein assemblies such as the Hepatitis B Virus capsid[67], our study is to our knowledge, the first example of HDX-MS analysis applied to such a multicomponent system aimed at characterizing a protein on the surface of an intact virion. We show that at neutral pH, membrane association of full-length HA on virus does not alter the behavior of HA relative to BHA (Figure 2.2). It should be noted that the complexity of the whole virus sample greatly limited the sequence coverage and data quality for the full-length HA thus far, and similar pH activation experiments with full virus have been challenging due to the heterogeneity of specimens once pH-dependent structural changes are triggered. Hence, we cannot rule out the possibility that the full-length HA interaction with membrane and matrix may alter activation and play a role during fusion.[65,66] Future advances in instrumentation that allow more complex samples to be analyzed may allow for a more complete activation of full-length HA on the surface of virus.

EXPERIMENTAL PROCEDURES

Influenza and BHA preparation

X31 (H3N2) influenza A virus grown in allantoic fluid of embryonated chicken eggs purified by density gradient was purchased from Charles River Laboratories. Viral stocks (2 mg/mL) were centrifuged at 2,320 relative centrifugal force (rcf) at 4°C for 5 min to remove residual egg protein contaminates. Virus in the supernatant was pelleted by centrifugation at 25,000 rcf for 15 min at 4 °C, and concentrated in HBS (150 mM NaCl, 10 mM HEPES pH 7.4, and 0.02% NaN_3). Bromelain cleaved hemagglutinin (BHA) was generated by digestion of 30 mg of whole virus with 30mg of bromelain in 150 mM NaCl, 10 mM HEPES pH 7.8, 1 mM EDTA, 25 mM β-mercaptoethanol and 0.02% NaN_3. Viral particles were pelleted by ultracentrifugation, and additional digestions were performed twice thereafter. Soluble BHA was purified via size exclusion chromatography (GE-Superdex 200) in HBS, and concentrated via spin filtration. BHA purity was assessed by SDS-PAGE and native PAGE.

Hydrogen/Deuterium-Exchange (HDX)

Hydrogen deuterium exchange reactions of whole virus were initiated by diluting concentrated viral stocks into deuterated buffer: HBS, 85% D_20 (Cambridge Isotope Labs), for a final virus concentration of 2 mg/mL per reaction. HDX reactions of BHA at pH 7.4 were conducted in parallel under the exact conditions as whole virus, with a final BHA concentration of 100 µg/mL. Exchange reactions were quenched with equal volumes of ice-cold quench buffer (500 mM TCEP [tris(2-carboxyethyl) phosphine], 4 M Urea, 0.2% formic acid (FA)) containing 30 ug/mL porcine pepsin (Worthington Labs) for a final pH of 2.5. The BHA containing samples were digested on ice for 5 min, rapidly frozen in liquid nitrogen and stored at -80 °C until analysis. Whole virus samples were quenched, and digested with quench buffer and pepsin for 2 min on ice, and pelleted at 25,000 rcf at 4 °C for 3 min. After pelleting, the peptide containing supernatant was rapidly frozen in liquid nitrogen so that the total digestion time was 5 min to match the BHA samples. An undeuterated control was prepared in the sample buffer conditions as above, replacing the D_2O with Optima pure water (Fisher Scientific). A "zero" time point used to account for "IN" exchange during digestion, was prepared by diluting BHA or whole virus into quenched D_2O buffer, and digesting as above. Fully deuterated whole virus and BHA standards were prepared by denaturing samples at 80 °C in 30 mM DTT, 1.5 M Gdn-HCl, diluting into deuteration buffer, incubating overnight at 50 °C, and quenching as described above.

HDX of BHA at pH approaching activation

Exchanges were initiated in duplicate by diluting 10-15 µg of BHA into deuteration buffer (150 mM NaCl, 10 mM Na_3PO_4, 0.02% NaN_3, 85% D_2O) adjusted for a final pH* of 7.5, 6.5 and 5.9, where pH* is the measured value for each reaction in D_2O. Exchanges at pH* 5.6 were performed using 10 mM Citrate and 10 mM HEPES in place of Na_3PO_4 for optimal buffer capacity. All exchanges were performed at 22 °C, quenched with ice-cold quench buffer (200 mM TCEP, 0.2% FA), to a final pH of 2.5, digested with 30 µg of porcine pepsin for 5 min, frozen in liquid nitrogen and stored at -80°C until analysis. Since the intrinsic amide proton exchange (k_{ch}) rate is highly pH-dependent, and under our conditions the exchange is base-catalyzed ($k_{\mathrm{OH}}[\mathrm{OH}^-]$), incubation times were adjusted using the Arrhenius equation (1) below where E_a is the activation energy, A is the frequency factor, assuming constant temperature (23°C) and $k_{\mathrm{OH}}[\mathrm{OH}^-]$ for each pH condition.[48] The pH* 6.5 and 5.9 time points were adjusted to match the pH* 7.5 time points ranging from 10 sec to 30 min. The pH* 5.6 samples were adjusted to mimic pH* 7.5 incubation times of 3 sec, 10 sec, 20 sec, 30 sec, and 1 min. All reactions contained 0.5 µg/mL of the tetrapeptide, PPPI (AnaSpec), as an internal standard to probe the intrinsic amide exchange rate.[49] Data from each pH condition were adjusted in the time dimension to match the exchange for the PPPI (Figure S7).

$$k_{\mathrm{ch}} \sim k_{\mathrm{OH}}[\mathrm{OH}^-] = A\exp(-\mathrm{E}_a/RT)[\mathrm{OH}^-] \qquad (2.1)$$

HDX of pre- and post-fusion BHA

100 µg of concentrated pre-fusion BHA in HBS was acidified to pH 4.9 (with 2.5 mM Citrate pH 3.0), incubated for three hours at 22 °C, and reneutralized to pH 7.4, yielding an acid-triggered post-fusion BHA stock. A matched pre-fusion BHA stock was prepared similarly to the acid-triggered BHA stock; however, pre-fusion BHA was added after reneutralization to prevent activation. Hydrogen deuterium exchange was initiated by diluting 5 µg of pre-fusion or acid-triggered BHA into HBS (85% D_2O) for 3 sec, 1 min, 30 min and 20 hrs in duplicate. All samples along with undeuterated, “zero” and fully deuterated samples were quenched as described above.

Mass spectrometry

Undeuterated BHA peptides were identified by exact mass and MS/MS spectra on a Waters Synapt HDMS. Samples were thawed on ice for 5 min, manually injected onto a 100 µL loop and peptides were trapped onto a 1.7 µm 1x17 mm BEH reverse phase C_{18} (Waters) trap column at 200uL/min with 0.1% trifluoroacetic acid (TFA) buffer. The peptides were separated using a Hypersil 2.1 µm 1x50 mm C_{18} (Thermo Scientific) reverse phase column running a gradient of 10% to 50% solvent B for 10 min (solvent A: 0.05% TFA, 5% acetonitrile [ACN]; solvent B: 0.05% TFA, 80% ACN). The injection loop, lines and columns were kept on melting ice in an insulated container to minimize back exchange. Sample carryover was minimized by rapid cycling from 10% to 100% B, while the syringe, loop and trap column were washed by injecting a series of 10% formic acid, 80% methanol, 2:1 isopropanol-ACN, and 80% ACN.[68] For each resolved isotopic envelope, mass shifts were calculated by fitting to a tailored binomial distribution within the semi-automated HX-Express v2 software.[43] Experimental error was calculated using the standard deviation from duplicate measurements. For glycopeptides the average of all observable glycoforms is reported. Percent exchange was calculated, at each time point relative to the zero and fully deuterated standards.

Small Angle X-Ray Scattering (SAXS)

SAXS measurements were conducted on beam line 4-2 at the Stanford Synchrotron Radiation Laboratory implementing online size exclusion using a Precision S200 column (GE) as previously described.[31] Buffers for size exclusion were 150 mM NaCl, 0.02% NaN_3 and 0.25% n-dodecyl maltoside (n-DDM) with 20 mM HEPES 20 mM Citrate at pH 7.5 or pH 5.2. The flow from the column was passed through a capillary cell and 1 sec X-ray exposures were collected every 5 sec. Scattering data were scaled for the transmitted beam intensity at each exposure, and azimuthally averaged. R_G and I(0) for each frame were batch analyzed using autoRg[69], and frames with stable R_G values were merged in primus.[70] The particle distance distribution function [P(r)] plots were generated from GNOM[71] and used for *ab initio* shape reconstruction with DAMMIN.[35] The bead models were aligned with SUPCOMB13[72], and spatially filtered using DAMFILT.[73]

Liposome Preparation and Fluorescence Spectroscopy

Liposomes were prepared by mixing DOPC (dioleoyl-phosphatidylcholine) (Avanti Polar Lipids) and bovine brain Calbiochem® disialoganglioside GD_{1a} (Millipore) in a 100:5 molar ratio, and dried under nitrogen gas. The lipid films were re-suspended in liposome buffer (HBS with 10 mM Na-Citrate, and 25 mM sulforhodamine-B (Sigma-Aldrich)), extruded through a 100 nm polycarbonate membrane (Avanti Polar Lipids) after 10 liquid nitrogen freeze/thaw cycles, and purified over a PD-10 desalting column (GE Healthcare). 3 µg of BHA were bound to GD_{1a} liposomes in liposome buffer and the solution was acidified from a pH range of pH 6.25 to pH 5.0 for 4500 sec postacidification. The BHA-mediated SRB dequenching was monitored at 22 °C with excitation/emission at 565/585 nm on a Varian Cary Eclipse Fluorescence Spectrophotometer. Reported fluorescence intensities were normalized at a given time point after acidification, relative to an average non-acidified time point, and an averaged maximally dequenched intensity, generated upon liposome disruption with Triton-X100 (Sigma-Aldrich).

Dynamic Light Scattering

0.9 mg/mL of BHA was measured at pH 7.4 (150 mM NaCl, 10 mM HEPES pH 7.4), pH 6.0, pH 5.5 and pH 5.0 (150 mM NaCl, 10 mM HEPES, 10 mM Na-citrate) by collecting three sets of thirty acquisitions at 20 °C for 10 sec on a DynaPro Nanostar (Wyatt Technology) for each BHA pH condition. Dynamic light scattering was used to calculate the radius of hydration for BHA at various the pH conditions. The data was fit assuming a spherical model using the Wyatt Dynamics analysis software package and the error reported as standard deviation of the triplicate set of thirty acquisitions.

CHAPTER II FIGURES

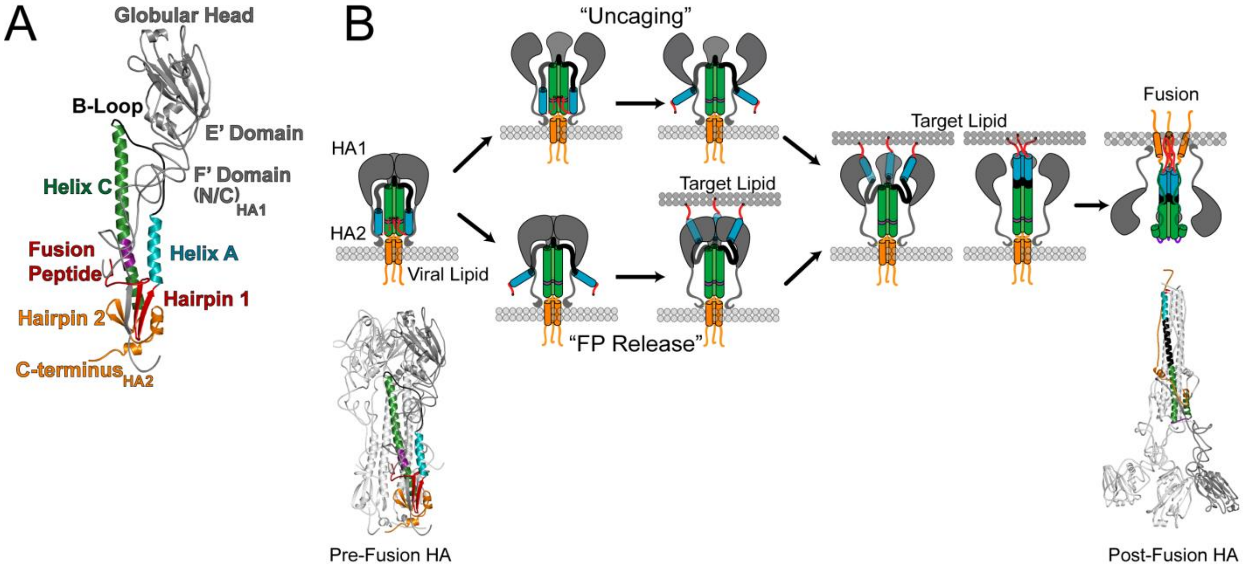

Figure 2.1 Structural Organization and Activation Models of Influenza HA. A) The structural organization of pre-fusion HA color-coded on one protomer for clarity (PDB 2HMG) [1]. HA1 residues grey; HA2 residues 1-39 red (1-20 fusion peptide, FP), 40-52 cyan, 53-69 black (B-loop), 70-105 and 113-123 green, 106-112 purple (kinked-loop), 124-175 orange. **B)** Two proposed HA activation schemes, colors of crystal structure and schematic subdomains related for clarity. In the top "Uncaging" model, pre-fusion HA initiates fusion via HA1 dissociation leading to release of FP and generating a membrane-active pre-hairpin intermediate; while the bottom "FP Release" model is initiated primarily via fusion peptide release which inserts into the target membrane followed by HA1 dissociation and pre-hairpin intermediate formation. Both models conclude with membrane fusion and post-fusion HA2 (PDB 1QU1, with HA1 lobes modeled from 2HMG). [1,3]

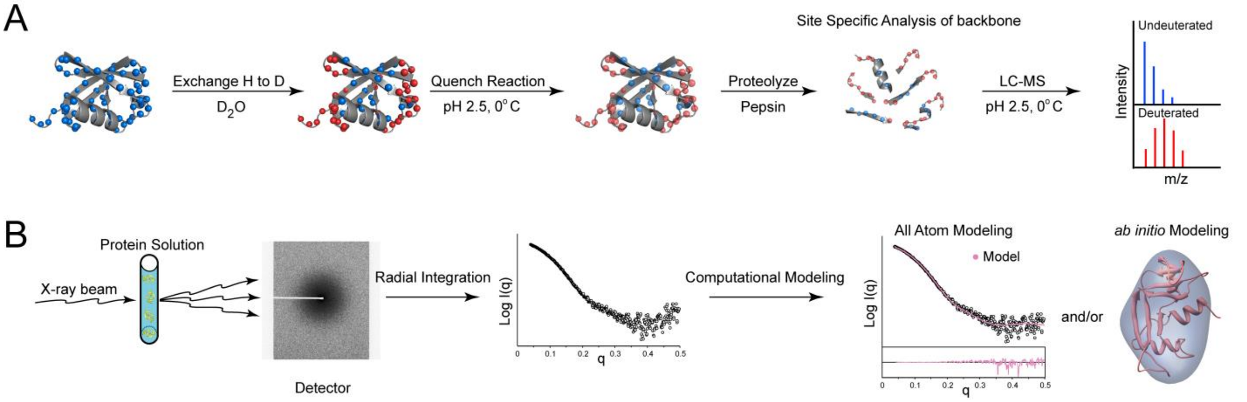

Figure 2.2 Solution Based Approaches for Protein Characterization A) Hydrogen-Deuterium Exchange Mass Spectrometry (HDX-MS). Exchange of backbone amide protons for deuterons is initiation by incubating a protein in deuterated buffer for various amounts of time, reaction is quenched at pH 2.5 and on ice, samples are denatured and digested, and mass shifts are analyzed by mass spectrometry. **B) Small Angle X-ray Scattering (SAXS).** Biological macromolecules in solution are irradiated with a monochromatic X-ray beam, which generate a characteristic scattering pattern. Computational methods such as all atom modeling can be used to compare high resolution models and/or structures relative to the solution-phase data or *ab initio* shape reconstruction can be used to generate low resolution morphological information.

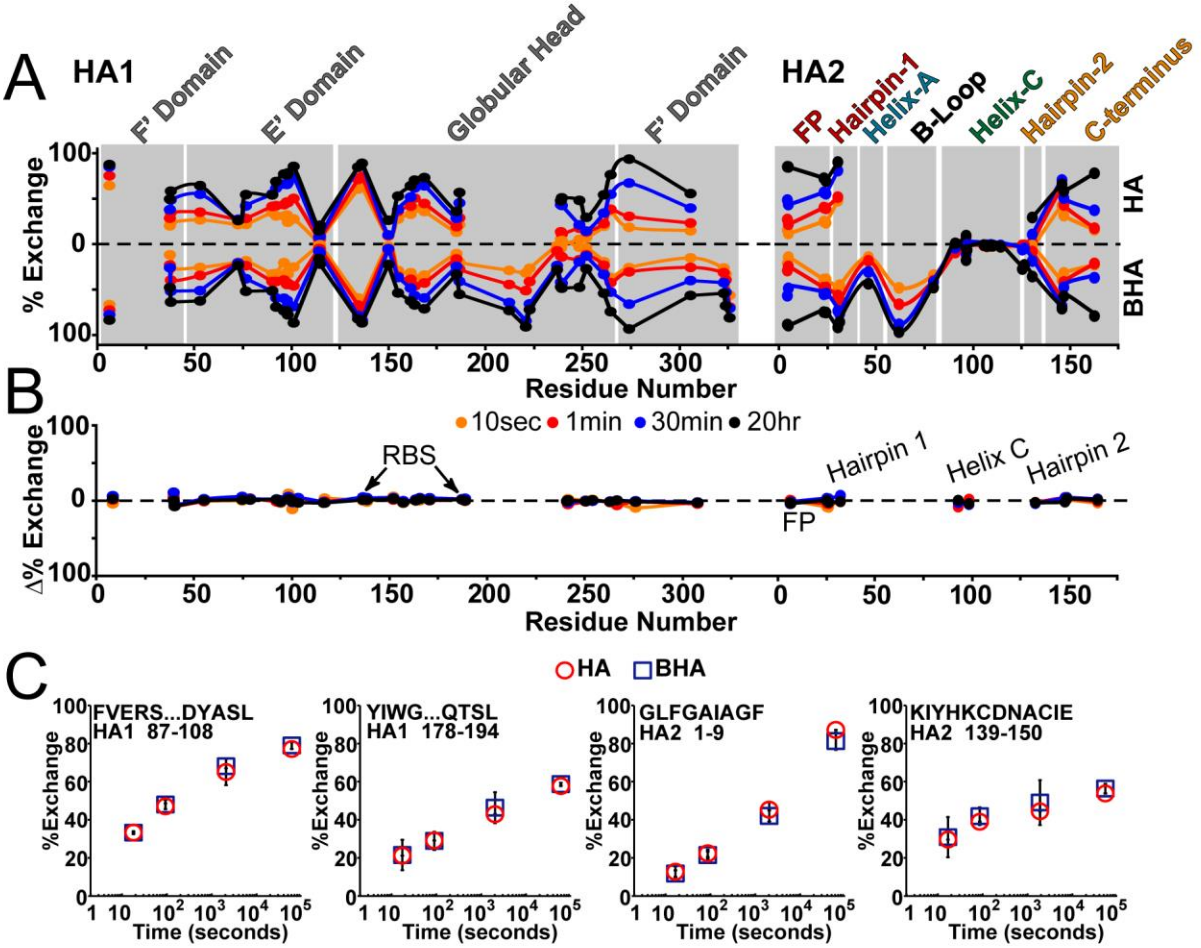

Figure 2.3 HDX Comparison of X31 H3N2 Virion-associated HA vs BHA. A) Percent exchange profiles at pH* 7.5 for all observable peptides in HA1 and HA2 for intact HA in viral membrane (top) and BHA (bottom), subdomain colors pertain to Figure 2.2A and throughout the manuscript. Data for each peptide is plotted at the midpoint of the primary sequence for each time point. Lines connecting each point indicate continuous sequence coverage while discontinuity in the lines reflects missing sequence coverage. **B)** HDX difference profiles show no significant differences between BHA and full-length HA on virus. **C)** Individual exchange profiles of representative HA1 and HA2 peptides show no difference in membrane-distal and membrane-proximal regions of full-length HA (red circles) versus BHA (blue squares). Error bars are the calculated standard error from duplicate measurements.

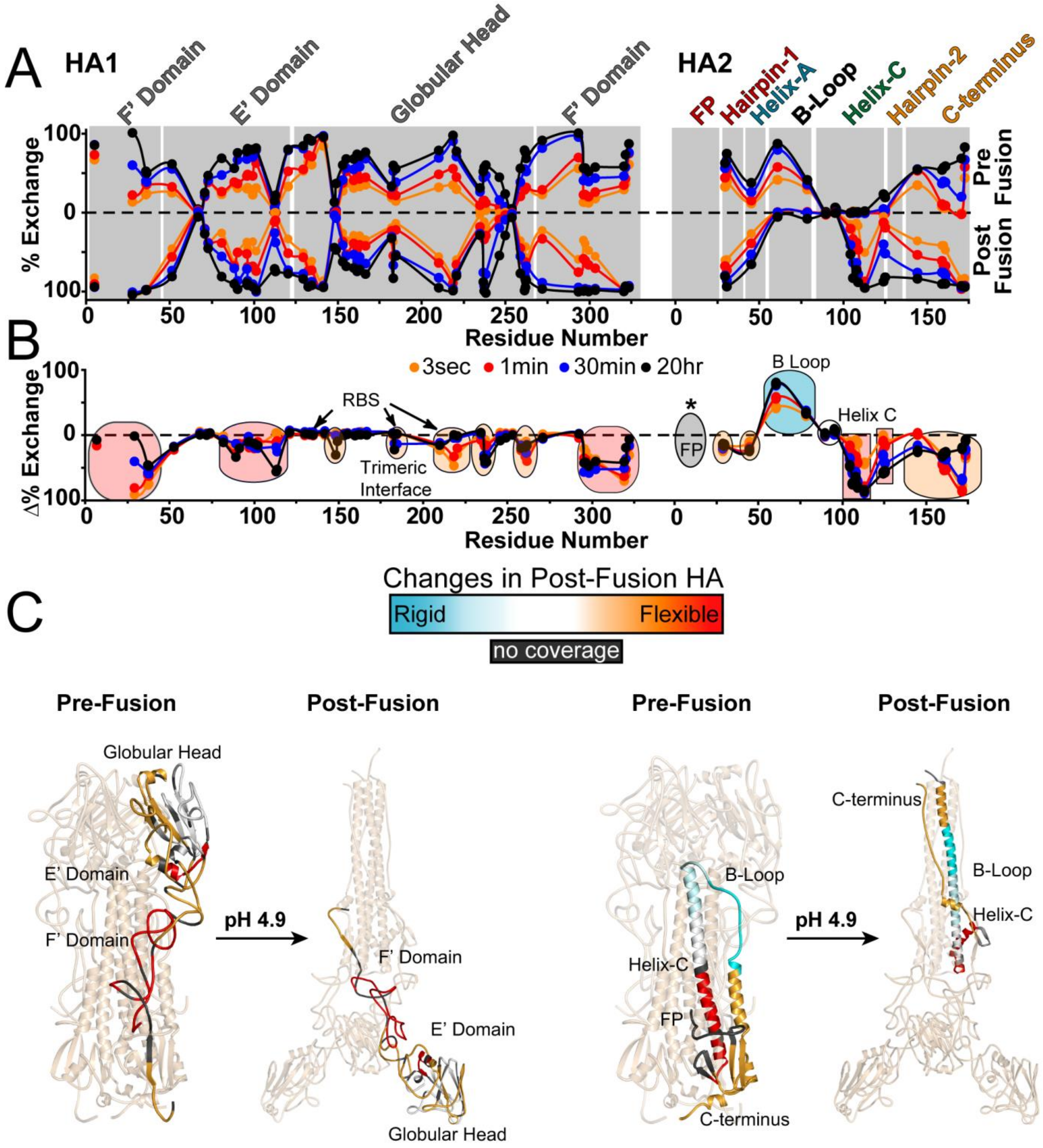

Figure 2.4 HDX Comparison of Pre-fusion and Post-fusion BHA A) Butterfly plots comparing exchange profiles of pre-fusion (top) versus post-fusion (bottom) BHA after 3 sec (orange), 1 min (red), 30 min (blue) and 20 hrs (black) of exchange at pH* 7.5. The line connecting each point indicates continuous sequence coverage, while discontinuity in the lines reflects missing sequence coverage. Structural organization corresponds to Figure 2.2A throughout the text. **B)** Exchange differences plotted above or below the axis correspond to regions of BHA that gain or lose protection in post-fusion BHA, respectively. **C)** Areas in post-fusion BHA that become highly flexible (red), moderately flexible (orange) or more protected (cyan) relative to the pre-fusion conformation, are mapped onto the pre- and post-fusion trimer, 2HMG. HA1 lobes were modeled onto 1QU1 to reflect the post-fusion state (PDB: 2HMG and 1QU1).[1,3] Individual exchange plots with error bars are shown in Figure S2.5.

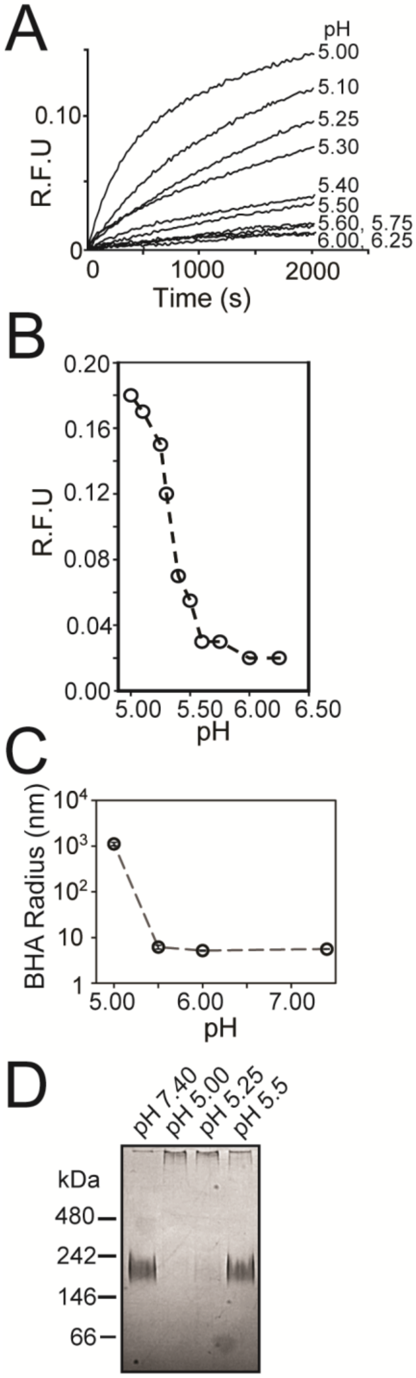

Figure 2.5 BHA Induced Liposome Dequenching and Native PAGE Near Fusion. A) Fluorescence monitoring BHA induced pH-dependent sulforhodamine-B liposome leakage at 22 °C **B)** Fluorescence intensity at the final time point for each pH show minimal leakage between pH 6.25 and pH 5.5 and a major increase in activity between 5.5 and 5.0. **C)** Radius of hydration of BHA at pH 7.4, 6.0, 5.5, 5.0 by dynamic light scattering at 20 °C. Error bars represent the standard deviation from more than 3 experiments. **D)** pH-dependent aggregation of BHA at 22 °C in the absence of detergent visualized by Native PAGE indicates aggregation does not occur at pH 5.5 or higher.

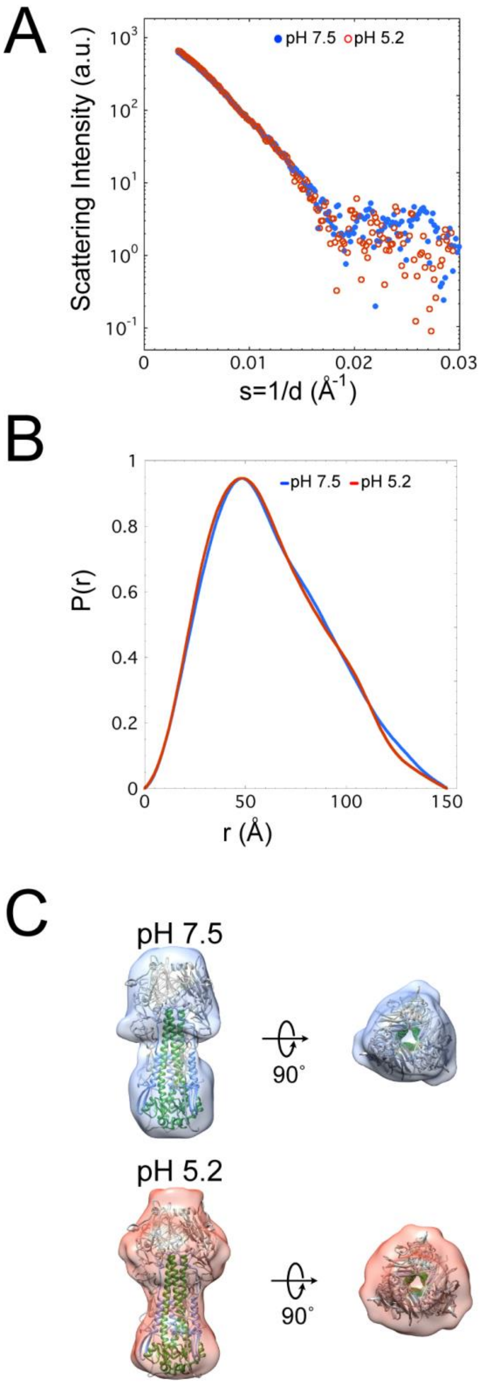

Figure 2.6 Small Angle X-ray Scattering (SAXS) of BHA at pH 7.5 and pH 5.2. A) SAXS patterns for BHA eluted from an in-line size exclusion chromatography column equilibrated with 150 mM NaCl, 20mM HEPES, 20 mM Na-citrate, 0.25% n-dodecylmaltoside, 0.02% NaN_3 at 22 °C where the blue and red dots represent buffer conditions for pH 7.5 and pH 5.2 respectively. **B)** Pairwise mass distribution (P(r)) plots for BHA at pH 7.5 (blue) and pH 5.2 (red). DAMMIN reconstructions of BHA at pH 7.5 (blue) and pH 5.2 (red).

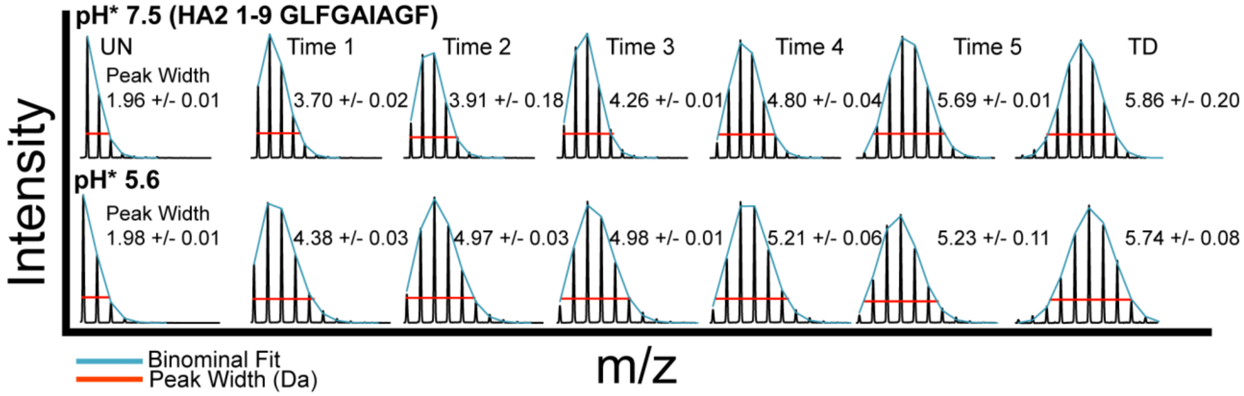

Figure 2.7 Peak Width Analysis of Raw Spectral HDX Data for the Fusion Peptide. Average peak width at 20% peak height with errors from duplicate measurements are shown for the two extreme pH* conditions, with pH* 7.5 on top and pH* 5.6 on bottom. Mass to charge (m/z) on x-axis relative to the intensity shown on the y-axis. pH* 5.6 envelopes do not show extensive peak width broadening as observed in Figure S2.4.

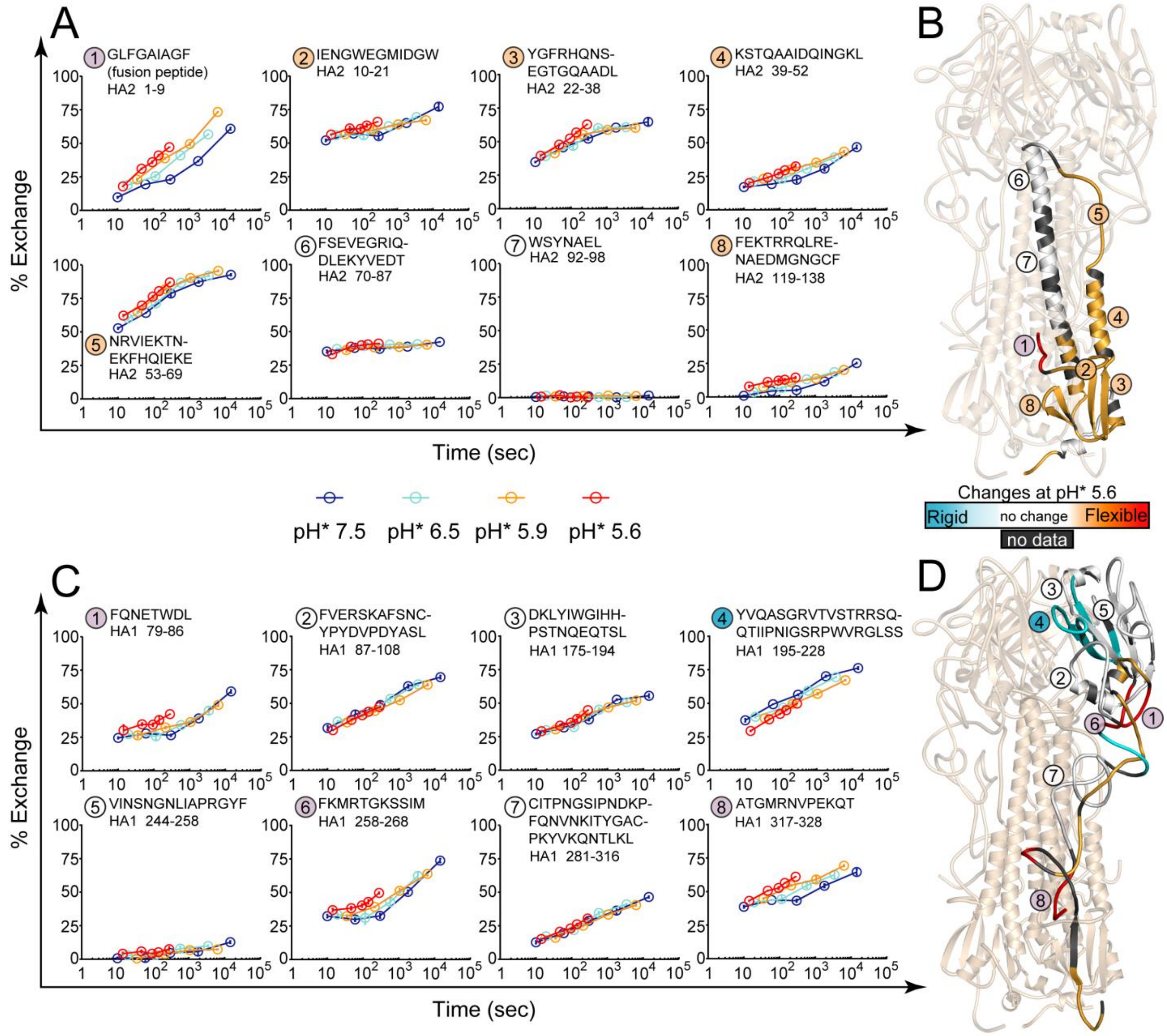

Figure 2.8 Dynamic Changes in BHA Upon Acidification. A) Exchange profiles of selected HA2 peptide shown at pH* 7.5 (blue dots), 6.5 (cyan dots), 5.9 (orange dots) and 5.6 (red dots), with error bars representing the standard error from duplicate measurements. Acidic HDX time points were scaled relative to pH* 7.5 using the fits of the internal standard (Figure S2.7). The exchange profiles for all individual peptides are shown in Figure S2.8. **B)** Corresponding HA2 peptides mapped onto the HA2 domain of the pre-fusion BHA structure (PDB: 2HMG), where regions of increased dynamics (red) and increased protection (blue) at pH* 5.6. No differences indicated by white, and no coverage is grey. **C)** Exchange profiles for selected HA1 peptides represented as in A). **D)** Corresponding HA1 peptides mapped onto the HA1 domain of pre-fusion BHA structure (PDB: 2HMG) represented as in B).

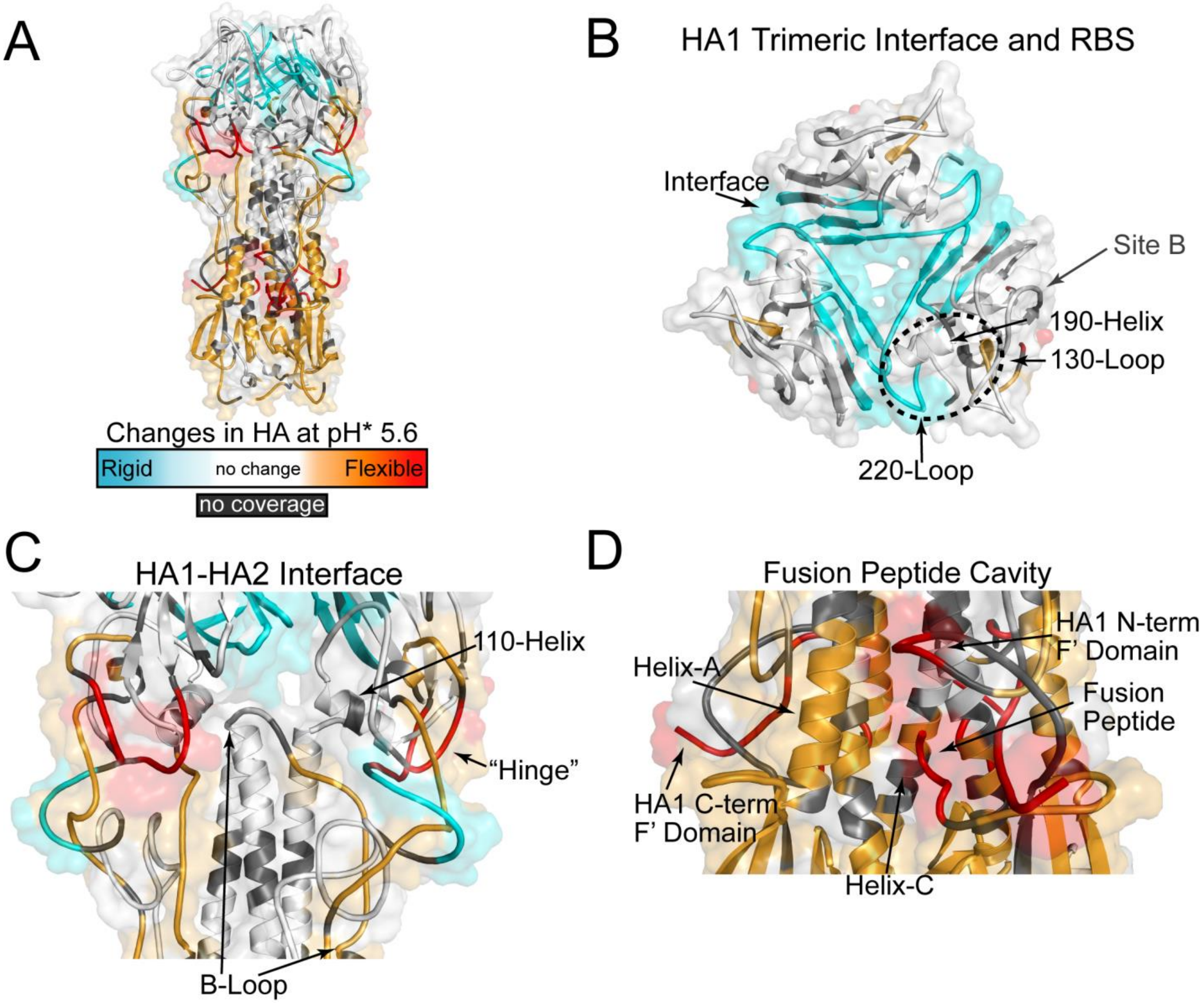

Figure 2.9 Regions of pH-Dependent Changes in BHA. A) All peptides are mapped on the trimeric pre-fusion BHA structure (PDB:2HMG) where peptides that are more dynamic at pH* 5.6 are red, peptides that are more protected are cyan, white indicates no change, and grey is no coverage. **B)** Top-view of the HA1 globular head. The dashes highlight the receptor binding site (RBS) composed of the 130-Loop, 190-Helix and 220-Loop, adjacent to the HA1-HA1 trimeric interface and the antigenic Site B is indicated in grey. **C)** Close-up view of the fusion peptide cavity with the HA1 F' Domain and HA2 elements highlighted. **D)** Close-up view of the HA1-HA2 interface, where the HA1 110-Helix and "hinge" peptides from the E' Domain, and N- and C-terminial regions of the HA2 B-loop are highlighted.

CHAPTER II REFERENCES

1. Wilson, I.A., Skehel, J.J. & Wiley, D.C. Structure of the haemagglutinin membrane glycoprotein of influenza virus at 3 A resolution. *Nature* **289**, 366-73 (1981).
2. Bullough, P.A., Hughson, F.M., Skehel, J.J. & Wiley, D.C. Structure of influenza haemagglutinin at the pH of membrane fusion. *Nature* **371**, 37-43 (1994).
3. Chen, J., Skehel, J.J. & Wiley, D.C. N- and C-terminal residues combine in the fusion-pH influenza hemagglutinin HA(2) subunit to form an N cap that terminates the triple-stranded coiled coil. *PNAS* **96**, 8967-72 (1999).
4. Konermann, L., Vahidi, S. & Sowole, M.A. Mass spectrometry methods for studying structure and dynamics of biological macromolecules. *Anal Chem* **86**, 213-32 (2014).
5. Orban, T., Gupta, S., Palczewski, K. & Chance, M.R. Visualizing water molecules in transmembrane proteins using radiolytic labeling methods. *Biochemistry* **49**, 827-34 (2010).
6. Garcia, N.K., Guttman, M., Ebner, J.L. & Lee, K.K. Dynamic changes during acid-induced activation of influenza hemagglutinin. *Structure* **23**, 665-676 (2015).
7. Lim, X.X., Chandramohan, A. & Anand, G.S. Temperature-dependent Conformational Dynamics in Whole Dengue Viral Particles by Hydrogen/Deuterium Exchange Mass Spectrometry. . *Presentation given at: 63rd American Society for Mass Spectrometry. 2015 May 31-June 4; St. Louis, Missouri.* (2015).
8. Xu, G. & Chance, M.R. Radiolytic modification and reactivity of amino acid residues serving as structural probes for protein footprinting. *Anal Chem* **77**, 4549-55 (2005).
9. Konermann, L. & Pan, Y. Exploring membrane protein structural features by oxidative labeling and mass spectrometry. *Expert Rev Proteomics* **9**, 497-504 (2012).
10. Gau, B.C., Sharp, J.S., Rempel, D.L. & Gross, M.L. Fast photochemical oxidation of protein footprints faster than protein unfolding. *Anal Chem* **81**, 6563-71 (2009).

11. Iacob, R.E., Murphy, J.P., 3rd & Engen, J.R. Ion mobility adds an additional dimension to mass spectrometric analysis of solution-phase hydrogen/deuterium exchange. *Rapid Commun Mass Spectrom* **22**, 2898-904 (2008).

12. Englander, S.W. Hydrogen exchange and mass spectrometry: A historical perspective. *J Am Soc Mass Spectrom* **17**, 1481-9 (2006).

13. Kiselar, J.G. & Chance, M.R. Future directions of structural mass spectrometry using hydroxyl radical footprinting. *J Mass Spectrom* **45**, 1373-82 (2010).

14. Coales, S.J., Tuske, S.J., Tomasso, J.C. & Hamuro, Y. Epitope mapping by amide hydrogen/deuterium exchange coupled with immobilization of antibody, on line proteolysis, liquid chromatography and mass spectrometry. *Rapid Communications in Mass Spectrometry* **23**, 639-647 (2009).

15. Jones, L.M., J, B.S., J, A.C. & Gross, M.L. Fast photochemical oxidation of proteins for epitope mapping. *Anal Chem* **83**, 7657-61 (2011).

16. Davenport, T.M. et al. Isolate-specific differences in the conformational dynamics and antigenicity of HIV-1 gp120. *J Virol* **87**, 10855-73 (2013).

17. Bale, S. et al. Ebola virus glycoprotein needs an additional trigger, beyond proteolytic priming for membrane fusion. *PLoS Negl Trop Dis* **5**, e1395 (2011).

18. Bale, S. et al. Structural basis for differential neutralization of ebolaviruses. *Viruses* **4**, 447-70 (2012).

19. Marcsisin, S.R. & Engen, J.R. Hydrogen exchange mass spectrometry: what is it and what can it tell us? *Analytical and bioanalytical chemistry* **397**, 967-972 (2010).

20. Hamuro, Y., Coales, S.J., Molnar, K.S., Tuske, S.J. & Morrow, J.A. Specificity of immobilized porcine pepsin in H/D exchange compatible conditions. *Rapid Commun Mass Spectrom* **22**, 1041-6 (2008).

21. Huang, R.Y. & Hudgens, J.W. Effects of desialylation on human alpha1-acid glycoprotein-ligand interactions. *Biochemistry* **52**, 7127-36 (2013).

22. Houde, D., Arndt, J., Domeier, W., Berkowitz, S. & Engen, J.R. Characterization of IgG1 Conformation and Conformational Dynamics by Hydrogen/Deuterium Exchange Mass Spectrometry. *Anal Chem* **81**, 5966 (2009).

23. Varki, A. et al. *Essentials of Glycobiology*, (Cold Spring Harbor Laboratory Press, Plainview, NY, 2009).

24. Iacob, R.E. & Engen, J.R. Hydrogen exchange mass spectrometry: are we out of the quicksand? *J Am Soc Mass Spectrom* **23**, 1003-10 (2012).

25. Marcsisin, S.R. & Engen, J.R. Hydrogen exchange mass spectrometry: what is it and what can it tell us? *Anal Bioanal Chem* **397**, 967-72 (2010).

26. Putnam, C.D., Hammel, M., Hura, G.L. & Tainer, J.A. X-ray solution scattering (SAXS) combined with crystallography and computation: defining accurate macromolecular structures, conformations and assemblies in solution. *Q Rev Biophys* **40**, 191-285 (2007).

27. Jacques, D.A. & Trewhella, J. Small-angle scattering for structural biology-Expanding the frontier while avoiding the pitfalls. *Protein Science* **19**, 642-657 (2010).

28. Mylonas, E. & Svergun, D.I. *Journal of Applied Crystallography* **40**, S245-S249 (2007).

29. Fischer, H., de Oliveira Neto, M., Napolitano, H.B., Craievich, A.F. & Polikarpov, I. The molecular weight of proteins in solution can be determined from a single SAXS measurement on a relative scale. *J. Appl. Cryst.* **43**, 101-109 (2010).

30. Petoukhov, M.V. & Svergun, D.I. Analysis of X-ray and neutron scattering from biomolecular solutions. *Curr Opin Struc Biol* **17**, 562-71 (2007).

31. Guttman, M., Weinkam, P., Sali, A. & Lee, K.K. All-atom ensemble modeling to analyze small-angle x-ray scattering of glycosylated proteins. *Structure* **21**, 321-31 (2013).

32. Guttman, M. & Lee, K.K. A functional interaction between gp41 and gp120 is observed for monomeric but not oligomeric, uncleaved HIV-1 Env gp140. *J Virol* **87**, 11462-75 (2013).

33. Guttman, M., Kahn, M., Garcia, N.K., Hu, S.L. & Lee, K.K. Solution structure, conformational dynamics, and CD4-induced activation in full-length, glycosylated, monomeric HIV gp120. *J Virol* **86**, 8750-64 (2012).

34. Hammel, M. et al. Solution structure of human and bovine beta(2)-glycoprotein I revealed by small-angle X-ray scattering. *J Mol Biol* **321**, 85-97 (2002).

35. Svergun, D.I. Restoring low resolution structure of biological macromolecules from solution scattering using simulated annealing. *Biophys J* **76**, 2879-86 (1999).

36. Svergun, D.I. & Koch, M.H. Advances in structure analysis using small-angle scattering in solution. *Curr Opin Struct Biol* **12**, 654-60 (2002).

37. Svergun, D.I., Petoukhov, M.V. & Koch, M.H. Determination of domain structure of proteins from X-ray solution scattering. *Biophys J* **80**, 2946-53 (2001).

38. Forster, F. et al. Integration of small-angle X-ray scattering data into structural modeling of proteins and their assemblies. *J Mol Biol* **382**, 1089-106 (2008).

39. Petoukhov, M.V., Eady, N.A.J., Brown, K.A. & Svergun, D.I. Addition of missing loops and domains to protein models by X-ray solution scattering. *Biophys J* **83**, 3113-3125 (2002).

40. Hammel, M. Validation of macromolecular flexibility in solution by small-angle X-ray scattering (SAXS). *Eur Biophys J* **41**, 789-99 (2012).

41. Weinkam, P., Pons, J. & Sali, A. Structure-based model of allostery predicts coupling between distant sites. *PNAS* **109**, 4875-80 (2012).

42. Schneidman-Duhovny, D., Hammel, M. & Sali, A. FoXS: a web server for rapid computation and fitting of SAXS profiles. *Nucleic Acids Res* **38**, W540-4 (2010).

43. Guttman, M., Weis, D.D., Engen, J.R. & Lee, K.K. Analysis of overlapped and noisy hydrogen/deuterium exchange mass spectra. *J Am Soc Mass Spectrom* **24**, 1906-12 (2013).

44. Skehel, J.J. et al. Changes in the conformation of influenza virus hemagglutinin at the pH optimum of virus-mediated membrane fusion. *PNAS* **79**, 968-72 (1982).

45. Park, H.E., Gruenke, J.A. & White, J.M. Leash in the groove mechanism of membrane fusion. *Nat Struct Biol* **10**, 1048-53 (2003).

46. Bizebard, T. et al. Structure of influenza virus haemagglutinin complexed with a neutralizing antibody. *Nature* **376**, 92-4 (1995).

47. Bai, Y., Milne, J.S., Mayne, L. & Englander, S.W. Primary structure effects on peptide group hydrogen exchange. *Proteins* **17**, 75-86 (1993).

48. Coales, S.J. et al. Expansion of time window for mass spectrometric measurement of amide hydrogen/deuterium exchange reactions. *Rapid Commun Mass Spectrom* **24**, 3585-92 (2010).

49. Zhang, Z., Zhang, A. & Xiao, G. Improved protein hydrogen/deuterium exchange mass spectrometry platform with fully automated data processing. *Anal Chem* **84**, 4942-9 (2012).

50. White, J.M., Delos, S.E., Brecher, M. & Schornberg, K. Structures and mechanisms of viral membrane fusion proteins: multiple variations on a common theme. *Crit Rev Biochem Mol Biol* **43**, 189-219 (2008).

51. Remeta, D.P. et al. Acid-induced changes in thermal stability and fusion activity of influenza hemagglutinin. *Biochemistry* **41**, 2044-54 (2002).

52. Krumbiegel, M., Herrmann, A. & Blumenthal, R. Kinetics of the low pH-induced conformational changes and fusogenic activity of influenza hemagglutinin. *Biophys J* **67**, 2355-60 (1994).

53. Doms, R.W., Helenius, A. & White, J. Membrane fusion activity of the influenza virus hemagglutinin. The low pH-induced conformational change. *J Biol Chem* **260**, 2973-81 (1985).

54. White, J.M. & Wilson, I.A. Anti-peptide antibodies detect steps in a protein conformational change: low-pH activation of the influenza virus hemagglutinin. *J Cell Biol* **105**, 2887-96 (1987).

55. Kemble, G.W., Bodian, D.L., Rose, J., Wilson, I.A. & White, J.M. Intermonomer disulfide bonds impair the fusion activity of influenza virus hemagglutinin. *J Virol* **66**, 4940-50 (1992).

56. Chen, J. et al. A soluble domain of the membrane-anchoring chain of influenza virus hemagglutinin (HA2) folds in Escherichia coli into the low-pH-induced conformation. *PNAS* **92**, 12205-9 (1995).

57. Fontana, J., Cardone, G., Heymann, J.B., Winkler, D.C. & Steven, A.C. Structural changes in Influenza virus at low pH characterized by cryo-electron tomography. in *J Virol*, Vol. 86 2919-29 (United States, 2012).

58. Mair, C.M., Ludwig, K., Herrmann, A. & Sieben, C. Receptor binding and pH stability - how influenza A virus hemagglutinin affects host-specific virus infection. *Biochim Biophys Acta* **1838**, 1153-68 (2014).

59. Weis, W.I. et al. The structure of a membrane fusion mutant of the influenza virus haemagglutinin. *EMBO J* **9**, 17-24 (1990).

60. Rachakonda, P.S. et al. The relevance of salt bridges for the stability of the influenza virus hemagglutinin. *FASEB J* **21**, 995-1002 (2007).

61. DuBois, R.M. et al. Acid stability of the hemagglutinin protein regulates H5N1 influenza virus pathogenicity. *PLoS Pathog* **7**, e1002398 (2011).

62. Xu, R. & Wilson, I.A. Structural characterization of an early fusion intermediate of influenza virus hemagglutinin. *J Virol* **85**, 5172-82 (2011).

63. Huang, Q., Opitz, R., Knapp, E.W. & Herrmann, A. Protonation and stability of the globular domain of influenza virus hemagglutinin. *Biophys J* **82**, 1050-8 (2002).

64. Bentz, J. Membrane fusion mediated by coiled coils: a hypothesis. *Biophys J* **78**, 886-900 (2000).

65. Lee, K.K. Architecture of a nascent viral fusion pore. *EMBO J* **29**, 1299-311 (2010).

66. Fontana, J. & Steven, A.C. At low pH, influenza virus matrix protein M1 undergoes a conformational change prior to dissociating from the membrane. *J Virol* **87**, 5621-8 (2013).

67. Bereszczak, J.Z., Watts, N.R., Wingfield, P.T., Steven, A.C. & Heck, A.J. Assessment of differences in the conformational flexibility of hepatitis B virus core-antigen and e-antigen by hydrogen deuterium exchange-mass spectrometry. *Protein Sci* **23**, 884-96 (2014).

68. Fang, J., Rand, K.D., Beuning, P.J. & Engen, J.R. False EX1 signatures caused by sample carryover during HX MS analyses. *Int J Mass Spectrom* **302**, 19-25 (2011).

69. Petoukhov, M.V., Konarev, P.V., Kikhney, A.G. & Svergun, D.I. ATSAS 2.1 - towards automated and web-supported small-angle scattering data analysis. *J. Appl. Cryst.* **40**, s223-s228 (2007).

70. Konarev, P.V., Volkov, V.V., Sokolova, A.V., Koch, M.H.J. & Svergun, D.I. PRIMUS: a Windows PC-based system for small-angle scattering data analysis. *J App Cryst* **36**, 1277-1282 (2003).

71. Svergun, D.I. Determination of the regularization parameter in indirect-transform methods using perceptual criteria. *J App Cryst* **25**, 495-503 (1992).

72. Kozin, M.B. & Svergun, D.I. Automated matching of high- and low-resolution structural models. *J App Cryst* **34**, 33-41 (2001).

73. Volkov, V.V. & Svergun, D.I. Uniqueness of ab-initio shape determination in small-angle scattering. *J. Appl. Cryst.* **36**, 860-864 (2003).

CHAPTER III: The Different Impacts of Stem Directed Inhibitors on the Conformational Dynamics of Influenza Hemagglutinin

INTRODUCTION

The high mutation rate of RNA viruses, such as influenza, imparts large genetic diversity within their surface antigens, which helps the virus evade the host antibody response, which in HA is predominately focused in the hypervariable HA1 head.[1-3] Recent isolation and co-crystallization of a number of broadly neutralizing antibodies (bnabs) with various HA isolates show bnabs can heterosubtypically bind the functionally conserved sequences at the HA2 fusion stem, and inspire hope for the development of a broad-spectrum vaccine.[4-10]

Although several of the stem directed bnabs have been isolated *in vitro* by phage display, some stem-directed bnabs such as FI6v3, which is capable of binding 11 of 16 subtypes, have been isolated from the immortalized B-cells of plasma donors.[4] Furthermore, examples of naturally produced stem targeting bnabs have been reported in humans either through vaccination[11] or during the course of infection[9,12,13], some of which display cross-reactivity to HAs from both groups .

Despite some minor overlap between epitopes, most of the characterized bnabs are group specific, generally targeting more group-1 isolates than group-2. The group-1 specific bnabs such as CR6261[5] and F10[8] bind the higher portion of the fusion domain via the heavy chain complementary determining region (CDR), while the paratopes of group-2 bnabs such as CR8020[6], utilize the CDR of both the heavy and light chain to bind closer to the base of the trimer. Distinct group-specific features of each epitope, such as the incorporation of an N-linked glycan in group-2 isolates (H3N2), and the extra half-turn at end of the short helix in group-1 isolates (H1N1) may be responsible for the limited cross-reactivity of most isolated bnabs. Recent reports of clinically relevant pan-inhibitory bnabs such as FI6v3 may accommodate the diversity of viral subtypes using both the heavy and light chain CDRs to recognize the fusion stem and circumvent the group-specific glycan near the epitope.[4,7]

Since pre-fusion HA is in a metastable conformation at neutral pH and undergoes a large structural transition to the ground state conformation in the presence of low pH, inhibitors that prevent these critical steps during viral entry likely stabilize the pre-fusion state.[14-20] It is hypothesized that such ligands stabilize the pre-fusion conformation by preventing the extrusion of the fusion peptide from the cavity at the base of the trimer and the reorientation of the short helix into the post-fusion conformation at low pH. However, only a few examples of bnabs that bind HAs from both groups have been isolated to date, and though these high resolution structures have been useful for recognizing functionally conserved and neutralization sensitive regions within HA2, it is still unclear whether antibody binding is localized to identical epitopes in both isolates, or if there are isolate specific effects that may manifest throughout the trimer.[4,7,9,21,22] Identifying these highly conserved and functionally important regions within HA2, which bnabs target has also assisted in the *de novo* computational design of small protein inhibitors such as HB36, which binds HA2 with high affinity.[23,24] HB36 and its progenitors were developed by first identifying binding commonalities between the two group-1 specific highly potent bnabs CR6261 and F10 in complex with HA, which both target the hydrophobic groove of the short helix and C-terminal fusion peptide, and then computationally docking disembodied side chains to this HA2 region.[23,24] Through iterative energy minimization and identification of scaffolds that could facilitate high affinity interactions early constructs of HB36 was created.

The crystal structures of early HB36 progenitors show that the small helical protein can accommodate a similar binding interface with almost identical rotamers as the bnabs from which it was developed, specifically the aromatic stacking of a Phe (HB36) and Trp21 (HA2).[23,24] Through collaboration between the Baker lab and Fuller lab, HB36.6 was optimized via yeast display and has been shown to have a dose-dependent protective effect in mice and ferrets that were challenged with lethal doses of A/California/07/2009 (H1N1) (Treants M.E. et al. manuscript in submission). While these molecules appear to have clinically promising effects, it is unknown at this time if HB36.6 elicits similar effects on HA as their lead molecules, F10 or CR6261, or similar stem directed bnabs such as FI6v3. In addition to bnabs, small molecules that prevent fusion have also been enticing topics of HA research. Previous crystal structures of group-2 HAs in complex with small molecule fusion inhibitor *tert*-butylhydroquinone (TBHQ) show that the interaction is formed at the interface between the short helix and long helix core from a neighboring protomer, which further supports this region as a key target for fusion inhibition.[25]

Here we use hydrogen-deuterium exchange, mass spectrometry (HDX-MS) to characterize the solution-phase conformational dynamics the complex of bnab, FI6v3 and the small protein inhibitor HB36.6 with the soluble bromelain cleaved HA ectodomain (BHA) of two isolates from each group; A/Puerto Rico/8/1934 (H1N1) and egg adapted X-31 A/Aichi/2/1968 (H3N2). We also use HDX-MS to study the impact of TBHQ binding to the H3 isolate in order to identify the structural determinants of fusion inhibition and neutralization. We report that the effects of binding FI6v3 antibody fab fragments for both isolates are localized to the epitope. While HB36.6 also locally stabilizes a portion of its binding site, it has additional long-range effects, including disorganization of the fusion peptide and the B-loop peptide near the H1-HA2 interface. Similarly, TBHQ stabilizes its corresponding binding site while also inducing minor destabilization within the fusion peptide.

RESULTS

Stem Targeting Proteins Prevent the pH-dependent Aggregation of Soluble HA

The pH-dependent conformational change of BHA in the absence of target membranes (Skehel 1982) forms large "rosette" aggregates when exposed to mildly acidic conditions(pH 5.25-5.0). In chapter II we have qualitatively shown that due to an increase in the hydrodynamic radius (R_H), acid-triggered H3 BHA does not enter the native PAGE matrix (Figure 2.4 C and D). Since native PAGE requires each sample to retain its native protein fold during sample staining, unfortunately, it is difficult to accurately quantify the extent of aggregation. The microheterogeneity intrinsic to highly glycosylated proteins, imparts an additional layer of complication to the analysis, thus this method is simply a qualitative assessment of low pH induced aggregation due to the acid triggered conformational change required for membrane fusion. Here aggregation was used as a surrogate for the structural rearrangement of BHA at low pH with native PAGE and DLS to assess the aggregation propensity of acid-treated unliganded BHA from H1 and H3 influenza virus, H1-FI6v3, H3-FI6v3 and H1-HB36.6 complexes, relative to a pre-fusion reference (Figure 3.1 and Table 3.1). At neutral pH and following incubation at pH 4.9, both H3-FI6v3 and H1-FI6v3 complexes entered the native PAGE matrix similarly, suggesting that the FI6v3 complexes retained its pre-fusion conformation (Figure 3.1). When visualized by native PAGE, H1-HB36.6was also found to prevent aggregation of BHA after incubation at pH 4.9 (Figure 3.1 B), indicating that the small protein, like FI6v3, also appears to prevent the structural rearrangements necessary for membrane fusion.

Due to the metastability of the pre-fusion state, HA is also susceptible to irreversible triggering to post-fusion HA when exposed to chaotropes and high heat. Using temperature induced aggregation, the thermal melting temperatures (T_m) of aggregation-onset for the unliganded BHAs, H1-FI6v3, H3-FI6v3 and H1-HB36.6 complexes was measured and reported in Table 3.1. The T_m of both unliganded BHAs was 63.7°C and 63.5°C for H3 and H1, respectively. Though these measurements were not performed in duplicate, the experimental values are consistent with values reported by circular dichroism, and fluorescence melting assays for several different HA isolates in the pre-fusion state.[18,25] Furthermore, the T_m of the FI6v3-BHA complexes were shifted to 75.5°C and 73.8°C for H3-FI6v3 and H1-FI6v3, respectively. HB36.6 bound to H1 BHA shifted the T_m modestly from 63.7°C to 66.5°C. The large shift in T_m suggests that FI6v3 prevents the pH-dependent conformational change of both HAs by stabilizing the pre-fusion conformation. Although the change in T_m for the H1-HB36.6complex was not as dramatic as the antigen-fab system, it appears that HB36.6 also stabilizes BHA but not to the same extent as FI6v3.

Biophysical Characterization of HA Bound to Stem Targeting Protein Inhibitors

The BHA trimer presents three binding sites for each stem-directed ligand examined in this chapter. To ensure a 3:1 binding event between each protein ligand and trimeric BHA, multi-angle light scattering (MALS) and DLS online with size exclusion chromatography (SEC) was used to determine the stoichiometry and radius of hydration (R_H) of the unliganded BHAs, H3-FI6v3, H1-FI6v3 and H1-HB36.6 complexes (Table 3.1 and Figure 3.2 A,D,G). The experimentally determined molecular weight of each analyte was within 2% of accuracy of the calculated molecular weight, which includes the average carbohydrate composition of each BHA subtype. The R_H of the unliganded H3 BHA trimer increased from 5.9 nm to 7.0 nm when bound to three FI6v3 fragment antigen binding (fab) segments, which is very similar to the increase of 5.6 nm to 6.9 nm for the H1 BHA trimer bound to three FI6v3 fabs. The R_H of three HB36.6 ligands bound to trimer H1 BHA increases marginally from 5.6 nm to 6.0 nm, which is expected since HB36.6 is considerably smaller than FI6v3 (13kDa vs. 50kDa respectively).

As a second approach, small angle X-ray scattering (SAXS) online with size exclusion chromatography (SEC) was used to determine the overall shape and size of the aforementioned complexes in solution (Figure 3.2 B,E,H). Fourier transformation of the scattering data was performed to obtain the interatomic distance distribution function P(r). Similar to the Patterson function in crystallography, P(r) or the radial Patterson function, can provide shape and volume information occupied by a protein in solution. However, due to the finite range of scattering data, P(r) calculations must assume that the radius is zero at the maximum linear dimension (D_{Max}), thus the uncertainty depends on the quality of data, and in practice one typically does not assign an error to D_{Max}. Furthermore, high quality SAXS data can be analyzed to derive the mass distribution within a particle commonly known as the radius of gyration (R_G) using two distinct mathematical models; the P(r) and the Guinier approximation. Since P(r) calculations use the entire dataset to calculate R_G values, the values from P(r) are thought to be more precise than from the Guinier approximation, which relies on linear extrapolation of data obtained from the initial q values. The reported R_G values from both models should be nearly identical, which also provide a measure of the experimental consistency and data robustness.

For each SAXS experiment, the D_{Max} and R_G were determined for each protein state (Table 3.1). Each reported R_G was consistent between the two analytical approaches. The high resolution BHA crystal structures show that H3 (Protein databank ID:3HMG) is longer than H1 (PDB ID:1RU7), which is consistent with the measured D_{Max} of the unliganded BHAs in solution; 15.1 nm (H3) and 13.4 nm (H1), and the R_G values of the unbound BHAs 4.7 nm (H3) and 4.5 nm (H1) also follow this trend. In the presence of FI6v3, the D_{Max} and R_G of both subtypes were much larger relative to the unliganded species; 18.0 nm, 5.4 nm (H3) and 18.3 nm, 5.4 nm (H1), while in the H1-HB36.6 complex, the D_{Max} increases slightly but the R_H remains the same relative to free BHA; 13.9 nm, 4.6 nm.

To verify that our solution-phase assemblies are consistent with the available crystal structures, all-atom models of the stem-targeting inhibitors bound to glycosylated BHA, were generated, and the theoretical scattering data for each model were analyzed with the FoXS webserver (Figure 3.2). The goodness of fit for each model is assessed by the reported by a χ value, which compares the theoretical fit of the model to the experimental data.[26,27] Both H3-FI6v3 (Figure 3.2 B,C) and H1-FI6v3models (Figure 3.2 E,F) were built with three Fab domains bound to the respective BHA timer as indicated in the H3 and H1 crystal structures (PDB ID: 3ZTJ and 3ZTN, respectively).[4] FoXS was used to identify the glycosylated H3-FI6v3 and H1-FI6v3 models whose theoretical SAXS curve fit the experimental SAXS data with the lowest χ value of 1.25 (H3) and 1.11 (H1). The agreement between the model and scattering data indicates that the solution conformations of the H3-FI6v3 and H1-FI6v3 were in accord with the available crystal structures. Likewise, a glycosylated H1-HB36.6 modeled with three HB36.6 monomers bound to the BHA trimer (Figure 3.2 H,I) was produced using the published crystal structure of an early generation HB36.3 bound to a group-1 BHA (PDB ID: 3R2X), which has a similar binding location but different affinity.[23] FoXS determined the lowest χ value for the H1-HB36.6 model was 1.31, and the theoretical SAXS profile of H1-HB36.6 fit well to the experimental SAXS data suggesting that the derived model is a good representation of the HB36.61-H1 complex in solution.

FI6v3 Stabilizes the H3 HA Short Helix and Fusion Peptide

To test the hypothesis that FI6v3 binding prevents HA-mediated infection by stabilizing pre-fusion HA, an HDX-MS comparison of the H3 BHA trimer both bound and unbound to the FI6v3 fab was performed (Figure 3.3). BHA obtain from H3N2 (X-31) was incubated with FI6v3 fabs and HDX-MS and compared to unliganded BHA as described in the experimental procedures. 90% sequence coverage of H3

BHA was obtained from 22 and 15 unique peptides for HA1 and HA2, respectively. Upon comparison of the FI6v3 bound state to the unliganded BHA, the HDX-MS data revealed the peptides that were protected from exchange, invariant (no change between the two states) or had greater deuterium uptake in the presence of the fab (Figure 3.3).

In the pre-fusion complex, residues from the FI6v3 heavy and light chains predominately contact the surface of the HA2 short helix (HA2 39-52, peptide 4, H3 numbering), which in the post-fusion conformation reorients ~180° from the viral membrane towards the target membrane forming the trimeric core of the extended helix. In the bound pre-fusion state, the peptide spanning the HA2 short helix exhibited the most protection from deuterium exchange throughout the entire data set, consistent with a direct protein-protein interaction. Downstream of the short helix, a peptide spanning the far C-terminus of the short helix and far N-terminus of the HA2 B-loop (HA2 53-69, peptide 2) also interacts with FI6v3, and displayed minor protection from deuterium exchange in the bound state. Additionally, the HA2 N-terminal fusion peptide (HA2 1-8, peptide 6) exhibited modest HDX protection in the presence of FI6v3 but only at the final time point, which suggests that FI6v3 binding may stabilize the hydrogen bonding network of the fusion peptide within the cavity of the HA trimer.

Regions adjacent to the binding site exhibited increased deuterium exchange in the presence of FI6v3 even though they do not exhibit direct interaction with the fab based upon the co-crystal structure.[4] An HA2 peptide at the base of the trimer (HA2 139-148, peptide 8) displayed enhanced exchange in the Fab-bound state, and deuterium incorporation of the HA2 hairpin-1 (HA2 22-38, peptide 9) downstream of the fusion peptide and upstream of the short helix was moderately elevated. Furthermore, an HA1 "hinge" peptide (HA1 259-268, peptide 1) located near the HA2 B-loop showed a slight increase in deuterium exchange in the complex. Invariant areas within BHA were primarily localized to the apex of the trimer in the HA1 head (HA1 43-63, peptide 7 and 88-108, peptide 5). Peptides located within the core of the fusion domain in the HA2 long helix (HA2 70-87, peptide 3) and the HA2 C-terminus also showed identical exchange kinetics between the unliganded and FI6v3 bound BHA.

FI6v3 Stabilizes the H1 HA Short Helix and Hairpin-1 but not the Fusion Peptide

To examine whether FI6v3 binding induces identical stabilization to the pre-fusion state of different isolates, an HDX-MS comparison of unliganded H1 BHA with an H1 BHA bound to an antibody fab fragment of FI6v3 was performed. Pre-fusion BHA from a group 1, H1N1 influenza virus (PR8) was isolated as mentioned in the experimental procedures. The overall sequence coverage of H1 BHA was greater than 90% and obtained by identifying 30 and 18 unique HA1 and HA2 peptides, respectively.

Although the two isolates examined here share 67.9 % sequence similarity in HA1 and 85% sequence similarity in HA2 (as calculated from the LALIGN webserver), the pepsin digest yielded a very different set of peptides from H3 BHA, with the exception of the N-terminal HA2 peptide (HA2 1-9, for both isolates). Upon comparison of the HDX-MS profiles for both isolates, it was evident that the fusion peptide of H1 was more dynamic than the H3 fusion peptide, even in the pre-fusion unliganded state (Figure 3.4 A). Furthermore, the H1-FI6v3 data set revealed that the exchange kinetics of the H1 fusion peptide between the free and bound state did not change upon ligand binding to the same extent as in the H3 data set where the H3 fusion peptide became more protected with FI6v3 (Figure 3.4 A). Upon closer examination of the two all-atom models generated by homology models from existing crystal structures, it appears that Y32 from the light chain ($Y32_{LC}$) is closer in proximity to the fusion peptide backbone in the H3 complex, while $Y32_{LC}$ in the H1 complex does not share the same distance constraints (Figure 3.4 B), possibly explaining why FI6v3 stabilizes the fusion peptide in the H3 isolate more than the H1 isolate.

In contrast to the H3 FI6v3 comparison, there was no evidence of enhanced exchange kinetics in any subdomain within the H1 BHA and all observable differences between the complex and free BHA trimer displayed protection from deuterium uptake (Figure 3.5, triangles). However, similar to the H3-FI6v3 HDX-MS analysis, one of the largest changes within the H1 data set was in an HA2 peptide spanning hairpin-1 and the HA2 short helix (HA2 34-54, peptide 4,H1 numbering), which becomes protected in the bound state. Additionally, peptides spanning the far C-terminus of the fusion peptide (HA2 17-21, peptide 5) just upstream of the HA2 34-54 peptide, exhibited a high degree of protection in the presence of the FI6v3 fab, and the middle of the fusion peptide (HA2 10-17, peptide 6) also showed some protection at a later time point.

Many regions with the H1-FI6v3 HDX comparison (Figure 3.5) also revealed other invariant regions within the membrane distal HA1 subunit (HA1 69-77, peptide 1, 151-175, peptide 8, and 198-205, peptide 9), as well as areas near the base of the trimer (HA1 264-271, peptide 10). Furthermore, many HA2 peptides just outside of the binding interface were unaffected within the complex such as the far C-terminal short helix and B-loop (HA2 55-59, peptide 3 and 64-80, peptide 2). This demonstrates that the effects of this antibody binding are highly localized and do not induce large-scale structural perturbations; rather the native, pre-fusion state appears to be recognized and stabilized by FI6v3 binding.

HB36.6 Destabilizes the H1 Fusion Peptide and B-loop

To test the hypothesis that HB36.6 inhibits HA by ordering the pre-fusion conformation in a similar fashion as stem directed bnabs, an HDX-MS comparison of free H1 BHA versus H1-HB36.6 was performed. The same HA sequence coverage as H1-FI6v3 was obtained for the H1-HB36.6 complex, and the two systems were directly compared (Figure 3.5, squares). In contrast to the H1-FI6v3 profile, the exchange profile of the HA2 short helix (HA2 34-54, peptide 4) did not change when associated with HB36.6. However, a peptide spanning the C-terminus of the short helix and B-loop (HA2 55-59, peptide 3) showed the largest increase in deuterium exchange in the presence of HB36.6 and the far N-terminus of the HA2 fusion peptide (HA2 1-9, peptide 7) was also more deuterated when bound. Similar to the H1-FI6v3 profile, a short peptide covering the far C-terminus of the fusion peptide (HA2 17-21, peptide 5) displayed the greatest degree of protection when bound to HB36.6. The deuterium uptake of the HA2 core (HA2 64-80, peptide 2) remained uniform upon HB36.6 association, as did peptides covering the termini of each subunit located near the base of the trimer (HA1 264-271, peptide 10 and HA2 10-17, peptide 6). While the exchange kinetics for the majority of peptides spanning HA1 (HA1 151-175, peptide 8 and 198-205, peptide 9) were unaffected by HB36.6, a peptide located at the HA1 “hinge” (HA1 69-77, peptide 1) was moderately protected at the first two time points.

Conditions Approaching H1 Fusion Activation Reveal a Common Stabilization Mode

The neutral pH data of H1 bound to HB36.6 and FI6v3 fabs suggests that while HB36.6 stabilizes a portion of the trimer near the C-terminal fusion peptide (HA2 17-21), the binding effects within the trimer are different. To deduce whether the observed stabilization in H1 when bound to FI6v3 and HB36.6 will be maintained during the low pH activation approaching fusion, HDX-MS experiments of free H1, H1-FI6v3 and H1-HB36.6 were performed (Figure 3.6). In both complexes, binding of FI6v3 or HB36.6 stabilized the pre-fusion state within the C-terminal fusion peptide even at pH 6.0 (HA2 17-21, peptide 3 in Figure 3.6). The short helix (HA2 34-54, peptide 4) that is stabilized by FI6v3 but not HB36.6, also remained stabilized in the H1-FI6v3 complex at pH 6.0, while the H1-HB36.6 complex was unperturbed by low pH. The middle portion of the fusion peptide (HA2 10-17, peptide 2) was relatively unaffected by FI6v3 binding under both solution conditions, however, at pH 6.0, H1-HB36.6 exhibited a moderate increase in deuterium exchange. Many regions remained invariant under all conditions probed for all three protein states, which suggest that the stabilization within the C-terminal fusion peptide (peptide 3) and the short helix (peptide 4) are what is responsible for inhibiting the conformational changes required for membrane fusion.

The N-terminal fusion peptide (HA2 1-9, peptide 1), however, exhibited some increase in deuterium uptake in both the unliganded H1 and H1-HB36.6 complex when incubated at pH 6.0. Furthermore, the HA1 helix located at the HA1-HA2 interface (HA1 113-117, peptide 8), showed the largest pH dependent increase in deuterium uptake within the whole dataset. The extent of magnitude for the HA1 portion of this interface was identical for the unliganded and both bound states, which suggest that while FI6v3 and HB36.6 both stabilize the HA2 stem, they do not appear to have an impact on HA1 dynamics when nearing fusogenic conditions. It also appears that the pH-dependent increase in flexibly within this interface was localized to the HA1 portion since the HA2 B-loop (HA2 64-73, peptide 5) remained unchanged under all conditions measured. This observation was also contrasting what was observed for the unliganded H3 isolate when approaching the pH of fusion, reported in chapter 2, where the HA1 head was rather unperturbed by low pH and the fusion stem was the most impacted.[28]

A Small Molecule Fusion Inhibitor Locally Impacts the H3 HA Short Helix and Fusion Peptide

The overall differences between the H1-HB36.6 and H1-FI6v3 HDX profiles indicate that not all stem-directed protein inhibitors elicit the same pattern of changes in HA. We sought to investigate the impact of a stem-targeting fusion inhibitor, *tert*-buylhydroquinone (TBHQ), on the overall conformational dynamics of the H3 BHA with HDX-MS. The overall peptide coverage was identical to that reported for H3-FI6v3, and of all the examined peptides, only three showed effects upon TBHQ binding. The HA2 short helix (HA2 39-52), and the B-loop (HA2 53-69) span the solvent accessible face of the binding site, and these regions were the only sites that were protected from deuterium exchange in the presence of TBHQ (Figure 3.6). Additionally, the HA2 N-terminal fusion peptide (HA2 1-8) was slightly more exchanged when BHA was bound to TBHQ, which was contrary to what was observed for the H3-FI6v3 complex (Figure 3.3 and Figure 3.6). The deuterium uptake of all other peptides encompassing both HA1 (HA1 109-119, 175-194 and 314-328) and HA2 (HA2 70-87 and 110-115) did not show major changes between the bound and free BHA trimer, suggesting TBHQ locally stabilizes the binding site, while allosterically destabilizing the fusion peptide cavity.

DISCUSSION

Each of the studied stem-directed molecules has been shown to inhibit HA mediated membrane fusion at low pH. While it is evident that targeting HA2 prevents the low pH structural transition required for viral replication, the mechanism of inhibition for each of these species is unclear. Here we use HDX-MS to determine whether FI6v3 binds both H1 and H3 epitopes in a similar manner and if binding induces similar local stabilization within the trimer. We also report data investigating the impact of HB36.6 binding to an H1 isolate to ascertain whether HB36.6 binding function is consistent with FI6v3, and if the low pH profile of H1-HB36.6 and H1-FI6v3 are also similar. Finally, we examine the H3-TBHQ complex to establish if the mechanism of targeting HA2 is universally to stabilize the pre-fusion state to prevent the low pH conformational change.

Local ordering of antigen epitopes has been shown to be a common property of highly potent bnabs that target the HIV envelope glycoprotein, while poorly neutralizing antibodies with little breadth often induce allosteric changes distal from the binding site.[29] Here, we observe an interesting parallel with influenza HA bnabs. While the group specific differences such as an additional turn in the short helix, or an N-linked glycan near the epitope, are thought to impact the breadth of group-1 and group-2 specific bnabs, respectively; FI6v3 is capable of binding genetically distinct HAs from both groups.[4] Likewise, FI6v3 only elicits local stabilization near the epitope. In contrast, HB36, which can target group-1 isolates only, induces structural changes beyond its immediate binding site, some of which are destabilizing.

Overall, both isolates exhibited stabilization within the short helix in the presence of the FI6v3 fabs; however, due to differences in amino acid sequence between each subtype, the magnitude of stabilization within these regions cannot be directly compared. The N-terminus of the fusion peptide is the only region that can be directly compared between both HAs, and even in the unbound state, it appears that H1 is more flexible than H3. Comparison of the FI6v3 complex suggests that binding H3 isolates may moderately stabilize this region, while the H1 subtype is unaffected. In the all atom models it appears that the light chain Y32 residue may participate in a hydrogen bonding network with the N-terminal fusion peptide backbone in H3 but not H1, which may explain why stabilization is only observed in the H3 complex. FI6v3 appears to significantly stabilize the C-terminal portion of the fusion peptide (HA2 17-21) exclusively monitored in H1, which is a common binding region for other group-1 specific stem directed bnabs such as F10 and CR6261, as well as the group-2 specific bnab CR8020.[5,8,30]

Understanding the modes of neutralization for bnabs is a sought after goal for the development of HA inhibitors such as the group-1 specific small helical protein HB36.6.[23,24] The binding interface between HA and HB36.6 was modeled after the said group-1 specific bnabs and preliminary data shows that HB36.6 can protect ferrets and mice from infection (Treants, M.E. et al. manuscript submitted). While FI6v3 is not identical to CR6261 and F10, some epitope features (such as the C-terminal fusion peptide) are shared, as mentioned above. In order to better understand the mechanism of HB36.6 binding and if the differences between FI6v3 and HB36.6 complexes may reveal why FI6v3 is pan-neutralizing and HB36.6 is group specific, we used HDX-MS to investigate the H1 bound HB36.6. Overall, the profiles of H1-FI6v3 and H1-HB36.6 were considerably distinct. In particular, the short helix is not affected by HB36.6 despite being involved in the interface. Furthermore, the C-terminal fusion peptide also showed extensive protected when bound to HB36.6, though to a lesser extent than FI6v3. In contrast to FI6v3, HB36.6 also allosterically induced some flexibility within the N-terminal fusion peptide and N-terminal portion of the B-loop, which suggests that binding does not simply have a local stabilizing effect within the pre-fusion state. Nonetheless the common binding mode between HB36.6 and FI6v3 appears to be within the C-terminal portion of the fusion peptide. We hypothesize that stabilizing this region prevents the release of the N-terminal fusion peptide from the cavity located at the base of the trimer, which in turn inhibits other necessary structural rearrangements required for fusion. This hypothesis is also supported by the observation that upon lowering the pH of both H1-FI6v3 and H1-HB36.6 to near fusion conditions (pH ~6.0); the C-terminal fusion peptide maintained the same extent of protection within both liganded states. While we are unable to draw parallels to the other bnabs from which HB36.6 was designed, it is likely that the epitope within those complexes would involve stabilization locally at the C-terminal fusion peptide and short helix.

The small molecule TBHQ was previously reported to bind in the pocket between the short helix and long helix of HA2, and stabilize the melting of HA compared to unliganded HA.[25]
H3-TBHQ also appears to order the short helix similar to the H3-FI6v3 bound sate. However, as with HB36.6, the fusion peptide also becomes more flexible when bound to TBHQ. These parallels, although observed for different subtypes with consequently different sequences, suggest that stabilization of either the short helix or far C-terminal fusion peptide may be sufficient for inhibiting HA mediated membrane fusion. Yet, the observed increased dynamics may be why the affinity of TBHQ was micromolar, which is less than ideal for potential drug candidates.

The differences observed when unliganded H1 approaches fusion activation conditions (pH 6.0) appeared to be focused within an HA1 peptide in the HA1-HA2 interface, and not the HA2 B-loop, which contrasts what was observed for the H3 isolate where the fusion peptide and HA1 “hinge” appear to drive

HA activation.[28] This contrast may be in part be explained by the fact that the H1 fusion peptide is already highly dynamic at neutral pH, even more so than the H3 isolate (Figure 3.4 A). It is possible that the acid stability observed for the H1 fusion peptide may be necessary to prevent inactivation prior full endosomal maturation that is required for membrane fusion (~pH 5.0). However, it has been shown previously that the membrane fusion kinetics of unique subtypes responds to low pH titrations differently, which may be exhibited by rapid inactivation.[31] It has also recently been demonstrated that acid activation and membrane fusion kinetics of HA from the same subtype but different isolates (in this case H3 variants) also have markedly distinctive fusion and activation profiles.[32]

These apparent isolate-specific differences in fusion activation mechanisms may shed light onto other contradictory reports in the literature. For example, White and Wilson were the first to propose that the fusion peptide release precedes full HA1 "uncaging".[33] However, the cryo-electron tomography data of the H2 ectodomain at low pH by Böttcher et al. showed an opening of a cavity at the HA1 head, which lead to the hypothesis that HA1 dissociation may drive membrane fusion.[34] Some other findings also suggest that such events may occur in concert as observed by two separate experiments from Kemble et al. and Fontana et al. Kemble et al. used conformational antibodies to probe epitopes in HA1 that are buried within the pre-fusion HA but exposed in acid-activated state. After covalently crosslinking the HA1 heads together, Kemble and colleagues found that although HA1 uncaging could not occur when incubated at low pH, both the fusion peptide and hidden epitopes within HA1 were uncovered, which suggest that minor structural perturbations within HA1 occur simultaneously with fusion peptide release.[35] Fontana et al. observed by cryo-electron tomography that a narrowing of the HA2 stalk occurred when whole virus was incubated at pH 4.9 prior to freezing, yet the HA1 head appeared to remain in the pre-fusion-like conformation.[36] Such discrepancies reported within the literature may in fact be due to the large extent of sequence variability inherent to HA and other RNA viruses. It is possible that due to the sequence differences within each subtype and consequently minor three-dimensional architecture, HAs from different groups and possibly even divergent subtypes, have different mechanisms of low-pH activation in order to undergo membrane fusion at the precise time for optimal genome release. Thus it is likely that comparisons of a broad range of subtypes will be necessary to refine and the proposed mechanisms of HA activation.

EXPERIMENTAL PROCEDURES

Influenza and BHA Preparation

Purified soluble ectodomain of influenza A hemagglutinin following bromelain cleavage of whole virus from subtypes X31 (H3N2) and PR8 (H1N1) was obtained from Charles Rivers Laboratory and purified as described in the experimental procedures from chapter II.

Hemagglutinin Stem Binder Protein Ligand Production and Purification

FI6v3 Fab Production and Purification

Using the Daedalus method, stable 293-Freestyle cells (Invitrogen) expressing and secreting full-length human FI6v3 broadly neutralizing IgG_1 antibodies were produced and donated to our lab as a kind gift from the Jesse Bloom Lab (Fred Hutchinson Cancer Research Center).[37] The cells were grown at 1×10^6 cells/mL in Freestyle 293 expression media (Gibco) shaking at 130 rpm, 37°C and 8% CO_2. Expression was confirmed by western blot analysis, and after 1 week 500mL of cell culture supernatant was reserved and filtered for IgG_1 purification over Protein A affinity resin (Pierce). FI6v3 was allowed to bind the resin at room temperature and following three PBS (10 mM Phosphate, 150 mM NaCl, 0.02% NaN_3, pH 7.5) washes, the IgG_1 was eluted with 100 mM Glycine pH 2.5. Fab fragments were prepared using the Pierce ™ Fab Preparation Kit. The concentrated FI6v3 stock was digested by immobilized Papain for 3 hours at 37°C in digestion buffer (3.5 mg/mL cysteine, pH 10). The slurry was spin filtered and washed to collect the F_c/Fab mixture and then loaded over Protein A affinity resin equilibrated with PBS. After washing the Protein A affinity resin three times with PBS, the FI6v3 Fab was eluted from the resin using a pH-gradient from pH 4.0 to 2.0, where the pH 4.0-pH 3.0 buffers were 200 mM sodium acetate and the pH 2.5-pH 2.0 were 200 mM Glycine. The Fab fractions were immediately neutralized to pH 7.5 using 1M Tris pH 8.0 and purity was analyzed via SDS-PAGE. The Fab containing fractions were concentrated and buffer exchanged to 2.5 mg/mL in PBS using a spin-filter with a molecular weight cutoff of 30KD and the molecular weight of the final product was verified by MALDI-TOF mass spectrometry. All FI6v3 fabs will simply be referred to as FI6v3 for simplicity unless otherwise noted.

HB36.6 Production and Purification

The small monomeric HB36.6 group-1 specific HA stem binder protein was designed and produced in collaboration between the Baker Lab (University of Washington Biochemistry Department) and the Fuller Lab (University of Washington Microbiology Department and Washington National Primate Research Center) as described similarly by Fleishman et al. [23]

Small Angle X-Ray Scattering (SAXS) and Modeling of HA-Stem Binder Complexes

1mg/mL H3-FI6v3, H1-FI6v3 and H1-HB36.6 complexes were made by incubating purified BHA of either subtype with a 3-fold molar excess of FI6v3 or HB36.6 (H1 BHA only at 4°C overnight to ensure a maximally bound state prior to size exclusion chromatography (SEC). Complexes were analyzed by SEC in-line with SAXS as described in chapter II.

All-Atom Ensemble Modeling of Glycosylated HA-Stem Binder Complexes

All-atom glycosylated models of unliganded BHA (H3 and H1 subtypes), were built using MODELER as previously described.[26,27,38-40] Ensembles of BHAs with FI6v3 Fab and BHA (H1) with HB36.6 were assembled with at least 30 individual models. Crystal structures of non- or partially glycosylated unliganded BHA (PDB ID: 3HMG and 1RU7), FI6v3 bound BHA (3ZTN and 3ZTJ) and the 1918 H1 BHA bound to a homologous HB36.6 construct (3R2X) were used as starting templates for generation of initial models .[4,16,23,41,42] BHA glycans were added based on known major glycoforms observed by mass spectrometry during HDX-MS analysis. Glycans were added and set as flexible residues during simulated annealing. Models were aligned and visualized with PyMOL (Delano). The FoXS web server [26,27] was used to calculate the theoretical SAXS profile of each model by implementing the Debye formula for spherical scattering[43], The goodness of fit (χ value) for each model relative to the experimental SAXS data of the corresponding protein complex was used to identify the models most consistent with the scattering data.[26,27]

Hydrogen Deuterium Exchange (HDX)

HA- Stem Binder Protein Complexes

Protein stocks of unliganded BHA, FI6v3 BHA (both subtypes) and HB36.6 in complex with H1 BHA were made as described above with the addition of 1 µM of the tetra peptides PPPI and PPPF to be used as an internal standard for the intrinsic exchange rate. HDX reactions of each stock were initiated by diluting 3 µg of the protein or complex into deuterated buffer (10 mM Hepes, 150 mM NaCl, 0.02% NaN_3) for a final pH of 7.5 and incubated at room temperature for 3 seconds, 20 seconds, 3.5 minutes or 30 minutes. All reactions were quenched with ice cold quench buffer (100 mM TCEP [tris(2-carboxyethyl) phosphine], 0.2% formic acid) for a final pH of 2.5, rapidly frozen in liquid nitrogen and stored at -80°C until analysis. Undeuterated controls were performed as above with optima pure (Thermo-Fisher) water in place of D_2O. To account for “in-exchange” during online-pepsin digestion (described in the mass spectrometry section below), a “zero” time point was made by diluting 3 µg of stock protein or complex into the quenched deuteration buffer and freezing as mentioned above. Fully deuterated “protein” stocks were prepared by denaturing BHA(H1 and H3) in 10 mM DTT, 3.5 M Gnd-HCl, 10 mM Hepes, 150 mM NaCl at 80°C for 30 minutes, and 3 µg denatured of BHA was added to deuteration buffer containing PPPI and PPPF for 30 minutes at 40°C. Fully deuterated “peptide” stocks were made by collecting the BHA pepsin peptides (either H1 or H3 subtypes) that were digested by the online-pepsin column and eluted from the liquid chromatography gradient used for mass spectrometry (explained in further detail below). Following elution, the BHA peptides were dried by speedvac, and resuspended in the fully deuterated denaturant buffer, and deuteration of fully deuterated “peptide” stocks was carried out identically to fully deuterated “protein” stocks. Both fully deuterated samples were frozen and stored for analysis as mentioned above.

H1 BHA pepsin digests used for initial mass spectrometry peptide identification were made by adding 30 µg of porcine pepsin (Worthington Labs) to quenched undeuterated H1 BHA sample and digesting on ice for 5 minutes and frozen until LC-MS analysis. Identical digests were reneutralized to pH 7.9 with 10M NaOH and fully deglycosylated with 1 µL of a 1U stock of N-Glycanase® (Prozyme) at 37°c for 1 hour. The deglycosylation reactions were quenched by re-acidifying to pH 2.5 with 2M HCl and frozen until LC-MS analysis.

H3 HA-TBHQ Small Molecule Complex

tert-butylhydroquinone was purchased from Sigma Aldrich at 97% purity and resuspended in 100% molecular biology grade DMSO (Sigma Aldrich) to a final stock concentration of 50 mM. H3 BHA was prepared as previously described. TBHQ-bound BHA was prepared by pre-incubating 10 µM BHA with 1 mM TBHQ in stock buffer (10 mM Hepes, 150 mM NaCl, 0.02% NaN_3, 2% DMSO, 6 µM PPPI) for at least 30 minutes to ensure an ~98% fully bound complex (K_D = 20 µM), and an unliganded BHA stock was prepared identically by including 2% DMSO without TBHQ. Deuteration reactions were initiated by diluting 7 µg of unliganded BHA or TBHQ complex into deuterated buffer (10 mM Hepes, 150 mM NaCl, 0.02% NaN_3) for a final pH of 7.5 and performed at room temperature with time points ranging from 3 seconds, 1 minute, 30 minutes and 20 hours. All reactions were quenched with ice cold quench buffer (100 mM, 0.2% formic acid) for a final pH of 2.5, and digested with 30 µg of porcine pepsin for 5 min, frozen in liquid nitrogen and stored at -80°C until analysis.

Mass Spectrometry

Identification of HA peptides

Undeuterated peptides of H3 BHA were identified as described in chapter II on a Waters Synapt G1 HDMS. H1 BHA peptides were identified by exact mass and tandem mass spectrometry using a Thermo Linear Trap Quadrupole Orbitrap Xcalibur 2.0 DS and Waters Synapt G2-Si. Tandem mass spectra were interpreted with the aid of Protein Prospector and Water's ProteinLynx Global SERVER^{TM}. Glycopeptides were identified using tandem spectra obtained from the enzymatically deglycosylated digests.[44]

Analysis of HA-Stem Binder Protein Complexes

Frozen HDX samples were thawed on ice for 5 minutes, manually loaded onto a 250 µL steel line UPLC (ultra-pressure liquid chromatography) loop and injected onto 2.1x50 mm cartridge filled with POROS® AL/20 resin containing immobilized porcine at 200 µL/min with solvent C (2% acetonitrile [ACN], 0.1% FA, 0.04% tri-fluoracetic acid [TFA] pH 2.5) and peptides were trapped onto 1.7 µm 1x17 mm BEH reverse phase C_{18} (Waters) trap column in-line with the pepsin column for 5 minutes.[45] The peptides were then resolved using a BEH 1.7 µm 1x100 mm C_{18} (Waters) reverse phase column running a gradient of 5% to 40% solvent B for 9 minutes (solvent A: 2% acetonitrile [ACN], 0.1% FA, 0.04% tri-fluoracetic acid [TFA] pH 2.5; solvent B: 100% ACN, 0.1% FA). The injection loop, pepsin, trap and analytical columns were kept at a constant 1°C within the Waters HDX manager module.

During the main chromatographic gradient, the pepsin column is switched offline and the LEAP Technologies dual arm PAL was programed to perform a series of pepsin column washes with two 250 µL injections of 2M guanidine hydrochloride (GndHCl), 0.1% TFA pH 2.2; one 250 µL 10% FA and one 250 µL injection of 0.1% FA with 200 µL/min of solvent C. After the main LC gradient, the pepsin column is back-flushed with 0.1% FA, 0.04% TFA at 100 µL/min for 15 minutes. During this time, the trap column was washed to minimize sample carryover by cycling through one 250 µL injection of 10% FA, one 250 µL injection of 50% tri-fluoroethanol, one 250 µL injection 80% methanol, one 250 µL injection of a 2:1 mixture of ACN to isopropanol and one 250 µL injection of 80% ACN[46] and re-equilibrated with solvent C for subsequent injections. Mass shifts of each resolved isotopic envelopes were calculated by fitting to a tailored binomial distribution within the semi-automated HX-Express v2 software (HX-Express.com).[47,48] Experimental error was calculated using the standard deviation from duplicate measurements. For glycoproteins the exchange for the major glycoform is reported. Percent exchange was calculated for each time point relative to the "zero" and fully deuterated standards. In a few cases where the signal for the fully deuterated "protein" standard was insufficient (presumably due to aggregation prior to digestion or altered digestion efficiency) the fully deuterated "peptide" standard was used to calculate the percent exchange. For each difference maps, the represented exchange differences were calculated as the largest deviation in the percent exchange within the time course.

Analysis of H3 HA-TBHQ Small Molecule Complex

Frozen HDX samples were analyzed exactly as described in chapter II using a Waters Synapt G1 HDMS. Downstream mass shift, percent exchange and experimental error was calculated for each observable peptide as cited above using the HX-Express v3 software.

Light Scattering of HA-Stem Binder Complexes

Multi-angle Light Scattering (MALS)

Unliganded BHA (H1 and H3), BHA bound to FI6v3 (H1 and H3) and H1 BHA bound to HB36.6 were made as described above for a final protein complex concentration of 1mg/mL. Complexes were resolved over a Sepax SRT SEC-300 5 µm 4.6x300mm column with an Agilent Technologies high pressure liquid chromatography (HPLC). The HPLC was coupled to a miniDAWN TREOS and Optilab T-rEX (Wyatt Technology) MALS detector and refractometer, respectively. Prior to purification, the SEC column was equilibrated in PBS for at least 12 hours to obtain a stable buffer baseline and the T-rEX reference cell was thoroughly purged. Each eluate peak was analyzed for molar mass and radius of hydration (R_H) using the ASTRA software package (Wyatt Technologies). The RI of each analyte was estimated by weighting the average RI for the carbohydrate and protein (dn/dc = 0.146 and 0.185, respectively) component by mass for each complex (http://www.ampolymer.com/dn-dcValues.html).[49,50]

Thermal Melting Curves and Aggregation Onset

The eluate peak of each complex analyzed by MALS was also collected for determination of melting and aggregation temperatures using a DyanPro NanoStar (Wyatt Technologies) dynamic light scattering (DLS) instrument. 10 µL of each complex was added to a quartz cuvette and covered with 10 µL of paraffin oil to prevent evaporation during temperature ramps. The initial temperature of each sample was set to 30°C and 10 acquisitions of 5 seconds were collected while increasing the temperature 1°C repeated 60 times until a final temperature of 90°C was reached. The initial onset of melting temperatures (T_m) was determined using the DYNAMICS software (Wyatt Technologies) by plotting temperature as a function of the observed radius. The cuvette was washed with 1% Hellmanex III (Sigma Aldrich) at 50°C between each experiment.

CHAPTER III FIGURES and TABLES

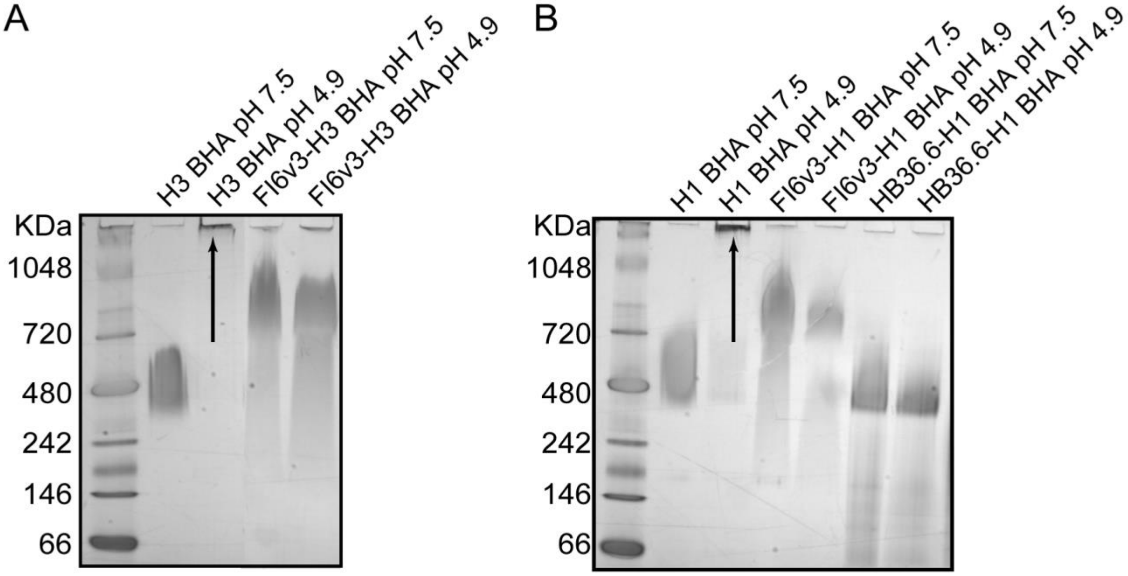

Figure 3.1 Native PAGE of BHA in Complex with Stem Directed Ligands. A) Aggregation profile of H3 bromelain cleaved HA (BHA) free or bound to FI6v3. **B)** Aggregation profile of H1 BHA free or bound to FI6v3 or HB36.6. In both A) and B) either free or liganded BHA was incubated for 30 minutes at pH 7.5 or pH 4.9 at 22°C. BHA aggregates do not enter the gel matrix.

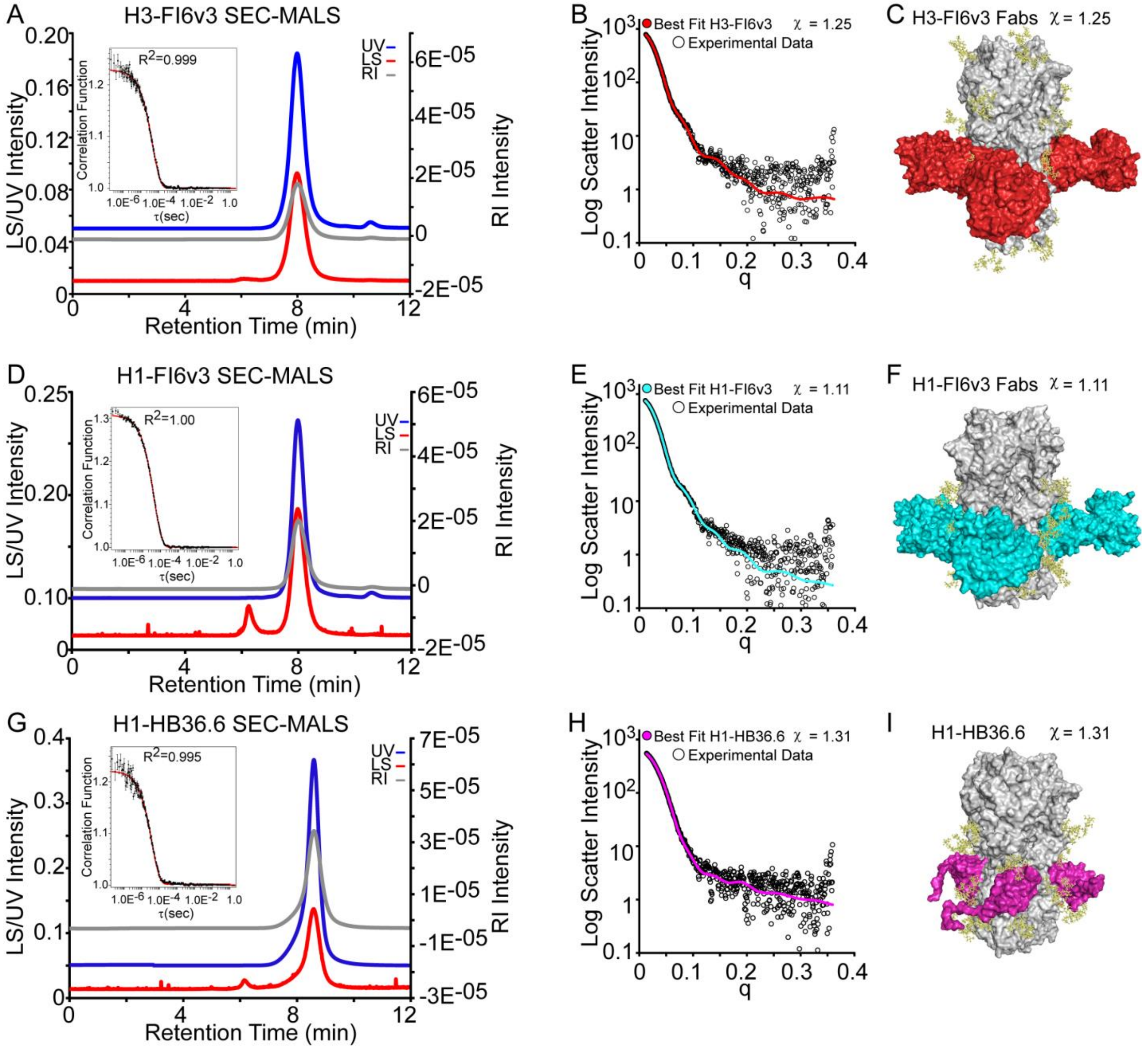

Figure 3.2 SEC-MALS, SAXS and Modeling of BHA with Stem Directed Ligands. A) Size exclusion chromatography (SEC) multiangle light scattering (MALS) data for H3-FI6v3. UV absorbance (blue) and light scattering (LS) (red) and refractive index (RI) (grey) intensities are shown as a function of retention time. The dynamic light scattering (DLS) correlation function for the complex is shown in the inset with the R^2 of the fit =0.999. **B)** Experimental SAXS data (black circles) for H3-FI6v3 and theoretical scattering curve (red fit) of an all-atom model of H3-FI6v3 showed in (B) with the goodness of fit, χ =1.25. **C)** Glycosylated (yellow sticks) all-atom model of H3-FI6v3 complex with three FI6v3 (red) bound to each HA (grey), using PDB ID: 3ZTJ as a template.[4] **D)** SEC-MALS traces and DLS correlation function (inset) for the H1-FI6v3 complex with parameters described as in A). The DLS R^2 of the fit =1.00 shown as the inset. **E)** Experimental SAXS data (black circles) for H1-FI6v3 complex and theoretical scattering curve (cyan fit) of an all-atom model of H1-FI6v3 shown in (D) with goodness of fit χ =1.11. **F)** Glycosylated (yellow sticks) all-atom model of H1-FI6v3 complex with three FI6v3 (cyan) bound to each HA (grey) PDB ID: 3ZTN as a template.[4] **G)** SEC-MALS traces and DLS correlation function (inset) for H1-HB36.6 complex with the parameters described as in A) where the DLS R^2 of the

fit =0.995.**H)** Experimental SAXS data (black circles) for H1-HB36.6 complex and theoretical scattering curve (magenta fit) of an all-atom model of H1-HB36.6 with three HB36.6 (magenta) bound to each HA (grey) shown in F) with χ =1.31. **I)** Glycosylated (yellow sticks) all-atom model of H1-HB36.6 using PDB ID: 3R2X as a template.[23]

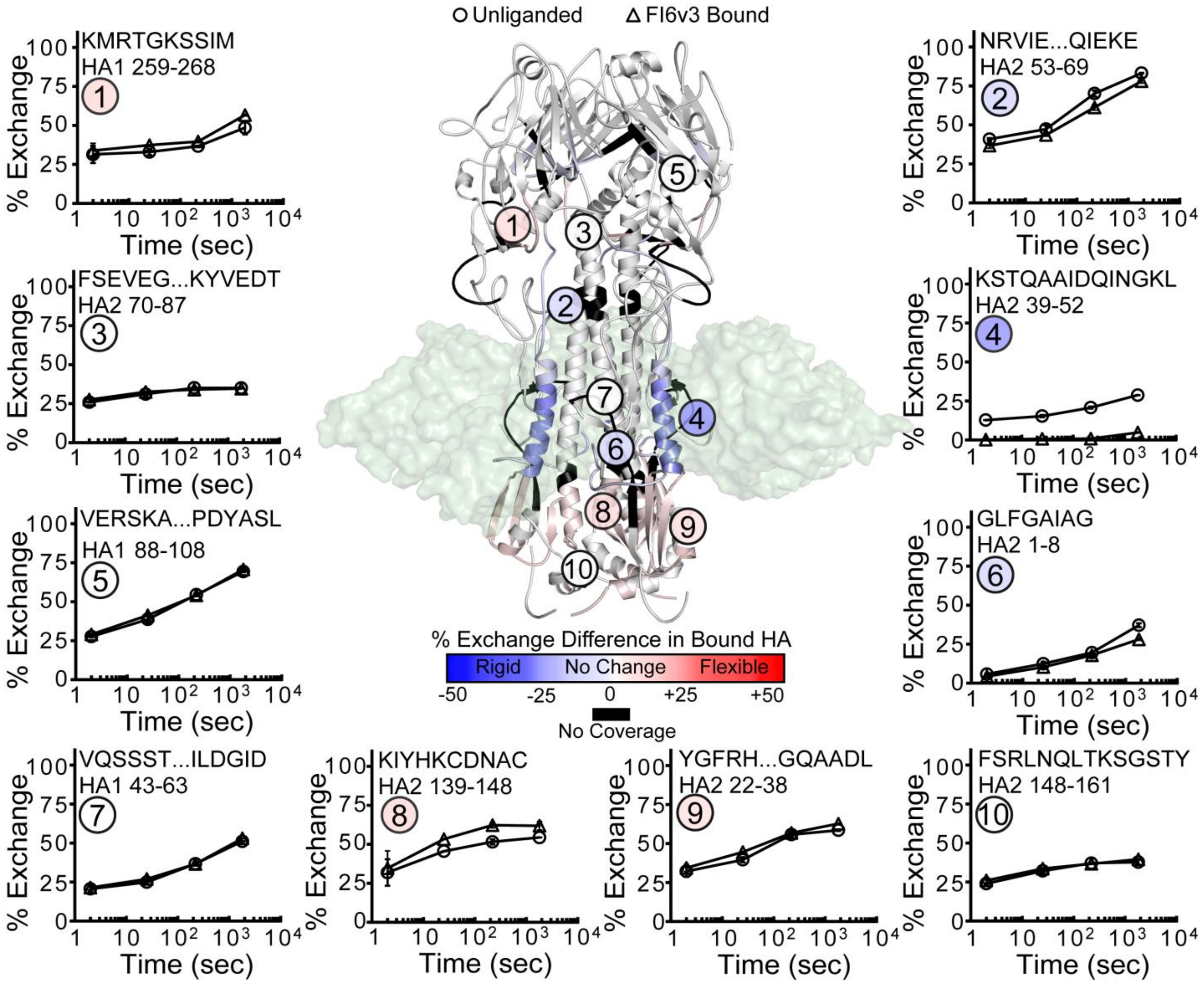

Figure 3.3 Dynamic Changes within H3-FI6v3 Complex at pH 7.5. Exchange profiles of selected HA1 and HA2 peptides are plotted for the unliganded state (circles) and the FI6v3 bound state (triangles). Error bars are the standard error from duplicate measurements and all colored differences on the structure are outside experimental error. The peptide sequence and subunit are designated within the exchange plots and the circled numbers indicate the position of each peptide on the H3-FI6v3 all-atom model. The FI6v3 is shown as a pale green surface representation, and the HA is colored as a percent exchange difference heat map. Blue represents regions that are more protected in the complex, white are no differences between the two datasets and red are regions that are more exchanged in the bound state. Regions colored black signify no peptide coverage.

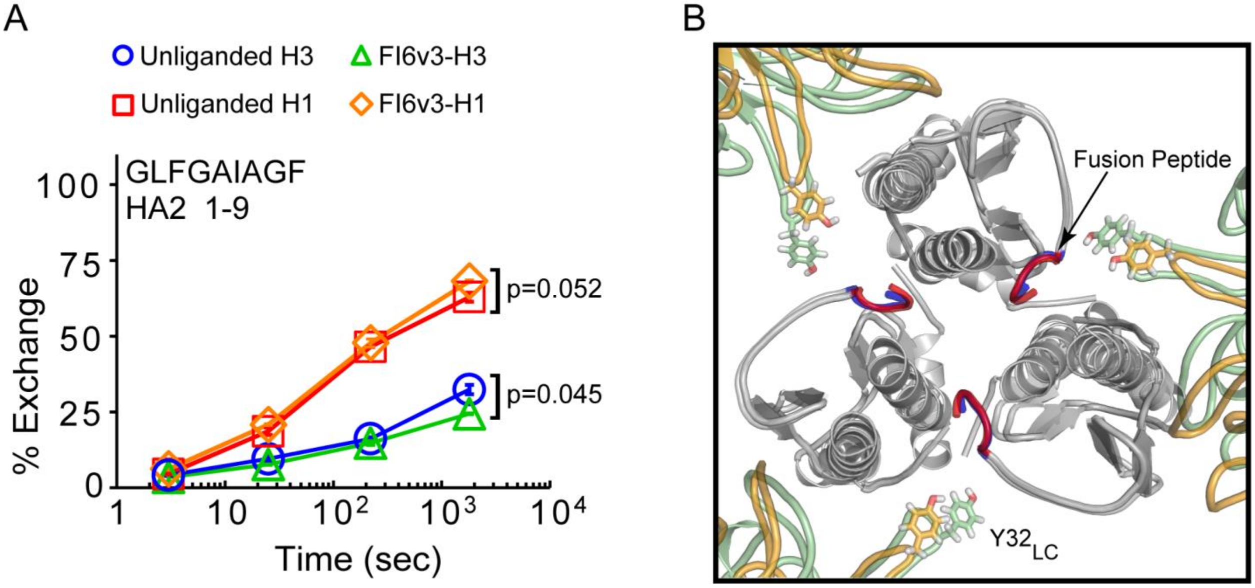

Figure 3.4 Fusion Peptide HDX Profile in H3- and H1-FI6v3 Complexes. A) The HDX-MS profile of the fusion peptide at neutral pH for the unliganded H3 (blue circle), bound to FI6v3 (green triangle), unliganded H1 (red square) and FI6v3 (orange diamond). Error bars are the standard error from duplicate measurements and all colored differences on the structure are outside experimental error. The p values were calculated using the excel T-test function. **B)** All-atom models of FI6v3 complexes where the H3 fusion peptide is blue, FI6v3 light chain (LC) bound to H3 is pale green, H1fusion peptide is red, FI6v3 LC is pale orange. The Y32 side chain is shown as sticks.

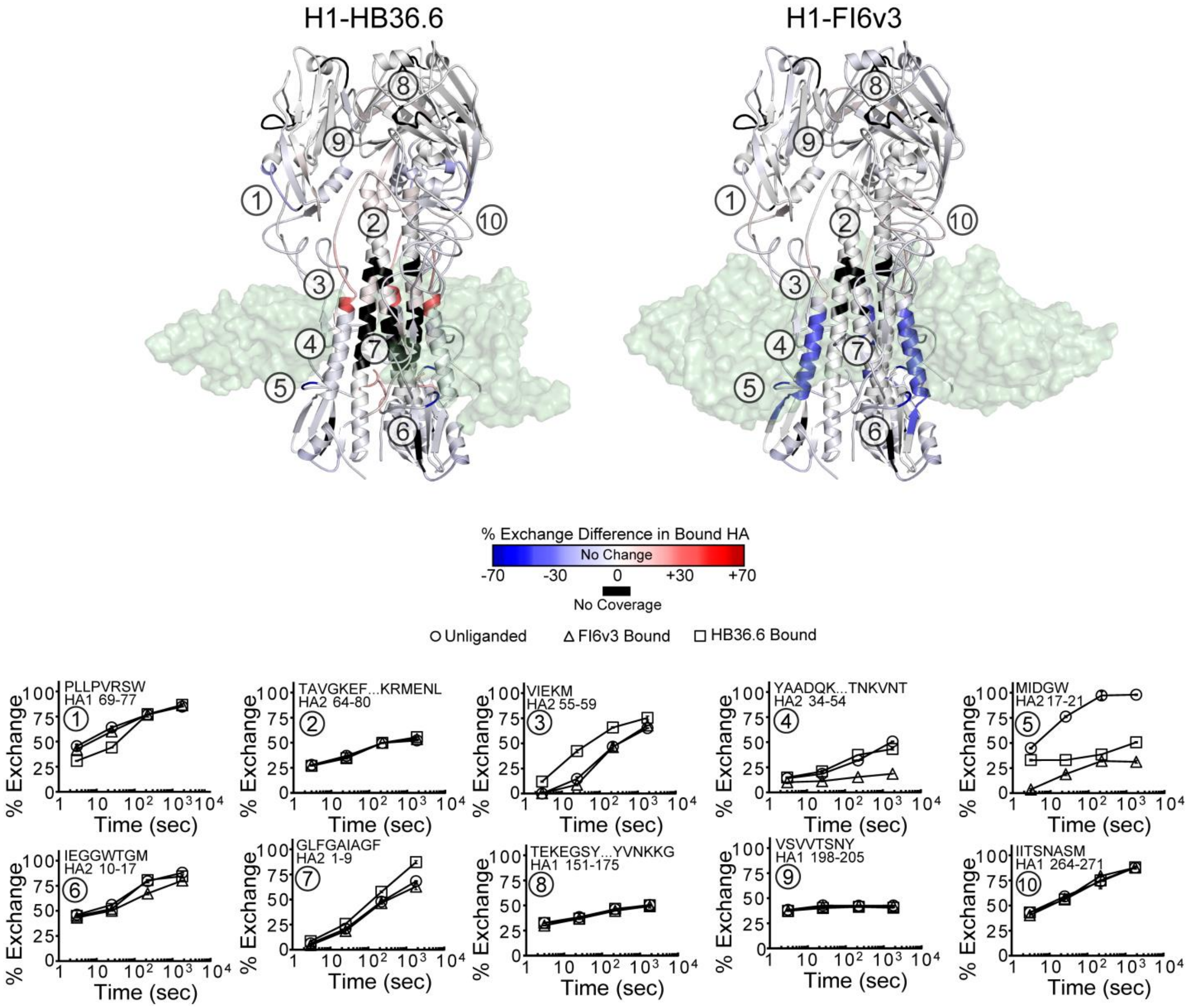

Figure 3.5 Dynamic Changes within H1-HB36.6 (left) and H1-FI6v3 (right) at pH 7.5. Exchange profiles of selected H1 peptides in the unliganded trimer (circles), H1-HB36.6 complex (squares) and H1-FI6v3 complex (triangles) where error bars are the standard error from duplicate measurements and all colored differences on the structure are outside experimental error. Plots are represented as in Figure 3.3 and the peptide numbers within each plot are designated within the three-dimensional structure within both complexes. The percent exchange difference heat maps are colored as in Figure 3.3. The two ligands are shown as surface representations and colored pale green.

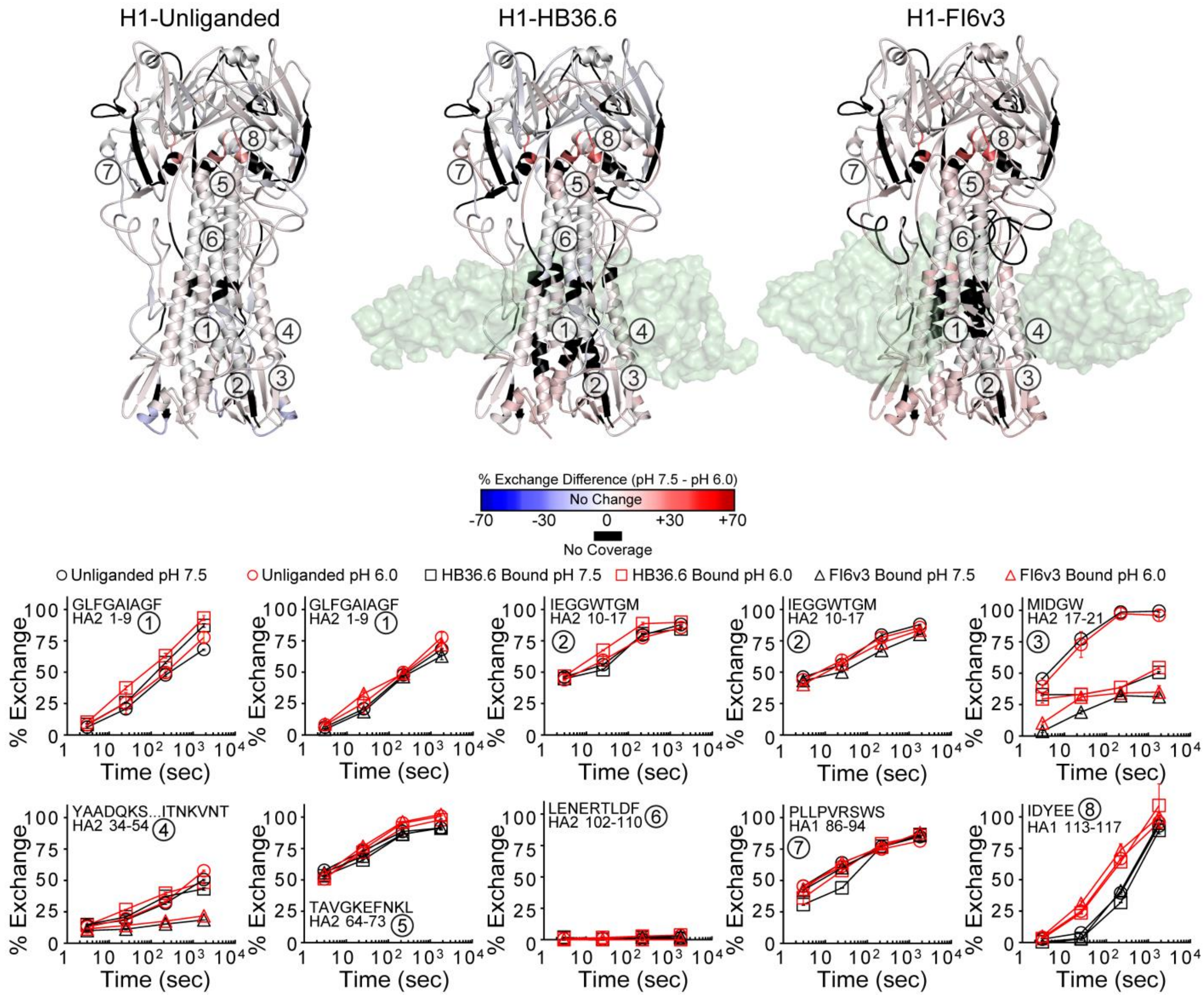

Figure 3.6 Dynamics of H1 (left), H1-HB36.6 (middle) and H1-FI6v3 (right) at a pH Approaching Fusion. Exchange plots of unliganded H1 at neutral pH (black circles) and at pH 6.0 (red circles) for selected peptides are shown, while the percent exchange difference between the neutral and low pH state for unliganded BHA are shown in the structure on the left from the PDB ID: 1RU7. Exchange plots for the H1-HB36.6 pH 7.5 (black squares) and at pH 6.0 (red squares) are shown for selected peptides and the percent exchange difference between the neutral state and low pH state for the H1-HB36.6 complex is shown on the all-atom model in the middle panel. The H1-FI6v3 exchange data for selected peptides at pH 7.5 (black triangles) and pH 6.0 (red triangles) are shown while the whole data set is shown as percent exchange difference between pH 7.5 and pH 6.0 for the H1-FI6v3 bound state on the all-atom model (right). The corresponding regions for each selected peptides are shown on all three structures and the heat map is colored as in Figure 3.3 and 3.4. Error bars are the standard error from duplicate measurements and all colored differences on the structure are outside experimental error.

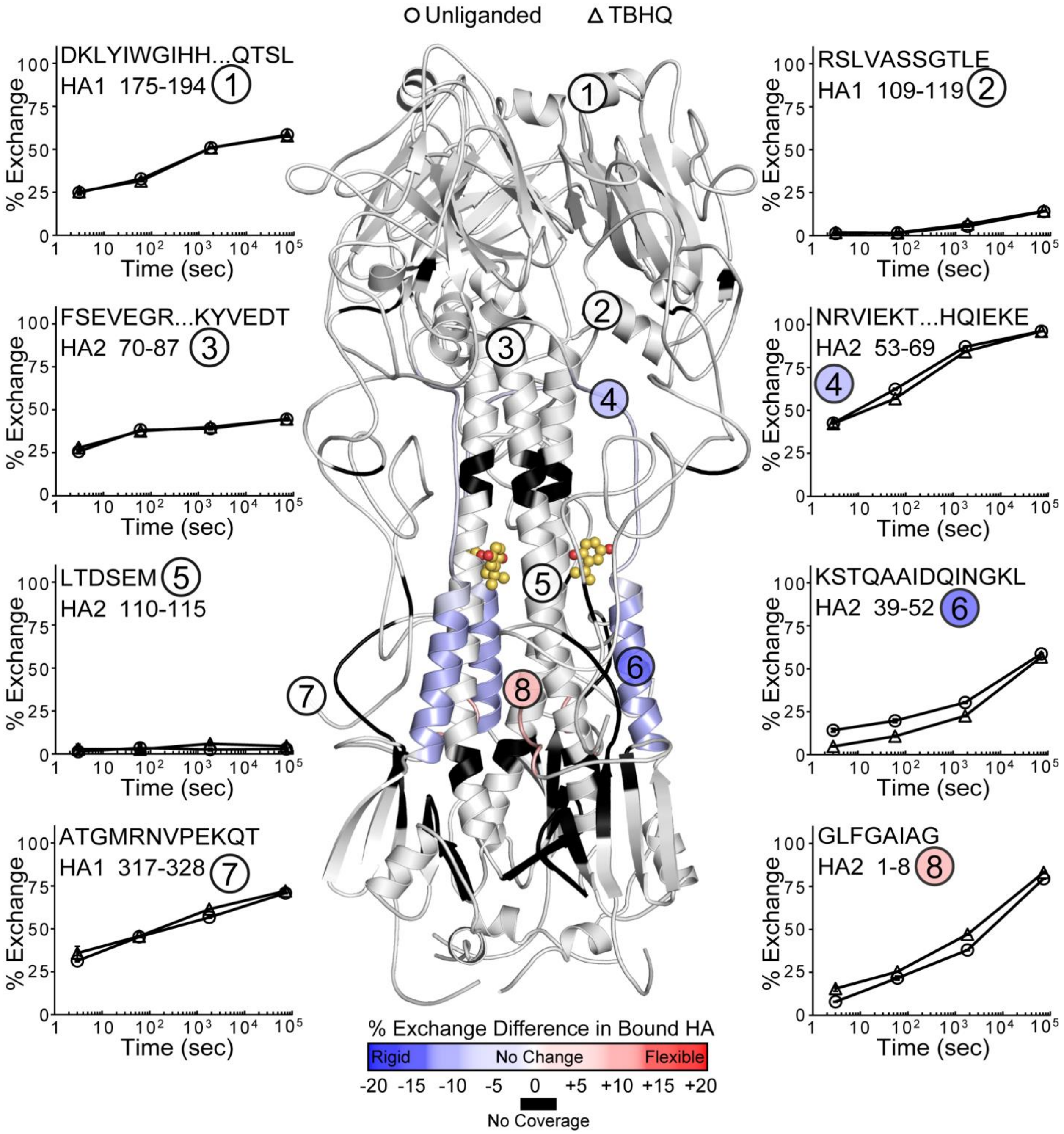

Figure 3.7 Dynamic Changes in H3-TBHQ Complex at pH 7.5. Exchange data is plotted as function of time for selected HA1 and HA2 peptides. The numbers correspond to the position of each sequence on the three-dimensional structure (middle panel) from PDB ID: 3EYM.[25] The percent exchange difference between unliganded and TBHQ bound H3 is shown for all peptides on the structure and colored as mentioned above. Error bars are the standard error from duplicate measurements and all colored differences on the structure are outside experimental error.

Protein	**Theoretical MW (KDa)**	**Experimental MW (KDa)**	**R_H[a] (nm)**	**R_G[b] (nm)**	**R_G[c] (nm)**	**D_{Max}[c] (nm)**	**T_m[d] (°C)**
BHA (H3)	210.0	212.8	5.9	4.7 ± 0.1	4.7±0.1	15.1	63.7
H3-FI6v3	359.0	366.7	7.0	5.4± 0.1	5.4±0.1	18.0	75.5
BHA (H1)	201.0	201.5	5.6	4.5± 0.1	4. 5±.01	13.4	63.5
H1-FI6v3	350.0	349.7	6.9	5.4 ± 0.1	5.4±0.1	18.3	73.8
H1-HB36.6	240.5	245.3	6.0	4.7±0.1	4.6±0.01	13.9	66.5

Table 3.1 Solution-phase Characterization of Stem Directed Ligands. Molecular Weight (MW), of Unliganded HA and HA Bound to Stem Directed Ligands. ***a***) Radius of Hydration (R_H) determined from SEC-DLS, ***b)*** Radius of Gyration (R_G) determined using the Guinier fit of the SEC-SAXS data, ***c)*** R_G and the maximum linear distance (D_{Max}) determined from real space SEC-SAXs data, ***d)*** Melting Temperature (T_m) determined from DLS.

CHAPTER III REFERENCES

1. Chen, R. & Holmes, E.C. Avian influenza virus exhibits rapid evolutionary dynamics. *Mol. Biol. Evol.* **23,** 2336-2341 (2006).
2. Wiley, D.C., Wilson, I.A. & Skehel, J.J. Structural identification of the antibody-binding sites of Hong Kong influenza haemagglutinin and their involvement in antigenic variation. *Nature* **289**, 373-8 (1981).
3. Gerhard, W., Yewdell, J., Frankel, M.E. & Webster, R. Antigenic structure of influenza virus haemagglutinin defined by hybridoma antibodies. *Nature* **290,** 713-717 (1981).
4. Corti, D. et al. A neutralizing antibody selected from plasma cells that binds to group 1 and group 2 influenza A hemagglutinins. *Science* **333**, 850-6 (2011).
5. Ekiert, D.C. et al. Antibody recognition of a highly conserved influenza virus epitope. *Science* **324**, 246-51 (2009).
6. Ekiert, D.C. et al. A highly conserved neutralizing epitope on group 2 influenza A viruses. *Science* **333**, 843-50 (2011).
7. Dreyfus, C., Ekiert, D.C. & Wilson, I.A. Structure of a classical broadly neutralizing stem antibody in complex with a pandemic H2 influenza virus hemagglutinin. *J Virol* **87,** 7149-7154 (2013).
8. Sui, J. et al. Structural and functional bases for broad-spectrum neutralization of avian and human influenza A viruses. *NSMB* **16**, 265-73 (2009).
9. Wu, Y. et al. A potent broad-spectrum protective human monoclonal antibody crosslinking two haemagglutinin monomers of influenza A virus. *Nat Commun* **6**, 7708 (2015).
10. Okuno, Y., Isegawa, Y., Sasao, F. & Ueda, S. A common neutralizing epitope conserved between the hemagglutinins of influenza A virus H1 and H2 strains. *J Virol* **67,** 2552-2558 (1993).
11. Wei, C.J. et al. Induction of broadly neutralizing H1N1 influenza antibodies by vaccination. *Science* **329**, 1060-1064 (2010).

12. Corti, D. et al. Heterosubtypic neutralizing antibodies are produced by individuals immunized with a seasonal influenza vaccine. *J Clin Invest* **120**, 1663-1673 (2010).

13. Wrammert, J. et al. Broadly cross-reactive antibodies dominate the human B cell response against 2009 pandemic H1N1 influenza virus infection. *The Journal of experimental medicine* **208**, 181-193 (2011).

14. Baker, D. & Agard, D.A. Influenza hemagglutinin: kinetic control of protein function. *Structure* **2**, 907-10 (1994).

15. Bullough, P.A., Hughson, F.M., Skehel, J.J. & Wiley, D.C. Structure of influenza haemagglutinin at the pH of membrane fusion. *Nature* **371**, 37-43 (1994).

16. Wilson, I.A., Skehel, J.J. & Wiley, D.C. Structure of the haemagglutinin membrane glycoprotein of influenza virus at 3 A resolution. *Nature* **289**, 366-373 (1981).

17. Carr, C.M., Chaudhry, C. & Kim, P.S. Influenza hemagglutinin is spring-loaded by a metastable native conformation. *PNAS* **94**, 14306-13 (1997).

18. Remeta, D.P. et al. Acid-induced changes in thermal stability and fusion activity of influenza hemagglutinin. *Biochemistry* **41**, 2044-2054 (2002).

19. Chen, J. et al. A soluble domain of the membrane-anchoring chain of influenza virus hemagglutinin (HA2) folds in Escherichia coli into the low-pH-induced conformation. *PNAS* **92**, 12205-12209 (1995).

20. Ruigrok, R.W. et al. Conformational changes in the hemagglutinin of influenza virus which accompany heat-induced fusion of virus with liposomes. *Virology* **155**, 484-97 (1986).

21. Russell, R.J. et al. H1 and H7 influenza haemagglutinin structures extend a structural classification of haemagglutinin subtypes. *Virology* **325**, 287-96 (2004).

22. Ha, Y., Stevens, D.J., Skehel, J.J. & Wiley, D.C. H5 avian and H9 swine influenza virus haemagglutinin structures: possible origin of influenza subtypes. *EMBO J* **21**, 865-75 (2002).

23. Fleishman, S.J. et al. Computational design of proteins targeting the conserved stem region of influenza hemagglutinin. *Science* **332**, 816-21 (2011).

24. Whitehead, T.A. et al. Optimization of affinity, specificity and function of designed influenza inhibitors using deep sequencing. *Nat Biotechnol* **30**, 543-8 (2012).

25. Russell, R.J. et al. Structure of influenza hemagglutinin in complex with an inhibitor of membrane fusion. *PNAS* **105**, 17736-41 (2008).

26. Schneidman-Duhovny, D., Hammel, M., Tainer, J.A. & Sali, A. Accurate SAXS profile computation and its assessment by contrast variation experiments. *Biophys J* **105**, 962-74 (2013).

27. Schneidman-Duhovny, D., Hammel, M. & Sali, A. FoXS: a web server for rapid computation and fitting of SAXS profiles. *Nucleic Acids Res* **38**, W540-544 (2010).

28. Garcia, N.K., Guttman, M., Ebner, J.L. & Lee, K.K. Dynamic changes during acid-induced activation of influenza hemagglutinin. *Structure* **23**, 665-676 (2015).

29. Guttman, M. et al. Antibody potency relates to the ability to recognize the closed, pre-fusion form of HIV Env. *Nat Commun* **6**, 1-11 (2015).

30. Friesen, R.H. et al. A common solution to group 2 influenza virus neutralization. *PNAS* **111**, 445-450 (2014).

31. Puri, A., Booy, F.P., Doms, R.W., White, J.M. & Blumenthal, R. Conformational changes and fusion activity of influenza virus hemagglutinin of the H2 and H3 subtypes: effects of acid pretreatment. *J Virol* **64**, 3824-3832 (1990).

32. Costello, D.A., Whittaker, G.R. & Daniel, S. Variations in pH sensitivity, acid stability, and fusogenicity of three influenza virus H3 subtypes. *J Virol* **89**, 350-360 (2015).

33. White, J.M. & Wilson, I.A. Anti-peptide antibodies detect steps in a protein conformational change: low-pH activation of the influenza virus hemagglutinin. *J Cell Biol* **105**, 2887-96 (1987).

34. Bottcher, C., Ludwig, K., Herrmann, A., van Heel, M. & Stark, H. Structure of influenza haemagglutinin at neutral and at fusogenic pH by electron cryo-microscopy. *FEBS Lett* **463**, 255-259 (1999).

35. Kemble, G.W., Bodian, D.L., Rose, J., Wilson, I.A. & White, J.M. Intermonomer disulfide bonds impair the fusion activity of influenza virus hemagglutinin. *J Virol* **66**, 4940-4950 (1992).

36. Fontana, J., Cardone, G., Heymann, J.B., Winkler, D.C. & Steven, A.C. Structural changes in Influenza virus at low pH characterized by cryo-electron tomography. *J Virol* **86**, 2919-2929 (2012).

37. Bandaranayake, A.D. et al. Daedalus: a robust, turnkey platform for rapid production of decigram quantities of active recombinant proteins in human cell lines using novel lentiviral vectors. *Nucleic Acids Research* **39,** e143 (2011).

38. Sali, A. & Blundell, T.L. Comparative protein modelling by satisfaction of spatial restraints. *J Mol Biol* **234**, 779-815 (1993).

39. Weinkam, P., Pons, J. & Sali, A. Structure-based model of allostery predicts coupling between distant sites. *PNAS* **109**, 4875-4880 (2012).

40. Guttman, M., Weinkam, P., Sali, A. & Lee, K.K. All-atom ensemble modeling to analyze small-angle x-ray scattering of glycosylated proteins. *Structure* **21**, 321-331 (2013).

41. Weis, W.I., Brunger, A.T., Skehel, J.J. & Wiley, D.C. Refinement of the influenza virus hemagglutinin by simulated annealing. in *J Mol Biol*, Vol. 212 737-761 (1990).

42. Gamblin, S.J. et al. The structure and receptor binding properties of the 1918 influenza hemagglutinin. *Science* **303**, 1838-1842 (2004).

43. Debye, P. Zerstreuung von röntgenstrahlen. *Annalen der Physik* **351**, 809-823 (1915).

44. Baker, P.R., Trinidad, J.C. & Chalkley, R.J. Modification site localization scoring integrated into a search engine. *Mol Cell Proteomics* **10**, M111.008078 (2011).

45. Wang, L., Pan, H. & Smith, D.L. Hydrogen exchange-mass spectrometry: optimization of digestion conditions. *Mol Cell Proteomics* **1**, 132-138 (2002).

46. Fang, J., Rand, K.D., Beuning, P.J. & Engen, J.R. False EX1 signatures caused by sample carryover during HX MS analyses. *Int J Mass Spectrom* **302**, 19-25 (2011).

47. Weis, D.D., Engen, J.R. & Kass, I.J. Semi-automated data processing of hydrogen exchange mass spectra using HX-Express. *J Am Soc Mass Spectrom* **17**, 1700-1703 (2006).

48. Guttman, M., Weis, D.D., Engen, J.R. & Lee, K.K. Analysis of overlapped and noisy hydrogen/deuterium exchange mass spectra. *J Am Soc Mass Spectrom* **24**, 1906-1912 (2013).

49. Folta-Stogniew, E. Oligomeric states of proteins determined by size-exclusion chromatography coupled with light scattering, absorbance, and refractive index detectors. *Methods Mol Biol* **328**, 97-112 (2006).

50. Wen, J., Arakawa, T. & Philo, J.S. Size-exclusion chromatography with on-line light-scattering, absorbance, and refractive index detectors for studying proteins and their interactions. *Anal Biochem* **240**, 155-166 (1996).

CHAPTER IV: Head Directed Inhibition of Influenza Hemagglutinin

INTRODUCTION

The membrane-distal HA1 subunit of the influenza membrane fusion glycoprotein, hemagglutinin (HA), triggers endocytosis of the virus by binding to sialic acid (SA) receptors abundant on the cell surface glycocalyx.[1-3] Early NMR studies investigating the affinity of SA analogues for the receptor binding site (RBS) within individual protomers found that the affinity for sialic acid at each site is relatively weak (~2mM), yet due to the high density of HA (~300-500 spikes) on the viral surface and three binding sites per trimer, viral adsorption is likely mediated through avidity.[4-9] Some of the residues required for SA binding are functionally conserved, however, the surrounding footprint is a major target for neutralizing antibodies (nabs) that inhibit virus engulfment by sterically occluding SA from the RBS, and such residues are hypervariable in order to escape from neutralization antibodies.[10-20]

Broadly neutralizing antibodies (bnabs) targeting only the receptor pocket have been identified and, analogous to SA attachment, bivalency appears to enhance receptor binding inhibition.[18-20] Nevertheless, the affinities of these head directed antibodies are much higher affinity interactions than SA. The conserved nature of the RBS makes it an attractive target for the rational design of small molecule inhibitors. Similar to the small protein inhibitors that inhibit fusion by targeting the HA2 stem, HA1 bnabs are also being used as lead molecules for protein inhibitors that block receptor binding. The trimeric Head Binder protein was designed by the Baker lab to mimic HA1 specific bnabs, and each protomer consists of a RBS binding lobe linked by a glycine rich linker to a trimerization domain held together through electrostatic interactions. Head Binder has been preliminarily shown to inhibit H3 isolates *in vitro* and though it cannot bind group-1 subtypes, the determined dissociation constant is near picomolar (personal communication, Baker Lab). The stoichiometry of inhibition is apparently governed by a 1:1 interaction of trimeric Head Binder for trimeric HA; however, initial negative stain electron microscopy images suggest that each binding lobe may rapidly dissociate from its respective HA1 binding site. Despite extensive efforts, no high resolution crystal structures have been solved for the trimeric Head Binder alone or in complex with HA (personal communication, Baker Lab).

Downstream from viral attachment, the pH-dependent transition from pre-fusion HA to a membrane active state requires several structural rearrangements, one of which is the unclamping of HA1 from the metastable HA2.[21-23] Despite the observation that the fusion peptide is one of the major structural elements to respond first to conditions mimicking the maturing endosome (~pH 5.5), membrane fusion can be prevented by cross-linking of the HA1 heads, either by incorporation of cysteine pairs at the HA1-HA1 interface, or through a unique antibody-antigen interaction at a similar region.[21,24,25] Analogous to other HA1 directed nabs, the HA3 specific HC63 nab neutralizes virus by blocking receptor binding as well as preventing the low pH transition required for membrane fusion.[15,16] However, it is unclear if HC63 binding prevents the post-fusion state by preventing HA1 dissociation or by also inducing large scale changes distal from the unique epitope. The crystal structure revealed an unprecedented 2:1 stoichiometry of HC63 to the HA trimer, even though the remaining volume within the trimer is capable of accommodating an additional HC63 fab arm, and early solution-phase characterization by sedimentation equilibrium analytical ultracentrifugation (SE-AUC) suggest that the crystal structure is an authentic representation of the solution state of the antigen-fab complex.[16,26]

In order to better understand the binding modes of HA1 directed ligands with HA, we use hydrogen-deuterium exchange mass spectrometry (HDX-MS) to study the conformational dynamics of the soluble HA ectodomain, BHA, bound to HC63, trimeric Head Binder and the SA receptor analogue, α2,6 sialyllactose (α2,6 SAL). We find that stabilization within the HA1 head is sufficient to prevent the low pH transitions, as it appears that HC63 locally ordered its epitope and no other regions within the trimer. Small angle X-ray scattering (SAXS) and multi-angle light scattering (MALS) suggest that in solution the complex of HC63 and HA shows a 3:1 fabs per HA trimer, in contrast to the published crystallographic 2:1 stoichiometry. Furthermore, trimeric Head Binder appears to exhibit rapid binding kinetics and our data cannot distinguish between the different proposed binding states. We also find that

BHA fully saturated with α2,6 SAL causes organization of the RBS alone, without affecting the structure of HA2.

RESULTS

Head Targeting Proteins Shift the Aggregation Threshold of Soluble HA

In chapter II and III, we demonstrated the application of native PAGE and dynamic light scattering (DLS) to monitor the pH-dependent aggregation of the soluble bromelain cleaved HA (BHA) as a proxy for the low pH structural transition. Here we examine the propensity of aggregation for unliganded H3 BHA, HC63-BHA and Head Binder-BHA complexes when exposed to low pH (Figure 4.1 and Table 4.1). The complex of HC63 with BHA could qualitatively be resolved by native PAGE both at neutral pH and after incubation at pH 4.9. In contrast, when incubated at low pH, aggregates incapable of entering the native-PAGE matrix were observed in the well of the lane corresponding to the acidified Head Binder-BHA complex, which suggests that the Head Binder does not prevent the low pH transition of soluble HA.

To assess the extent in which HC63 prevents temperature induced BHA aggregation, and to also determine if the melting state of Head Binder-BHA is similar to that of free BHA, the melting temperatures (T_m) of HC63-BHA and Head Binder-BHA complexes were calculated and compared against unliganded BHA as reported in Table 4.1. The T_m of unliganded BHA was 63.7°C, while the T_m of HC63-BHA was shifted to 68.4°C. Head Binder-BHA was also moderately shifted from 63.7°C to 65°C. While the T_m shift of HC63-BHA was more modest than that observed for FI6v3-BHAs (Table 3.1 and 4.1), it is still possible that HC63-BHA inhibits the structural changes in HA by preventing the pH-dependent uncaging of HA2 as hypothesized by others when studying the fusogenicity of chemically cross-linked HA.[24,25] The change in T_m for the Head Binder-BHA was only shifted by less than 2°C than that measured for unbound BHA, which suggests that the Head Binder only marginally stabilizes BHA and to a lesser extent than HC63.

Biophysical Characterization of HA Bound to Head Targeting Protein Inhibitors

Previous analytical ultracentrifugation and X-ray crystallography of HC63-BHA have reported an unexpected 2:1 stoichiometry of HC63 fabs for trimeric BHA, even though trimeric BHA can apparently accommodate three HC63 fabs per trimer.[16,26] Similarly, structural data for the Head Binder-BHA complex is currently limited to all-atom modeling, which suggests a 1:1 binding of the Head Binder to trimeric BHA. To test whether the former structural characterization accurately represents the solution-phase state of BHA bound to HC63 and the Head Binder, multi-angle light scattering (MALS) and DLS online with analytical size exclusion chromatography (SEC) was used to determine the stoichiometry and radius of hydration (R_H) of free BHA, HC63-BHA and Head Binder-BHA complexes (Table 4.1). The experimentally determined molecular weight of HC63-BHA was within 3% of the calculated molecular weight for a 3:1 stoichiometry, when properly accounting for the glycan content, suggesting that the solution-phase state of trimeric BHA is fully bound to three fabs. The R_H of the unliganded H3 BHA trimer increased from 5.9 nm to 7.1 nm with HC63 present, which is very similar to the increase of 5.9 nm to 7.0 nm for H3 BHA bound to three FI6v3 fabs (Table 3.1). The experimental molecular weight of Head Binder-BHA determined by MALS was 232.7 KDa, which is less than the theoretically calculated value of 279.1 KDa. The Head Binder-BHA SEC-MALS profile showed extensive peak broadening, which is consistent with disassociation of the ligand during the course of the size exclusion chromatography. The R_H determined from SEC-DLS of the Head Binder-BHA was 6.0 nm and did not show a large change from the bound state, which may be due to the proposed ligand disassociation.

To determine the overall shape and size of the BHA complexes, analytical SEC with online small angle X-ray scattering (SAXS) was performed (Figure 4.2 and 4.3). The radius of gyration (R_G) was calculated with the Guinier approximation and the interatomic distance distribution function, P(r); and the P(r) function also provided the maximum linear dimension, D_{max}, for each complex (Table 4.1). The reported R_G values were consistent between the two analytical approaches, demonstrating the quality of the data. In the HC63-BHA both the R_G and D_{max} values increase from 4.7 nm and 15.1 nm, respectively, to 6.0 nm, 20.2 nm relative to the unliganded state. BHA also exhibits an increase in both the R_G and D_{Max} of 5.6 nm, 20.6 nm respectively, in the presence of the Head Binder.

Thirty all-atom models of either two or three HC63 fabs bound to a glycosylated trimeric BHA were generated as an additional method to compare the previously reported 2:1 stoichiometry against the 3:1 stoichiometry observed by SEC-MALS (Table 4.1 and Figure 4.2). With the aid of the FoXS webserver, the theoretical scattering profiles of each modeled HC63 binding mode were calculated and the goodness of fit (χ) compared to the experimental SAXS data was determined, where the lowest χ represents the best fit. The models of BHA bound to 3 HC63 fabs were the most consistent with the experimental SAXS data with a χ of 1.14, while the best fit HC63-BHA with a 2:1 stoichiometry was 1.57. Additionally, multiple ensemble searches (MES) of the submitted models (~30 models from each binding state) did not minimize χ lower than that calculated for the HC63-BHA model with 3 fabs bound, which further supports a 3:1 binding stoichiometry in solution, and HC63-BHA will refer to the complex with 3:1 stoichiometry throughout the remainder of the text unless otherwise noted.

Since there are no published crystal structures of the Head Binder-BHA, all-atom models of the free trimeric Head Binder were produced with MODELER where each binding domain within the trimer was treated as a flexible unit relative to the initial rigid body model provided by the Baker lab (Figure 4.3 A and B). When both the flexible and rigid free Head Binder models were submitted to FoXS, the flexible model fit the experimental SAXS profile dramatically better with a χ of 1.27, relative to χ of 4.32 for the rigid model. Previously collected electron microscopy data of the Head Binder-BHA suggests that there may be an ensemble of conformations, and it is unclear if each HA1 binding site is occupied in the presence of the trimeric Head Binder (personal communication Baker lab). Therefore, using the flexible Head Binder model a series of flexible and glycosylated Head Binder-BHA models were generated in which one, two or three of the binding lobes within the trimeric Head Binder was associated with trimeric BHA and the collection of ensembles were submitted to FoXS, which calculated the best fit model relative to the experimental scattering data (Figure 4.3 C and D). Based on the χ values for one (1.26), two (1.20) and three (1.30) Head Binder lobes bound to BHA, were essentially indistinguishable from one another, suggesting that this method could not definitively discriminate between the models and therefore could not discern the exact binding mode for the Head Binder-BHA complex.

HC63 Stabilizes the Trimeric Interface at the Apex of HA

It has been shown that cross-linking the globular head prevents the pH-dependent conformational change required to promote membrane fusion. Blocking this large-scale rearrangement would require some structural ordering to stabilize the metastable conformation of the pre-fusion trimer, which has been accomplished through the introduction of disulfide bonds, or by through protein-protein interactions such as in an antigen-antibody interface. HDX-MS was used to assess the solution-phase dynamics of BHA bound to the HC63 fab to test how HC63 stabilizes the pre-fusion conformation (Figure 4.4). As reported in chapter III, the sequence coverage of BHA bound to HC63 was over 90% for both HA1 and HA2 subunits. Comparison of the HC63-BHA complex to unliganded BHA was used to identify and localize changes upon ligand binding, with significant differences assessed from the error from duplicate measurements. The mass envelopes during the course of exchange were unimodal for both the free and bound state, indicative of a single, uniform exchanging species, supporting a complete 3:1 binding stoichiometry. A 2:1 stoichiometry would have likely resulted in uneven bimodal mass envelopes at the regions proximal to the Fab binding site, as 1 of the 3 lobes would have a distinct exchange profile.

The binding site of HC63 is located at the apex of the trimer spanning multiple peptides covering the trimeric interface (HA1 195-211, peptide 8 and 212-228, peptide 9), the receptor binding site (HA1 121-147, peptide 1, 178-194, peptide 7 and 212-228, peptide 9) and a portion of the seven-stranded β-sheet that is solvent accessible (HA1 162-174, peptide 5). All of the HDX kinetics for each peptide within the HC63 binding site exhibited protection to some extent while in the complex (Figure 4.4). The peptide spanning the outermost surface of the HA1-HA1 trimeric interface (HA1 212-228, peptide 9) showed the most dramatic change upon binding, while the solvent occluded inner portion of this interface (HA1 195-211, peptide 8) was protected to a lesser extent. The RBS (HA1 121-147, peptide 1, 178-194, peptide 7) and solvent accessible β-sheet (HA1 162-174, peptide 5) were intermediately protected in the complex, which is in good agreement with the binding footprint from the crystal structure and HC63-BHA model. Portions of HA1 distal from the binding site (HA1 109-120, peptide 3 and 259-268, peptide 10) were unaffected by the fab, which suggests that HC63 binding stabilizes HA1 head locally. Furthermore, the exchange profiles for nearly all regions within the fusion stem (HA2 1-8, peptide 2, 70-87, peptide 6) were identical in both the free and bound state of BHA; though the B-loop exhibited some slight protection but only at the third time point.

The Head Binder Stabilizes the Trimeric Interface and Receptor Binding Site of HA

To determine whether one, two or three binding lobes of the Head Binder were associated to each HA1 trimer within the complex, HDX-MS of the complex and free BHA was performed (Figure 4.5). The same sequence coverage reported above was also obtained for Head Binder-BHA. Similar to HC63-BHA, all mass envelopes displayed unimodal exchange profiles with no observable increase in isotopic peak widths, consistent with a homogenous complex in which, all three binding lobes were associated with BHA.

Overall, regions outside of the binding site included peptides near or within the HA1-HA2 interface (HA1 269-277, peptide 4) as well as the entirety of the HA2 stem (HA2 1-8, peptide 6). The binding domain of the complex is formed from peptides encompassing the RBS and HA1-HA1 trimeric interface (HA1 121-147, peptide 1, 152-174, peptide 3, 178-194, peptide 5 and 212-228, peptide 2). The RBS helix (HA1 178-194, peptide 5) showed the largest degree of protection within the Head Binder-BHA complex, as did the solvent accessible loop at the edge of the globular head (HA1 121-147, peptide 1) and the trimeric interface (HA1 212-228, peptide 2). The peptide spanning the RBS a protected region of the seven-stranded β-sheet within the globular head (HA1 152-174, peptide 3) exhibited slightly depressed deuterium incorporation when bound. These profiles were unable to describe whether each binding site within BHA was occupied differently from one another. However, it does appear that binding is limited to the globular head, and at the RBS, which was the intended binding site of this designed protein.

Sialic Acid Analogue Orders the HA Receptor Binding Site

To determine whether sialic acid binding acts locally within the HA1 RBS or if it triggers allosteric effects within the trimer to prime it for subsequent fusion activation, HDX-MS of BHA bound to α2,6 sialyllactose (α2,6 SAL) was compared against an unliganded BHA (Figure 4.6). All mass shifts were observed to be unimodal and consistent with a single exchanging population for both protein states. Furthermore, the peptide coverage analyzed within this experiment was consistent with that of the previously studied isolates reported above and in chapter II and II. Peptides whose sequences encompass the sialic acid binding groove exhibited protection from exchange in the liganded state. The solvent accessible loop (HA1 125-147, peptide 1) showed the greatest extent of protection within the whole data set, while the trimeric interface (HA1 212-228, peptide 3) displayed moderate exchange. The helix involved in receptor binding (HA1 178-194, peptide 5) was also protected in the presence of sialic acid but to a lesser extent than the previously mentioned sites. Furthermore, other regions within HA1 distal to the RBS (HA1 109-120, peptide 2 and 233-243, peptide 8) exhibited no change in exchange between the bound and free state of BHA. Additionally, HA2 peptides including B-loop (HA53-69, peptide 4 and 70-87, peptide 7) and coiled-coil core of the trimer (HA2 92-99, peptide 9) were also invariant between the two examined states. These data definitely show that sialic acid binding induces only small changes focused entirely within the RBS without inducing any large-scale changes to the rest of the trimer.

DISCUSSION

Influenza viral attachment and subsequent endocytosis is inhibited when neutralizing antibodies sterically occlude the HA1 receptor binding site from attaching to sialic acid moieties found on host cell surfaces. The H3 specific nab HC63 has been shown to bind HA1 to inhibit receptor attachment and prevent the low pH structural transition.[15,16] While it has been shown in solution and in the crystal structure that the stoichiometry of binding is an unprecedented 2:1 of fab:HA, our findings suggest HC63 binds HA in a more conventional 3:1 fashion.[26] The previously reported stoichiometry observed in the crystal structure was substantiated by SE-AUC, which is a technique that is independent of shape. SE-

AUC calculates the molecular weight of a protein in solution by relying on the Archimedes' principle in which, the mass of the protein acted on by the centrifugal force is calculated by the mass displaced by the solvent or buoyant molar mass.[27] In such analyses, the buoyant molar mass requires the use of the partial specific volume (v-bar), which is dependent upon the molecular composition. For glycoproteins, the v-bar must be calculated as a weight-average from both the protein and glycan composition within the glycoprotein, which can be difficult if the average glycan composition is unknown.[28] Unfortunately, the aforementioned SE-AUC study of HC63 did not properly account for the glycosylation of HA significantly offsetting v-bar, which would result in an artificially lower determined molecular weight, and therefore an incorrectly inferred stoichiometry.[26-28] Furthermore, in the same study did not include characterization of the unliganded BHA to validate their approach.

Similar to SE-AUC v-bar, the refractive index for SEC-MALS requires the correct calculation of the refractive index offset due to the glycan and protein composition within a glycoprotein analyte. The molecular weights measured by SEC-MALS are consistent with a trimer in complex with three HC63 fab lobes (table 4.1). Our all-atom modeling of either 2:1 and 3:1 HC63 bound to HA includes the HA glycans, which also contribute significantly to the X-ray scattering pattern of BHA and the theoretical scattering pattern generated from the 3:1 stoichiometric model fit the experimental SAXS data with a lower chi value. Overall our data strongly suggest that the previously reported stoichiometry is not reflective of the complex in solution. Therefore, the stoichiometry observed in the X-ray crystal structure is likely an artifact of crystallization conditions; nonetheless, the high resolution structure has been useful for identifying alternative modes of HA inhibition by nabs. We also determined by HDX-MS that HC63 stabilizes the HA1 epitope, and that HA1 uncaging is likely inhibited through the stabilizing contacts between HC63 and the HA1-HA1 interface. These findings are consistent with the previously observed instances of fusion inhibition when HA1 is chemically crosslinked to adjacent HA1 protomers.[24,25]

The small molecule receptor analogue α2,6 sialyllactose in complex with H3 BHA has a stabilizing effect solely within the receptor binding domain of HA1. To our knowledge, this is the first evidence that that receptor binding does not induce allosteric effects within the fusion domain of the trimer. While these stabilizing effects were outside of experimental error, the milimolar K_D for monovalent sialosides are not therapeutically suitable.[5,6] However, efforts to design multivalent sialosides show some promise with infection inhibition IC_{50} close to 2µM for some compounds.[29,30] More recently *in silico* design of multivalent sialosides have been able to generate stronger binders by using peptidic linkers attached to each sialoside, which results in a nanomolar K_D and may provide a useful therapeutic.[31]

The trimeric Head Binder protein targets the HA1 receptor binding domain with an effective K_D near picomolar and is another example of rational *in silico* design (communicated by Baker Lab). While our solution-based techniques could not conclusively establish the stoichiometry of binding, the increased molar mass via SEC-MALS and DLS suggested that the complex was formed for analysis. However, the SEC-MALS chromatography exhibited peak broadening, which is indicative of the complex dissociating during the run, and as a result the experimental molecular weight was much less than expected for a 1:1 association of trimeric Head Binder and HA. While the trimeric Head Binder may have picomolar affinity for the trimeric HA, we surmise that the interaction between the binding lobe protomer and HA1protomer is relatively weak and the trimerization domain within the Head Binder localizes three binding lobes within proximity with the HA trimer for polyvalent binding. The HA1 receptor binding specific bnabs exhibit similar avidity effects upon binding as do the polyvalent sialiosides versus the monovalent SAL analogues.

HDX-MS revealed that the Head Binder binds HA1 and stabilizes the binding interface within the receptor binding pocket and the adjacent HA1-HA1 interface, though in the presence of low pH, the Head Binder cannot prevent the conformational change associated with membrane fusion. The magnitude of stabilization in the HDX-MS data was relatively subtle for such a large binding footprint as compared to the HC63 fab. If the individual lobes of the head binder were undergoing rapid association/dissociation at each HA lobe, it might result in such a low degree of stabilization at the binding interface. Such fast kinetics would be consistent with the peak broadening observed by SEC-MALS. Since the Head Binder recognizes the sialic acid binding site, HA attachment is likely inhibited by similar mechanisms as HC63 and other HA1 directed nabs, which sterically blocks receptor binding.

EXPERIMENTAL PROCEDURES

Influenza and BHA Preparation

Please refer to chapter II for detailed procedure of H3 BHA preparation and purification.

H3 Hemagglutinin Head Targeting Protein Complexes

Neutralizing Antibody HC63 Fab Production and Purification

Stable 293-Freestyle cells capable of expressing and secreting full-length human HC63 neutralizing human IgG_1 were produced using the Daedalus method and were a kind gift from the Jesse Bloom Lab (Fred Hutchinson Cancer Research Center)[32]. The cells were cultured identical to the stable FI6v3 producing cell lines as mentioned in chapter III and HC63 protein expression was also confirmed by western blot analysis. The HC63 IgG_1 was purified over Protein A affinity resin identically to the procedure described for FI6v3 IgG_1 in chapter III. Following purification of full-length HC63, the same Pierce^{TM} Fab Preparation Kit and fab digestion protocol as mentioned in chapter III was implemented. The HC63 fab was eluted from the Protein A affinity resin with 200mM Glycine pH 2.5 and immediately neutralized to pH 7.5 using 1M Tris pH 8.0. HC63 fab purity was analyzed via SDS-PAGE and the molecular weight was verified by MALDI-TOF mass spectrometry. The HC63 fab containing fractions were concentrated and buffer exchanged to 10.5 mg/mL in phosphate-buffered saline (PBS) (10mM Phosphate, 150 mM NaCl, 0.02% NaN_3, pH 7.5) using a spin-filter with a molecular weight cutoff of 30KD. And hereafter all HC63 fabs will simply be referred to as HC63 for simplicity unless otherwise noted.

Head Binder Protein Production and Purification

The group-2 specific trimeric head targeting protein was designed, expressed and purified by Eva-Maria Strauch, Ph.D. in the Baker Lab (University of Washington Biochemistry Department). The accurate molecular weight of the protomer was determined by MALDI-TOF mass spectrometry.

Small Angle X-Ray Scattering (SAXS) and Modeling of H3 Head Targeting Protein Complexes

1mg/mL HC63-BHA and Head Binder-BHA complexes were made by mixing purified BHA with a 3-fold molar excess of HC63 or Head Binder. The solutions were allowed to incubate at 4°C overnight to ensure a maximally bound state prior to SEC in-line with SAXS, as described in detail previously in chapter II. The free Head Binder was also analyzed by SEC in-line with SAXS as described in detail previously in chapter II; with the exception that the detector distance was changed to 1.7 m to obtain a maximum resolution conducive for smaller proteins.

All-Atom Ensemble Modeling of Glycosylated HA-Head Binding Complexes

All-atom glycosylated models of unliganded H3 BHA, BHA bound to either HC63 or the Head Binder were generated using MODELER as described in chapter III. Crystal structures of non- or partially glycosylated unliganded BHA (3HMG), HC63 bound BHA (1KEN) were used as alignment templates for generation of the initial three-dimensional models, and the BHA glycan positions were mapped out and implemented as described in chapter III. The published crystal structure of HC63 only contains two of three HA1 subunits in complex with two HC63 fabs, though the remaining unbound HA1 volume appears capable of accommodating a third HC63 fab arm. Thus, two different HC63-BHA ensembles were created in which, two or three HC63 fab arms were modeled bound to the BHA trimer. All-atom models of the free trimeric Head Binder and the trimeric Head Binder bound to three HA1 heads were provided by the Baker lab. The accurate mass of the Head Binder was determined by MALDI-TOF mass spectrometry confirmed the provided protein sequence. For the free Head Binder ensembles, the glycine linkers connecting the binding domains to the trimerization domain were left unrestrained to allow them to sample conformational space while the trimerization fold was restrained as a rigid-body in the template. As for the BHA bound Head Binder three different ensembles were created in which one, two or three binding domains of the Head Binder were bound one, two or three HA1 subunits, respectively, within the BHA trimer while constraining the Head Binder trimerization domain to the rigid-body template.

Consistency of the models to the experimental SAXS data was analyzed with FoXS as described in chapter III. Due to the intrinsic flexibility and possible stoichiometric intricacies associated with each H3 HA head targeting protein complex, FoXS was also used for multiple ensemble searches (MES) of conformations within a collection of submitted ensembles with distinct conformations (at least 30 all-atom ensembles) to determine whether a single state or a combination of states was sufficient for minimizing the χ value.

Hydrogen Deuterium Exchange (HDX)

HA-Head Targeting Protein Complexes

Protein stocks of unliganded BHA, HC63 BHA and Head Binder in complex with H3 BHA were prepared as described above with the addition of 1 µM of the tetra peptides PPPI and PPPF to be used as an internal standard for the intrinsic exchange rate. Samples were prepared and HDX reactions of each protein stock or complex were initiated and quenched as indicated in chapter III and all reaction were performed on the same day for comparison. Undeuterated, “zero” time points and fully deuterated “protein” and “peptide” controls were made identically to those described in chapter III.

H3 HA-α2,6 Sialyllactose Receptor Analogue Complex

HA human receptor analogue α2,6 sialyllactose (α2,6 SAL) and sucrose were purchased from Sigma Aldrich at 97% purity. A deuterated stock of either 200 mM α2,6 SAL or sucrose was made by resuspending either glycan in 85% D_2O and dried under vacuum , this process was repeated at least three times for α2,6 SAL to exchange amide protons with deuterons prior to resuspension in deuteration buffer (10 mM Hepes, 150 mM NaCl, 0.02% NaN_3). Undeuterated glycan stocks were made similarly to the deuterated stocks with the use of optima pure water in place of D_2O. H3 BHA in complex with α2,6 SAL was prepared by pre-incubating 10 µM BHA with 100 mM undeuterated α2,6 SAL in a final stock buffer (10 mM Hepes, 150 mM NaCl, 0.02% NaN_3, 6 µM PPPI) for at least 30 minutes to ensure an ~98% fully bound complex (K_D = 2 mM), and the unliganded BHA stock was prepared identically by substituting 100 mM sucrose (Sigma Aldrich) in place of α2,6 SAL to match the viscosity of the bound state. Deuteration reactions were initiated by diluting 7 µg of α2,6 SAL bound to BHA into the α2,6 SAL deuteration buffer for a final pH of 7.5 and performed at room temperature with time points ranging from 3 seconds, 1 minute, 30 minutes and 20 hours, while the unliganded BHA reactions replaced α2,6 SAL deuteration buffer with the sucrose deuteration buffer and carried out identically. All reactions were quenched with ice cold quench buffer (100 mM TCEP, 0.2% formic acid [FA]) for a final pH of 2.5, and digested with 30 µg of porcine pepsin for 5 min, frozen in liquid nitrogen and stored at -80°C until analysis. All undeuterated, "zero" and fully deuterated standards were prepared as in chapter III ; however, the addition of 100 mM sucrose was used to account for differences in viscosity.

Mass Spectrometry

Identification of BHA peptides

Undeuterated peptides of H3 BHA were identified on a Waters Synapt G1 HDMS with the identical liquid chromatography and mass spectrometry parameters as reported in chapter II.

Analysis of HA-Head Targeting Protein Complexes

Please refer to chapter III for a detailed description of the Waters Synapt G2 HDMS analysis protocol and downstream mass shift and percent exchange calculations.

Analysis of HA-α2,6 Sialyllactose Receptor Analogue Complex

HDX samples were analyzed on Waters Synapt G1 HDMS as described in chapter II. Mass shifts, percent deuteration and experimental error for each observable peptide were calculated as described in chapter III with the updated HX-Express v2 software (Guttman 2013b, HXMS.com).

Light Scattering of HA-Head Targeting Protein Complexes

Multi-angle Light Scattering (MALS)

Stocks of unliganded H3 BHA and H3 BHA bound to HC63 or Head Binder were made as described above for a final protein complex concentration of 1mg/mL and purified via HPLC SEC with online MALS as explained in the chapter III. Molecular mass and radius of hydration (R_H) was calculated using ASTRA software package (Wyatt Technologies).

Thermal Melting Curves and Aggregation Onset

The eluate peak of each complex analyzed by MALS was also collected for determination of melting and aggregation temperatures using a DyanPro NanoStar (Wyatt Technologies) dynamic light scattering (DLS) instrument. Samples were prepared, melting temperatures (T_m) and onset of aggregation was determined as in chapter III.

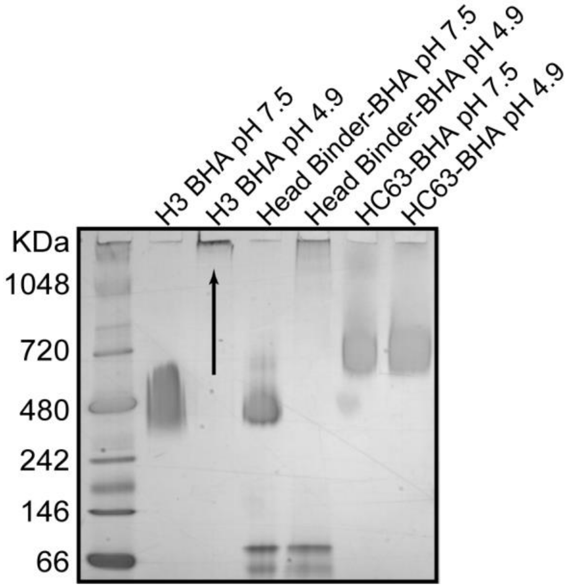

Figure 4.1 Native PAGE of BHA in Complex with Head Directed Ligands. Aggregation profile of unliganded BHA, Head Binder-BHA complex, and HC63-BHA complex. All BHA states were incubated at neutral pH or pH 4.0 prior to loading, BHA aggregates do not enter the gel matrix.

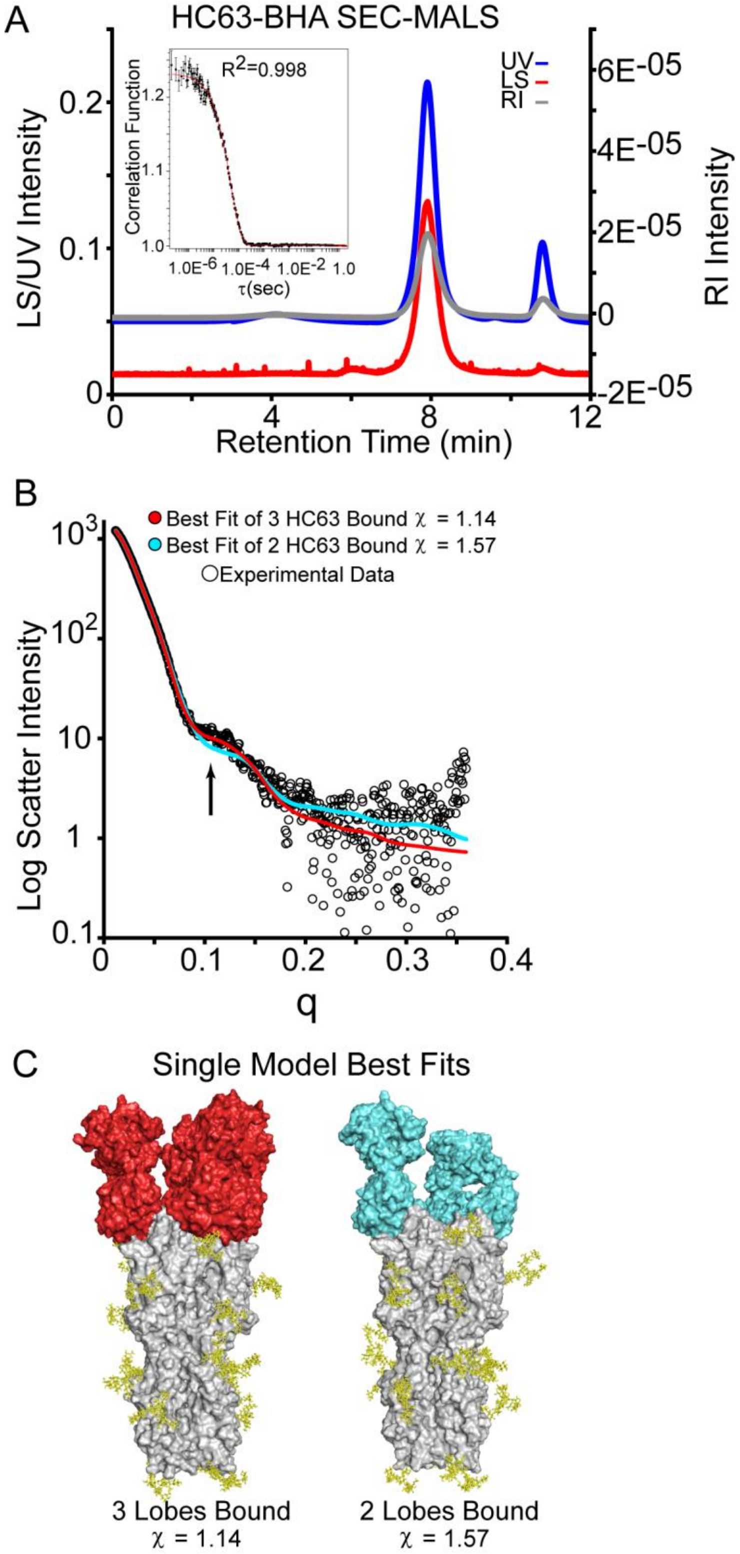

Figure 4.2 SEC-MALS, SAXS and Modeling of HC63-BHA. A) Size exclusion chromatography (SEC) multiangle light scattering (MALS) and dynamic light scattering (DLS) for HC63-BHA complex. The

UV absorbance intensity (blue), MALS intensity (red) and refractive index (RI) intensity (grey) are shown as a function of time. The correlation function (inset) for the DLS data is also shown with the R^2 fit=0.998. **B)** Experimental SAXS data (black circles) for HC63-BHA complex and theoretical scattering curve of all-atom models of either 3:1 stoichiometry (red fit) or 2:1 stoichiometry (cyan fit), with goodness of fit χ=1.14 and 1.57, respectively. **C)** Glycosylated (yellow) all-atom models of HC63-BHA complex with 3:1 HC63 (red) bound to a single HA trimer (grey) or 2:1 HC63 (cyan) bound to a single HA trimer (grey). The PDB ID: 1KEN was used as an initial template.[16]

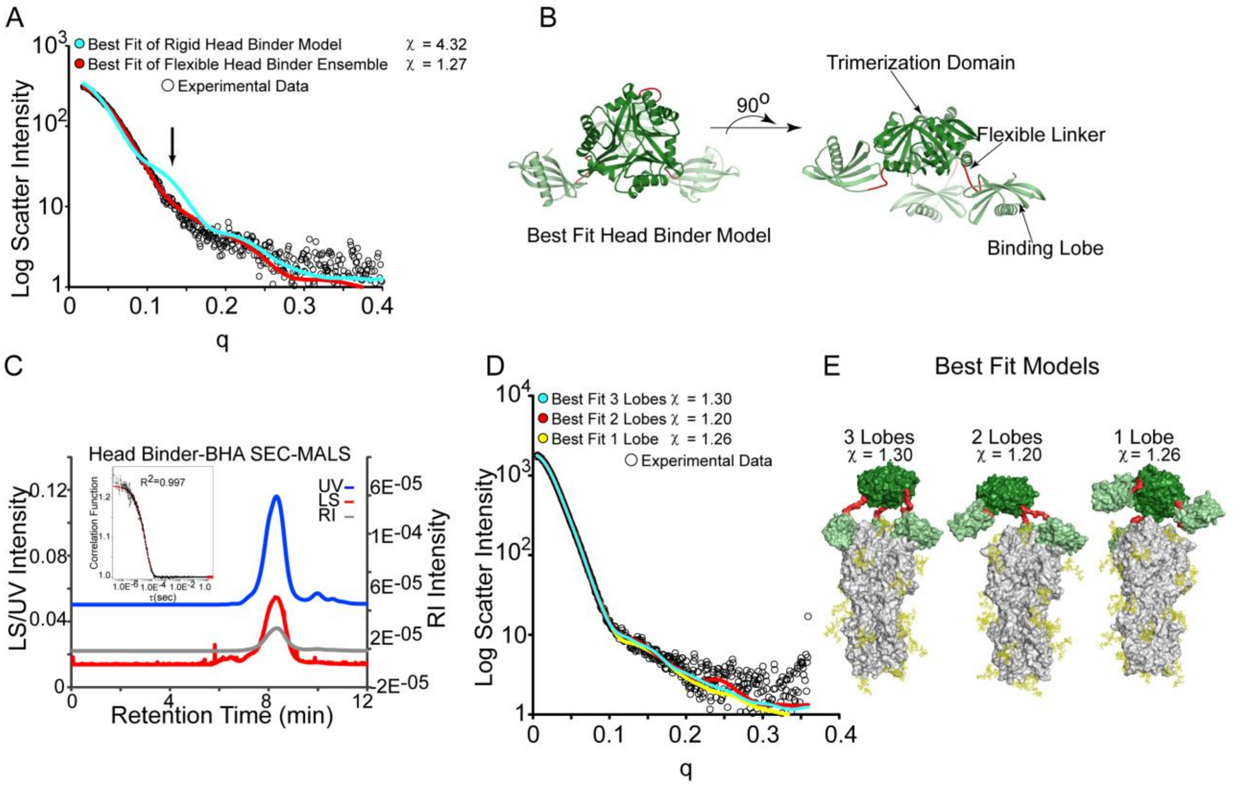

Figure 4.3 SEC-MALS, SAXS and Modeling of Head Binder and Head Binder-BHA. A) Experimental SAXS data (black circles) for Head Binder alone from SEC, and theoretical scattering curve of rigid body model (cyan fit) and flexible ensemble (red fit) with χ= 4.32 and 1.27, respectively. **B)** Best selected all-atom model of Head Binder alone where the trimerization domain shown in dark green, flexible linker shown in red and binding lobes shown in pale green. Initial model provided by the Baker Lab. **C)** Size exclusion chromatography (SEC) multiangle light scattering (MALS) and DLS data for the Head Binder-BHA complex. All parameters are as described in figure 4.2 A with the DLS (inset) R^2 fit=0.997. **D)** Experimental SAXS data (black circles) for Head Binder-BHA, theoretical scattering of all-atom models with 3 binding lobes bound to H3 (cyan fit), 2 binding lobes bound to H3 (red fit) and 1 binding lobe bound to H3 (yellow), with χ of 1.30, 1.20, and 1.26, respectively. **E)** All-atom ensembles of the single best fit model from (C), where the Head Binder domains are colored as in (B) and glycosylated H3 HA is shown in grey with glycans in yellow.

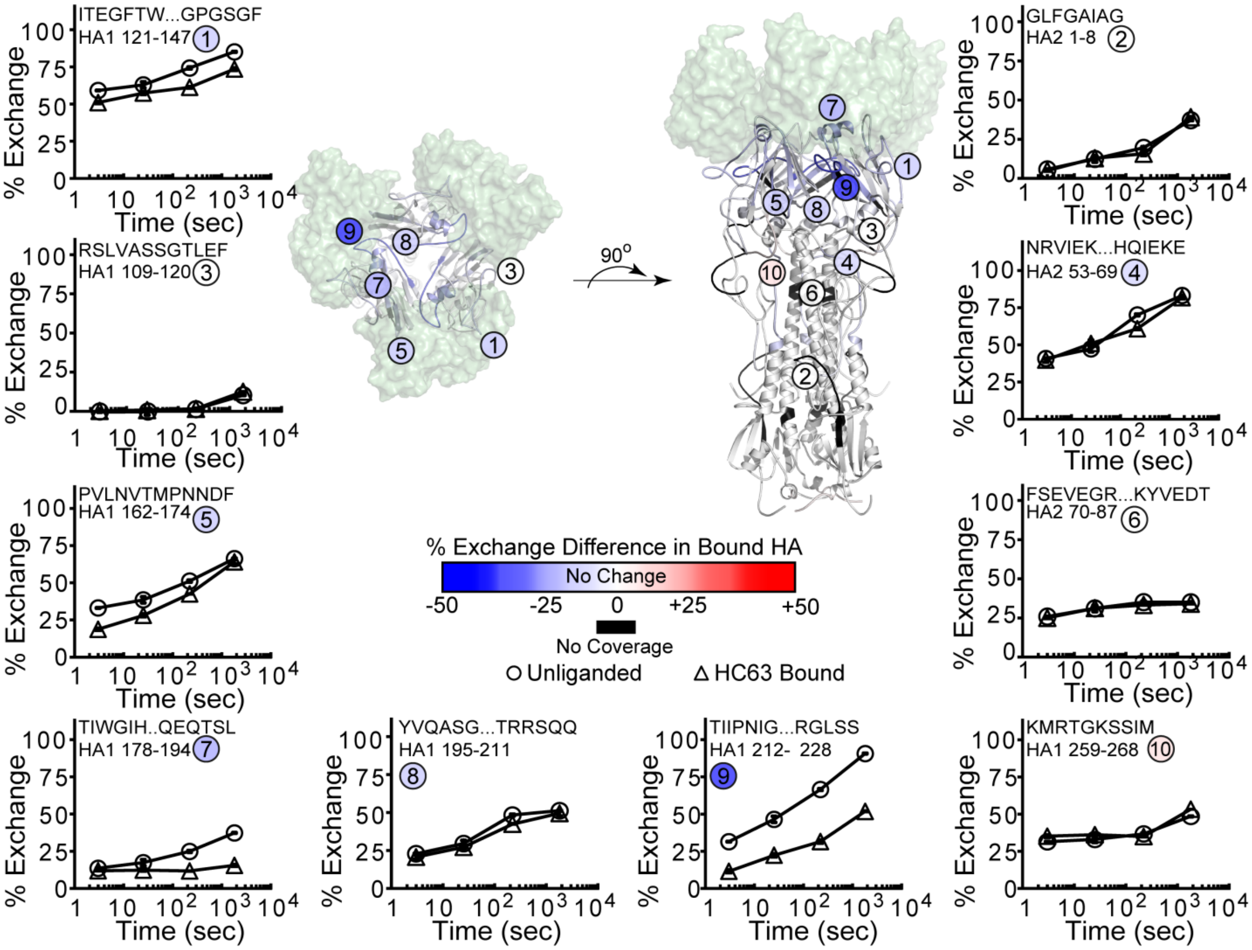

Figure 4.4 Dynamic Changes within HC63-BHA Complex at pH 7.5. Exchange profiles of selected HA1 and HA2 peptides are plotted as function of time for the unliganded (circles) and the HC63 bound (triangles) data sets. The sequences and subunits are denoted for each peptide and given a number that corresponds to the peptide position within the three-dimensional structure (middle panel) from the all-atom model in Figure 4.2. The percent exchange difference between the free state and bound state is plotted on the structure for all the observed peptides and the heat map corresponds to regions that are more protected in the bound state (blue), invariant regions (white), more flexible in the bound state (red) and no coverage (black). HC63 fabs are shown in green.

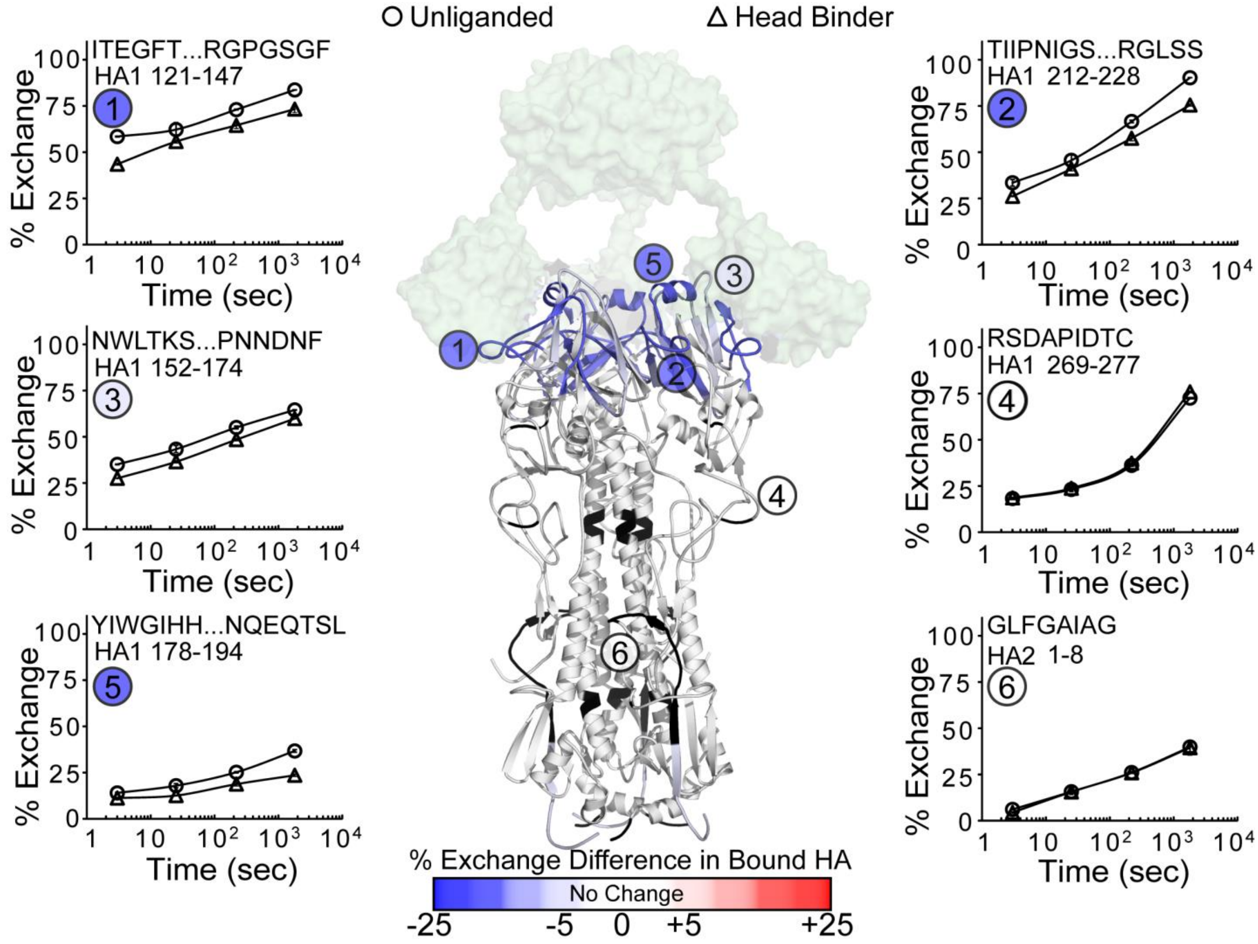

Figure 4.5 Dynamic Changes within Head Binder-BHA Complex at pH 7.5. Selected peptides for the exchange data is plotted as function of time for the unliganded state (circles) and Head Binder complex (triangles). The peptide position and sequence are shown for each plot with a circled number that corresponds to the position within the structure in the middle panel provided from the all-atom model. The percent exchange difference between the free and bound state are represented as in Figure 4.4. The Head Binder is shown in green.

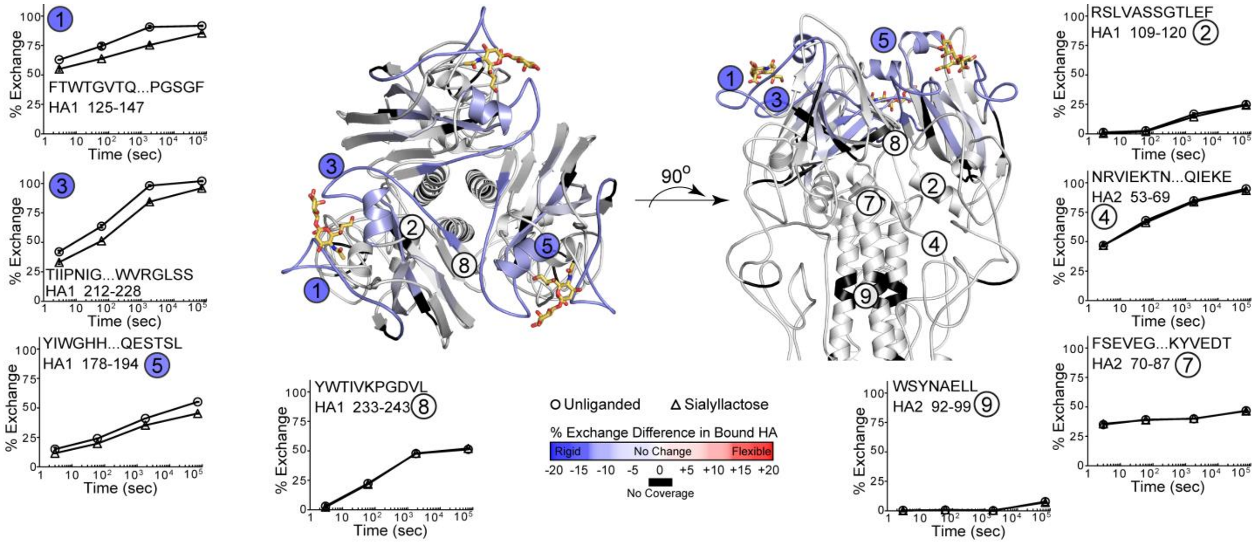

Figure 4.6 Dynamic Changes within the Receptor Binding Domain of α2,6 SAL-BHA. Selected peptides for the exchange data represented as a function of time for unliganded (circles) and α2,6 sialyllactose-bound (α2,6 SAL-BHA triangles) BHA. The peptide location and sequence are provided for each plot and given a number that corresponds to the three-dimensional location within the H3 structure bound to α2,6 sialyllactose shown as yellow sticks in PDB ID: 2YPG.[33] The percent exchange difference between the free and bound state is plotted within the trimer and colored as in Figure 4.4.

Protein	**Theoretical MW (KDa)**	**Experimental MW (KDa)**	**R_H [a] (nm)**	**R_G [b] (nm)**	**R_G [c] (nm)**	**D_{Max} [c] (nm)**	**T_m [d] (°C)**
BHA (H3)	210.0	212.8	5.9	4.7 ± 0.1	4.7±0.1	15.1	63.7
HC63-BHA	355.2	345.1	7.1	6.0±0.1	6.1±0.1	20.2	68.4
Head Binder-BHA	279.1	232.7	6.0	5.5±0.1	5.6±0.1	20.6	65.0

Table 4.1 Solution-phase Characterization of Head Directed Ligands. Molecular Weight (MW) of Unliganded H3 HA and H3 Bound to Head Directed Ligands. ***a)*** Radius of Hydration (R_H) determined from SEC-DLS, ***b)*** Radius of Gyration (R_G) determined using the Guinier fit of the SEC-SAXS data, ***c)*** R_G and the maximum linear distance (D_{Max}) determined from real space SEC-SAXs data, ***d)*** Melting Temperature (T_m) determined from DLS.

CHAPTER IV REFERENCES

1. Palese, P. & Compans, R.W. Inhibition of influenza virus replication in tissue culture by 2-deoxy-2, 3-dehydro-N-trifluoroacetylneuraminic acid (FANA): mechanism of action. *J Gen. Virol.* **33,** 159-163 (1976).
2. Skehel, J.J. & Wiley, D.C. Receptor binding and membrane fusion in virus entry: the influenza hemagglutinin. *Annu Rev Biochem* **69,** 531-569 (2000).
3. Rogers, G.N. & Paulson, J.C. Receptor determinants of human and animal influenza virus isolates: differences in receptor specificity of the H3 hemagglutinin based on species of origin. *Virology* **127,** 361-373 (1983).
4. Harris, A. et al. Influenza virus pleiomorphy characterized by cryoelectron tomography. *PNAS* **103,** 19123-19127 (2006).
5. Sauter, N.K. et al. Hemagglutinins from two influenza virus variants bind to sialic acid derivatives with millimolar dissociation constants: a 500-MHz proton nuclear magnetic resonance study. *Biochemistry* **28,** 8388-96 (1989).
6. Sauter, N.K. et al. Binding of influenza virus hemagglutinin to analogs of its cell-surface receptor, sialic acid: analysis by proton nuclear magnetic resonance spectroscopy and X-ray crystallography. *Biochemistry* **31,** 9609-9621 (1992).
7. Hanson, J.E., Sauter, N.K., Skehel, J.J. & Wiley, D.C. Proton nuclear magnetic resonance studies of the binding of sialosides to intact influenza virus. *Virology* **189,** 525-533 (1992).
8. Ha, Y., Stevens, D.J., Skehel, J.J. & Wiley, D.C. X-ray structures of H5 avian and H9 swine influenza virus hemagglutinins bound to avian and human receptor analogs. *PNAS* **98,** 11181-11186 (2001).
9. Stevens, J. et al. Structure of the uncleaved human H1 hemagglutinin from the extinct 1918 influenza virus. *Science* **303,** 1866-1870 (2004).
10. Connor, R.J., Kawaoka, Y., Webster, R.G. & Paulson, J.C. Receptor specificity in human, avian, and equine H2 and H3 influenza virus isolates. *Virology* **205**, 17-23 (1994).

11. Matrosovich, M. et al. Early alterations of the receptor-binding properties of H1, H2, and H3 avian influenza virus hemagglutinins after their introduction into mammals. *J Virol* **74,** 8502-8512 (2000).

12. Wiley, D.C., Wilson, I.A. & Skehel, J.J. Structural identification of the antibody-binding sites of Hong Kong influenza haemagglutinin and their involvement in antigenic variation. *Nature* **289,** 373-8 (1981).

13. Gerhard, W., Yewdell, J., Frankel, M.E. & Webster, R. Antigenic structure of influenza virus haemagglutinin defined by hybridoma antibodies. *Nature* **290,** 713-717 (1981).

14. Bizebard, T. et al. Structure of influenza virus haemagglutinin complexed with a neutralizing antibody. *Nature* **376,** 92-94 (1995).

15. Knossow, M. et al. Mechanism of neutralization of influenza virus infectivity by antibodies. *Virology* **302,** 294-8 (2002).

16. Barbey-Martin, C. et al. An antibody that prevents the hemagglutinin low pH fusogenic transition. *Virology* **294,** 70-4 (2002).

17. Lee, P.S. et al. Heterosubtypic antibody recognition of the influenza virus hemagglutinin receptor binding site enhanced by avidity. *PNAS* **109,** 17040-17045 (2012).

18. Xu, R., McBride, R., Nycholat, C.M., Paulson, J.C. & Wilson, I.A. Structural characterization of the hemagglutinin receptor specificity from the 2009 H1N1 influenza pandemic. *J Virol* **86,** 982-90 (2012).

19. Xu, R. et al. A recurring motif for antibody recognition of the receptor-binding site of influenza hemagglutinin. *N SMB* **20,** 363-370 (2013).

20. Lee, P.S. et al. Receptor mimicry by antibody F045-092 facilitates universal binding to the H3 subtype of influenza virus. *Nat. Comm.* **5** (2014).

21. White, J.M. & Wilson, I.A. Anti-peptide antibodies detect steps in a protein conformational change: low-pH activation of the influenza virus hemagglutinin. *JCB* **105,** 2887-2896 (1987).

22. Bottcher, C., Ludwig, K., Herrmann, A., van Heel, M. & Stark, H. Structure of influenza haemagglutinin at neutral and at fusogenic pH by electron cryo-microscopy. *FEBS Lett* **463,** 255-259 (1999).

23. Huang, Q. et al. Early steps of the conformational change of influenza virus hemagglutinin to a fusion active state: stability and energetics of the hemagglutinin. *Biochim Biophys Acta* **1614,** 3-13 (2003).

24. Godley, L. et al. Introduction of intersubunit disulfide bonds in the membrane-distal region of the influenza hemagglutinin abolishes membrane fusion activity. *Cell* **68,** 635-645 (1992).

25. Kemble, G.W., Bodian, D.L., Rose, J., Wilson, I.A. & White, J.M. Intermonomer disulfide bonds impair the fusion activity of influenza virus hemagglutinin. *J Virol* **66,** 4940-50 (1992).

26. Gigant, B. et al. A neutralizing antibody Fab-influenza haemagglutinin complex with an unprecedented 2:1 stoichiometry: characterization and crystallization. *Acta Crystallogr D Biol Crystallogr* **56,** 1067-1069 (2000).

27. Lebowitz, J., Lewis, M.S. & Schuck, P. Modern analytical ultracentrifugation in protein science: a tutorial review. *Protein Science* **11,** 2067-2079 (2002).

28. Lewis, M.S. & Junghans, R.P. Ultracentrifugal analysis of molecular mass of glycoproteins of unknown or ill-defined carbohydrate composition. *Methods Enzymol* **321,** 136-149 (2000).

29. Glick, G.D., Toogood, P.L., Wiley, D.C., Skehel, J.J. & Knowles, J.R. Ligand recognition by influenza virus. The binding of bivalent sialosides. *J Biol Chem* **266,** 23660-23669 (1991).

30. Lees, W.J., Spaltenstein, A., Kingery-Wood, J.E. & Whitesides, G.M. Polyacrylamides bearing pendant alpha-sialoside groups strongly inhibit agglutination of erythrocytes by influenza A virus: multivalency and steric stabilization of particulate biological systems. *J Med. Chem.* **37,** 3419-3433 (1994).

31. Waldmann, M. et al. A nanomolar multivalent ligand as entry inhibitor of the hemagglutinin of avian influenza. *J Am Chem Soc* **136,** 783-788 (2014).

32. Bandaranayake, A.D. et al. Daedalus: a robust, turnkey platform for rapid production of decigram quantities of active recombinant proteins in human cell lines using novel lentiviral vectors. *Nucleic Acids Research* **39,** e143 (2011).

33. Lin, Y.P. et al. Evolution of the receptor binding properties of the influenza A(H3N2) hemagglutinin. *PNAS* **109,** 21474-21479 (2012).

Chapter V: Perspectives and Future Directions

The aim of this dissertation was to i) monitor regions within HA that respond to low pH, and ii) investigate various modes of HA inhibition either at the HA1 head or HA2 stem. Although chapter II describes the low pH fusion activation profile of the group-2 H3 isolate, in which the fusion peptide appears to show the largest degree of destabilization; new data reported in chapter III investigating group-1 H1 isolates supports the notion that fusion activation may be highly subtype specific, and in some cases may vary among divergent isolates.[1,2] Between these two comparisons, it is possible that fusion activation in group-1 subtypes is initiated within the HA1 head, rather than the fusion elements, which is consistent with the proposed fusion mechanism from the Herrmann group, where the HA1 head must first open to allow water into the core of the trimer before the release of the fusion peptide.[3] Furthermore, the overall HDX profile of the fusion peptide in both examined H3 and H1 isolates, even at neutral pH, suggests large differences in the conformational dynamics that may govern membrane fusion. It is possible that such mechanistic variations reflect the virological adaptations reflective for each specific group, though it is strongly cautioned to make broad assumptions of an entire group based upon a single isolate characterization. High resolution crystal structures of several HA isolates from each group have shown that the overall architecture is somewhat distinctive between the two groups.[4-6] Thus, it is advised that future studies should make an effort to examine multiple subtypes from each group in an attempt to comprehensively probe the impact sequence variability has within the context of a three-dimensional protein structure and its inherent stability in the pre-fusion state and consequently during the course of acid-activation.

The type of HDX implemented in this dissertation was "continuous-labeling", in which a protonated HA (or HA complex) was incubated in D_2O, and the isotope exchange of the amide proton for deuterium was monitored as a function of incubation time.[7] In this scenario, the protein conformation is under equilibrium conditions and all exchangeable sites should uptake deuterium in a uniform fashion, as a function of their local intrinsic folding and unfolding rate in solution. While these experiments were capable of identifying isolate specific differences of HA as a function of pH, there is still a wealth of mechanistic information missing. For example, it appears that the fusion peptide pocket in H3 responds to low pH before the HA1-HA1 interface; however, it is still unknown whether fusion peptide deployment precedes the re-folding of the B-loop into a helix, or if these occur in a concerted manner. HDX "pulse-labeling" experiments are non-equilibrium kinetic experiments that have been useful to assess aspects of the "protein-folding problem" for proteins systems such as lysozyme, and to identify short-lived intermediates during a functional conformational change.[8,9] Thus, "pulse-labeling" HDX-MS would be apt for studying the low pH transition of HA from the pre-fusion to post-fusion conformation. Such an experiment would involve varying the time in which HA is incubated in a low pH environment (~pH 5.0) that will trigger the post-fusion state, and then rapidly pulsing each time point with deuterium (~pH 8.0) prior to quench and digestion. It would be interesting to determine if the previously observed pH-dependent isolate specific differences are maintained during fusion, and these experiments may help delineate observed discrepancies throughout the literature.[3,10,11]

Complementary to HDX-MS, which is highly influenced by secondary structure, oxidative labeling analyzed by mass spectrometry utilizes hydroxyl radicals generated rapidly by either synchrotron X-ray radiolysis of water or UV laser photolysis of hydrogen peroxide to covalently modify solvent accessible amino acid side chains within the tertiary or quaternary structure of a protein and/or complex.[9,12-15] By probing side-chain reactivity to radicals in bulk solvent, oxidative radical labeling allows solvent-accessible protein surfaces to be mapped.[14-19] Furthermore, the versatility of the both methods to be performed under a broad range of solution conditions enables the analysis of large dynamic protein systems that require atypical environments (e.g. detergents, low pH).[9,20] In a similar fashion to HDX-MS, oxidative labeling can be used to monitor the changes in side chain burial or exposure of a protein in chemical equilibrium, or by studying the kinetics of a protein folding/re-folding experiment. Using oxidative labeling in conjunction with "pulse-labeling" HDX experiments to monitor the transition from pre-fusion to post-fusion HA will provide insight into the steps required to organize the 3-dimension architecture necessary for productively carrying out membrane fusion. Furthermore, the reports of whole virus HDX-MS can also be used to probe any differences between the liberated HA ectodomain and the full-length HA *in situ*. With better instrumentation, sample handling protocols, and software it will be exciting to see how the field of HA activation and membrane fusion will progress.

In addition to group specific fusion activation, antibody mediated neutralization in most cases is highly type specific due to low sequence conservation at the immunodominate HA1 head.[21,22] The goal of current influenza vaccinology is to induce highly potent and broadly specific neutralizing antibodies to hemagglutinin in the effort to create a universal vaccine. Recent developments in the design of pre-fusion HA2 constructs as well as novel strategies focusing the immune response towards HA2 show much promise.[23-27] Understanding the structural mechanisms of antibody mediated neutralization within HA can aid in the development of universal vaccines and rational drug design for HA-targeting therapeutics.

In chapter III and IV, it was confirmed that the two different modes of antibody-antigen complexes; HC63-BHA and FI6v3-BHA indicate that it is possible for antibodies to prevent the low pH transition by i) cross-linking the HA1-HA1 interface to prevent HA1 "uncaging" and ii) targeting the stem to prevent the deployment of the fusion peptide and trimerization of the HA2 short helix. However, the large differences in the extent of stabilization (e.g. ΔT_m of 6.6°C between the two binding modes) suggests that stabilizing the HA2 stem may be a better strategy for preventing the low pH transition than stabilizing the HA1 head. Preventing the release of the fusion peptide either directly by stabilizing the fusion peptide cavity, or indirectly by preventing the association of the short helices within the trimer, are likely effective avenues for rational designed therapeutics such as the HB36.6 HA2 targeting protein inhibitor. However, it appears that the overall stabilization within the H1-HB36.6 complex was localized to the C-terminal fusion peptide only, and while binding does induce high destabilization in HA2 such effects do not appear to impact the protection efficacy in mice and ferrets (Treants M.E. et al. manuscript in submission). Yet, it is likely that by optimizing HB36.6 in a way that mitigates the destabilization upon binding, and by mirroring the stabilization observed for the FI6v3 HA complex, it may be possible to produce a higher affinity and potentially broader targeting ligand.

With regards to the low affinity target of the HA1 receptor binding pocket, it has been shown that multivalent sialiosides interacting within this domain can sufficiently target HA, and in some cases inhibit viral infection.[28-32] The sialosides are usually ligated through a flexible polyethylene glycol (PEG) linker that may contribute an entropic cost in binding of the ligand to the HA1 head and resulting in a micromolar K_D, which may explain why after 30 years of research these efforts are still therapeutically unsuccessful.[33,34] A more recent study using peptidic linkers in place of PEG for a panel of multivalent sialosides designed *in silico* have generated potential inhibitors that have enhanced the K_D from micromolar to nanomolar and may be clinically promising.[35]

The Head Binder analyzed by HDX-MS, SAXS and MALS reported in chapter IV, has a reported K_D of ~picomolar for the HA1 receptor binding domain (personal communication from the Baker Lab), yet the rapid association/dissociation kinetics appear to complicate full characterization and may be due to i) the low affinity interaction within each binding lobe per protomer and ii) the intrinsic flexibility within the peptidic linker. Therefore, it may be advantageous to optimize the Head Binder by either shortening the linker length, and/or introducing a sialoside within each domain to enhance the binding to the receptor binding pocket. The required multivalent association that is necessary for a tight interaction between HA1 and sialic acid analogues contrast what has been observed for the stem targeting small molecule TBHQ, which binds each protomer in a 1:1 stoichiometry with moderate affinity K_D of ~micromolar.[36] While it is unclear at this moment why such interactions differ, it is possible that the multibasic and hydrophobic patches lining the HA2 fusion stem may provide a better target for a wider range of molecules.

Taken together, this dissertation highlights the ability of solution-phase techniques for structural analysis and structure determination, which in combination with known high-resolution data can be used to investigate viral glycoproteins in multiple functional states. The use of HDX-MS, SAXS and MALS has also been paramount for reinterpreting crystallographic data and the erroneous solution-phase analyses that have been previously published for the HC63 antibody. These findings stress the importance of implementing hybrid approaches that can monitor large dynamic events and also be used to validate static high resolution structures, which may not always reveal what occurs under native solution conditions.[37-39]

It is likely that solution-phase techniques such as structural mass spectrometry, SAXS and electron microscopy will continue to provide unprecedented insight into the most dynamic stages of the infectious cycles of multiple pathogenic viruses as few other techniques are capable of probing these states in such detail, and recent implementation of single-molecule Förester resonance energy transfer used to monitor the conformational ensembles of HIV envelope on the surface of whole virus may also be implemented for studying HA activation.[32] Current tactics that attempt to unify a range of data from solution-phase albeit lower techniques and classical methods will provide a deeper and comprehensive understanding of the structure-function relationship between highly dynamic, variable and complex viral glycoproteins than any single method alone can provide.[40] Integrative structural biology of viral glycoproteins is thus poised to move from the realm of providing static snapshots of beginning and end states towards shedding light on the dynamic processes and conformational changes that drive their function.

CHAPTER V REFERENCES

1. Costello, D.A., Whittaker, G.R. & Daniel, S. Variations in pH sensitivity, acid stability, and fusogenicity of three influenza virus H3 subtypes. *J Virol* **89,** 350-360 (2015).
2. Puri, A., Booy, F.P., Doms, R.W., White, J.M. & Blumenthal, R. Conformational changes and fusion activity of influenza virus hemagglutinin of the H2 and H3 subtypes: effects of acid pretreatment. *J Virol* **64,** 3824-3832 (1990).
3. Böttcher, C., Ludwig, K., Herrmann, A., van Heel, M. & Stark, H. Structure of influenza haemagglutinin at neutral and at fusogenic pH by electron cryo-microscopy. *FEBS Lett*, **463,** 255-259 (1999).
4. Russell, R.J. et al. H1 and H7 influenza haemagglutinin structures extend a structural classification of haemagglutinin subtypes. *Virology* **325,** 287-296 (2004).
5. Ha, Y., Stevens, D.J., Skehel, J.J. & Wiley, D.C. H5 avian and H9 swine influenza virus haemagglutinin structures: possible origin of influenza subtypes. *EMBO J* **21,** 865-875 (2002).
6. Mair, C.M., Ludwig, K., Herrmann, A. & Sieben, C. Receptor binding and pH stability - how influenza A virus hemagglutinin affects host-specific virus infection. *Biochim Biophys Acta* **1838,** 1153-1168 (2014).
7. Marcsisin, S.R. & Engen, J.R. Hydrogen exchange mass spectrometry: what is it and what can it tell us? *Anal BioAnal Chem* **397,** 967-972 (2010).
8. Konermann, L. & Simmons, D.A. Protein-folding kinetics and mechanisms studied by pulse-labeling and mass spectrometry. *Mass Spectrom Rev* **22,** 1-26 (2003).
9. Konermann, L., Vahidi, S. & Sowole, M.A. Mass spectrometry methods for studying structure and dynamics of biological macromolecules. *Anal Chem* **86,** 213-32 (2014).
10. White, J.M. & Wilson, I.A. Anti-peptide antibodies detect steps in a protein conformational change: low-pH activation of the influenza virus hemagglutinin. *JCB* **105,** 2887-2896 (1987).

11. Kemble, G.W., Bodian, D.L., Rose, J., Wilson, I.A. & White, J.M. Intermonomer disulfide bonds impair the fusion activity of influenza virus hemagglutinin. *J Virol* **66,** 4940-4950 (1992).

12. Kiselar, J.G., Maleknia, S.D., Sullivan, M., Downard, K.M. & Chance, M.R. Hydroxyl radical probe of protein surfaces using synchrotron X-ray radiolysis and mass spectrometry. *Int J Radiat Biol* **78,** 101-14 (2002).

13. Kiselar, J.G. & Chance, M.R. Future directions of structural mass spectrometry using hydroxyl radical footprinting. *J Mass Spectrom* **45,** 1373-1382 (2010).

14. Maleknia, S.D., Brenowitz, M. & Chance, M.R. Millisecond radiolytic modification of peptides by synchrotron X-rays identified by mass spectrometry. *Anal Chem* **71,** 3965-3973 (1999).

15. Hambly, D.M. & Gross, M.L. Laser flash photolysis of hydrogen peroxide to oxidize protein solvent-accessible residues on the microsecond timescale. *J Am Soc Mass Spec* **16,** 2057-2063 (2005).

16. Xu, G. & Chance, M.R. Hydroxyl radical-mediated modification of proteins as probes for structural proteomics. *Chem Rev* **107,** 3514-43 (2007).

17. Xu, G. & Chance, M.R. Radiolytic modification and reactivity of amino acid residues serving as structural probes for protein footprinting. *Anal Chem* **77,** 4549-4555 (2005).

18. Gau, B.C., Sharp, J.S., Rempel, D.L. & Gross, M.L. Fast photochemical oxidation of protein footprints faster than protein unfolding. *Anal Chem* **81,** 6563-6571 (2009).

19. Chen, J., Rempel, D.L., Gau, B.C. & Gross, M.L. Fast photochemical oxidation of proteins and mass spectrometry follow submillisecond protein folding at the amino-acid level. *J Am Chem Soc* **134,** 18724-18731 (2012).

20. Konermann, L. & Pan, Y. Exploring membrane protein structural features by oxidative labeling and mass spectrometry. *Expert Rev Proteo* **9,** 497-504 (2012).

21. Gerhard, W., Yewdell, J., Frankel, M.E. & Webster, R. Antigenic structure of influenza virus haemagglutinin defined by hybridoma antibodies. *Nature* **290,** 713-717 (1981).

22. Wiley, D.C., Wilson, I.A. & Skehel, J.J. Structural identification of the antibody-binding sites of Hong Kong influenza haemagglutinin and their involvement in antigenic variation. *Nature* **289,** 373-378 (1981).

23. Yassine, H.M. et al. Hemagglutinin-stem nanoparticles generate heterosubtypic influenza protection. *Nature Medicine* **21**, 1065-1070 (2015).

24. Kanekiyo, M., Wei, C.J., Yassine, H.M. & McTamney, P.M. Self-assembling influenza nanoparticle vaccines elicit broadly neutralizing H1N1 antibodies. *Nature* ***499,*** 102-106 (2013).

25. Impagliazzo, A. et al. A stable trimeric influenza hemagglutinin stem as a broadly protective immunogen. *Science* **349,** 1301-1306 (2015).

26. Krammer, F. et al. Assessment of Influenza Virus Hemagglutinin Stalk-Based Immunity in Ferrets. *J Virol* **88,** 3432-3442 (2014).

27. Eggink, D., Goff, P.H. & Palese, P. Guiding the immune response against influenza virus hemagglutinin toward the conserved stalk domain by hyperglycosylation of the globular head domain. *J Virol* **88,** 699-704 (2014).

28. Gamian, A., Chomik, M., Laferriere, C.A. & Roy, R. Inhibition of influenza A virus hemagglutinin and induction of interferon by synthetic sialylated glycoconjugates. *J Microbiol* **37,** 233-237 (1991).

29. Glick, G.D., Toogood, P.L., Wiley, D.C., Skehel, J.J. & Knowles, J.R. Ligand recognition by influenza virus. The binding of bivalent sialosides. *JBC* **266,** 23660-23669 (1991).

30. Sauter, N.K. et al. Crystallographic detection of a second ligand binding site in influenza virus hemagglutinin. *PNAS* **89,** 324-328 (1992).

31. Lees, W.J., Spaltenstein, A., Kingery-Wood, J.E. & Whitesides, G.M. Polyacrylamides bearing pendant alpha-sialoside groups strongly inhibit agglutination of erythrocytes by influenza A virus: multivalency and steric stabilization of particulate biological systems. *J Med Chem* **37,** 3419-3433 (1994).

32. Munro, J.B. et al. Conformational dynamics of single HIV-1 envelope trimers on the surface of native virions. *Science* **7,** 759-763 (2014).

33. Jencks, W.P. On the attribution and additivity of binding energies. *PNAS* **78,** 4046-4050 (1981).

34. Page, M.I. & Jencks, W.P. Entropic contributions to rate accelerations in enzymic and intramolecular reactions and the chelate effect. *PNAS* **68,** 1678-1683 (1971).

35. Waldmann, M. et al. A nanomolar multivalent ligand as entry inhibitor of the hemagglutinin of avian influenza. *J Am Chem Soc* **136,** 783-788 (2014).

36. Russell, R.J. et al. Structure of influenza hemagglutinin in complex with an inhibitor of membrane fusion. *PNAS* **105,** 17736-17741 (2008).

37. Garcia, N.K., Guttman, M., Ebner, J.L. & Lee, K.K. Dynamic changes during acid-induced activation of influenza hemagglutinin. *Structure* **23,** 665-676 (2015).

38. Barbey-Martin, C. et al. An antibody that prevents the hemagglutinin low pH fusogenic transition. *Virology* **294,** 70-74 (2002).

39. Gigant, B. et al. A neutralizing antibody Fab-influenza haemagglutinin complex with an unprecedented 2:1 stoichiometry: characterization and crystallization. *Acta Crystallogr D Biol Crystallogr* **56,** 1067-1069 (2000).

40. Ward, A.B., Sali, A. & Wilson, I.A. Biochemistry. Integrative structural biology. *Science* **339,** 913-915 (2013).

SUPPLEMENTAL FIGURES

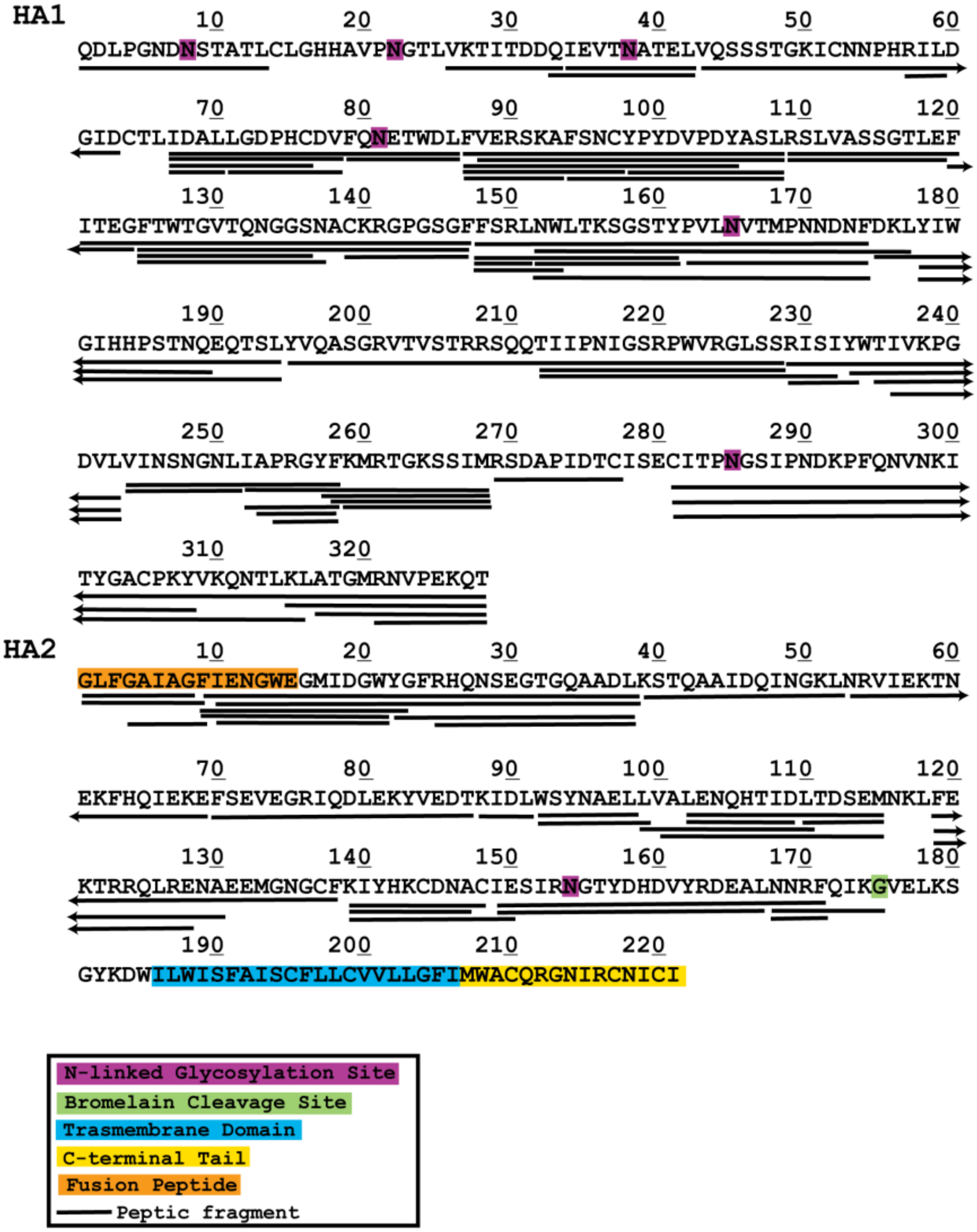

Figure S2.1: HDX-MS Sequence Coverage of BHA. Numbering of H3 BHA isolated from influenza A/Aichi/68 as denoted by Wilson et al. [1] Solid black line under the primary sequence represents observed peptic fragments for HA1 and HA2. N-linked glycosylation sites (purple), bromelain cleavage site (green), HA2 N-terminal fusion peptide (orange), unresolved transmembrane domain (blue) and C-terminal tail (yellow).

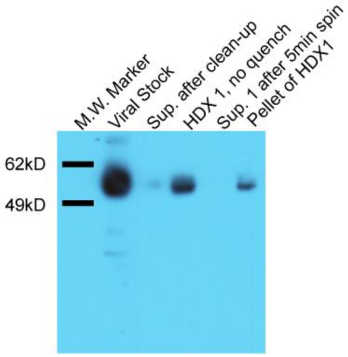

Figure S2.2: Whole Virus Western Blot During HDX. Whole virus and HDX preparations were carried out as in main-text methods in Optima Pure water instead of D_2O. Viral stock was used as an HA1 standard after high speed spin to remove residual egg protein, and a supernatant aliquot was taken following pelleting (“Sup. after clean-up”).“HDX1” was not quenched, an aliquot was taken prior to pelleting (main-text methods). Following 5min pelleting, an aliquot of the supernatant (“Sup.1”) and pellet was taken. Anti-HA1 monoclonal antibody (Millipore), which binds to a linear epitope of HA1 was used 1:100 and HA1 was visualized via HRP-conjugate anti-mouse secondary. An anti-HA1 antibody was used under the assumption that if HA were shed from the viral surface, only HA1 would be detected in the supernatant since HA2 is anchored in the viral membrane and would pellet with virus, since HA1 was only detected in the starting material and pellet, and not the supernatant after pelleting, all HA monitored via HDX was native HA.

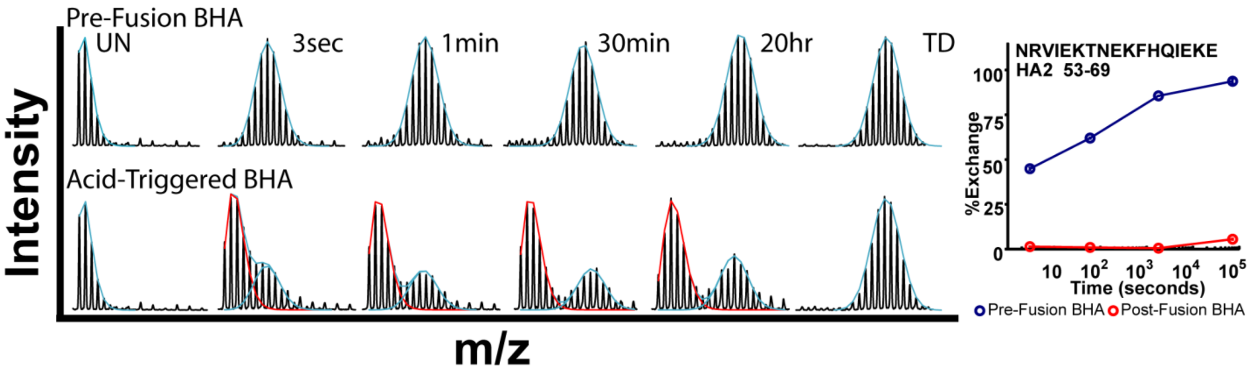

Figure S2.3. Example of Bimodal Deconvolution of Post-Fusion BHA in Acid-Triggered BHA HDX-MS Raw Spectra. Binomial fitting of pre-fusion BHA spectra (light blue line) displayed kinetics reflective of a homogenous population undergoing EX2 exchange. Raw spectral data for acid-triggered BHA exhibited spectral broadening and distinct bimodal distributions where the population of each species remained constant overtime, indicative of two distinct conformations undergoing EX2 exchange during HDX. Bimodal deconvolution was used to identify deuterium kinetics for post-fusion BHA (red line) by constraining one population to the pre-fusion envelope (light blue). [2,3] This specific example of the B-loop serves as a proof of principle for analysis of this system since one would expect the transition from loop-to-helix in post-fusion BHA (red dots) to generate a highly protected species relative to the exposed pre-fusion species (blue dots), which is observed in the exchange plot. [4,5]

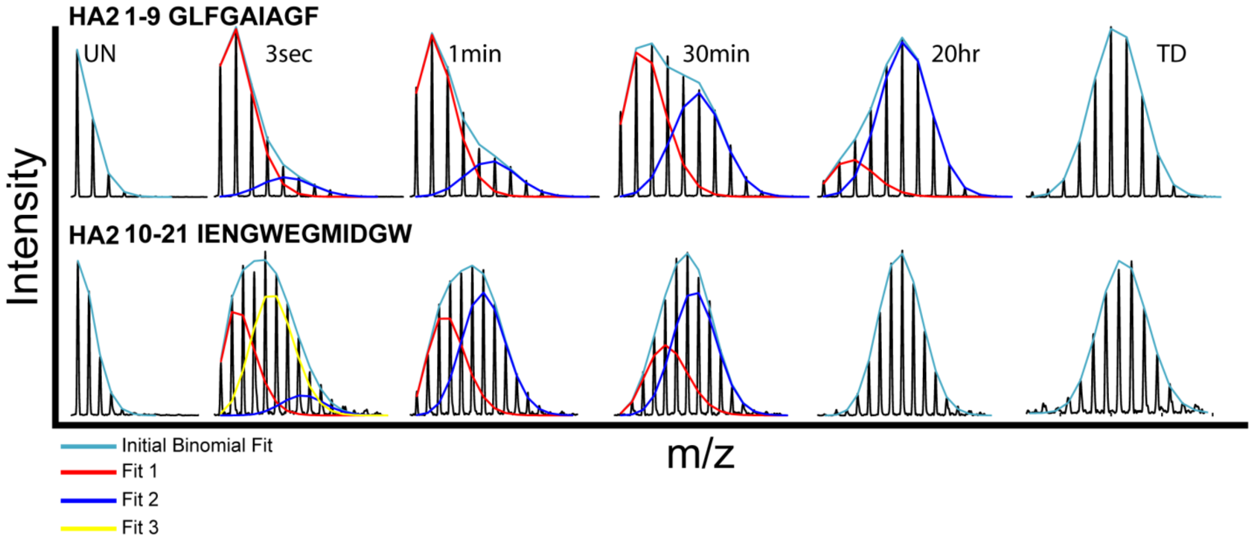

Figure S2.4. Fusion Peptide Raw Spectral Data in Acid-Triggered BHA. Raw spectral HDX data for the fusion peptide in acid-triggered BHA exhibits mixed exchange kinetics distinctive of species observed in Figure S2.3. Since the relative populations within the spectral data change as a function of time, and a portion of the sample contains pre-fusion BHA; it is difficult to definitively decipher the kinetics of post-fusion BHA. This type of kinetics was only observed in this region of acid-triggered BHA. Furthermore, previously published data suggests this site promotes aggregation in acid-triggered BHA. [6-8]

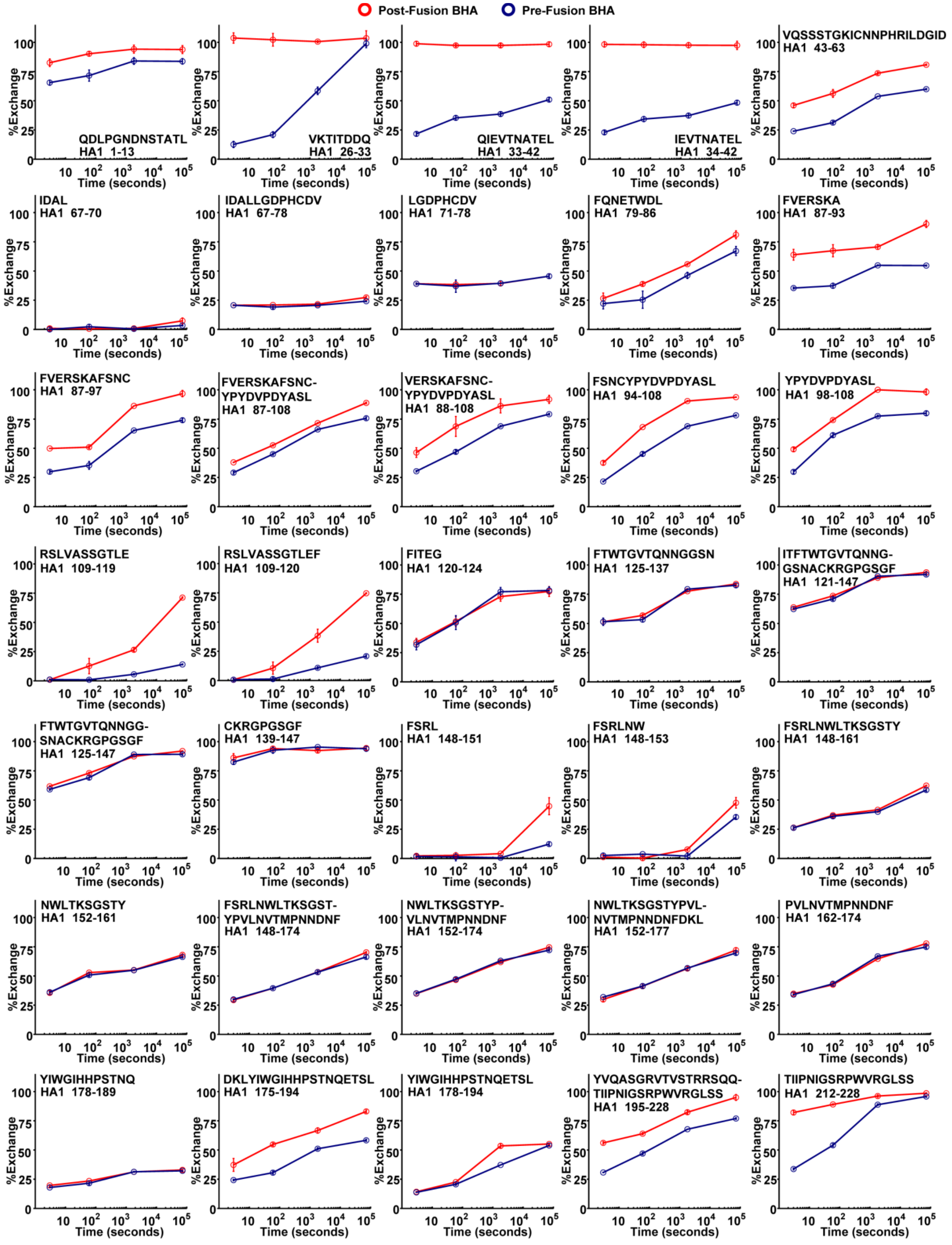
Post-Fusion BHA
Pre-Fusion BHA
%Exchange
Time (seconds)
0
25
50
75
100
10
10^2
10^3
10^4
10^5
QDLPGNDNSTATL HA1 1-13
VKTITDDQ HA1 26-33
QIEVTNATEL HA1 33-42
IEVTNATEL HA1 34-42
VQSSSTGKICNNPHRILDGID HA1 43-63
IDAL HA1 67-70
IDALLGDPHCDV HA1 67-78
LGDPHCDV HA1 71-78
FQNETWDL HA1 79-86
FVERSKA HA1 87-93
FVERSKAFSNC HA1 87-97
FVERSKAFSNC-YPYDVPDYASL HA1 87-108
VERSKAFSNC-YPYDVPDYASL HA1 88-108
FSNCYPYDVPDYASL HA1 94-108
YPYDVPDYASL HA1 98-108
RSLVASSGTLE HA1 109-119
RSLVASSGTLEF HA1 109-120
FITEG HA1 120-124
FTWTGVTQNNGGSN HA1 125-137
ITFTWTGVTQNNG-GSNACKRGPGSGF HA1 121-147
FTWTGVTQNNGG-SNACKRGPGSGF HA1 125-147
CKRGPGSGF HA1 139-147
FSRL HA1 148-151
FSRLNW HA1 148-153
FSRLNWLTKSGSTY HA1 148-161
NWLTKSGSTY HA1 152-161
FSRLNWLTKSGST-YPVLNVTMPNNDNF HA1 148-174
NWLTKSGSTYP-VLNVTMPNNDNF HA1 152-174
NWLTKSGSTYPVL-NVTMPNNDNFDKL HA1 152-177
PVLNVTMPNNDNF HA1 162-174
YIWGIHHPSTNQ HA1 178-189
DKLYIWGIHHPSTNQETSL HA1 175-194
YIWGIHHPSTNQETSL HA1 178-194
YVQASGRVTVSTRRSQQ-TIIPNIGSRPWVRGLSS HA1 195-228
TIIPNIGSRPWVRGLSS HA1 212-228

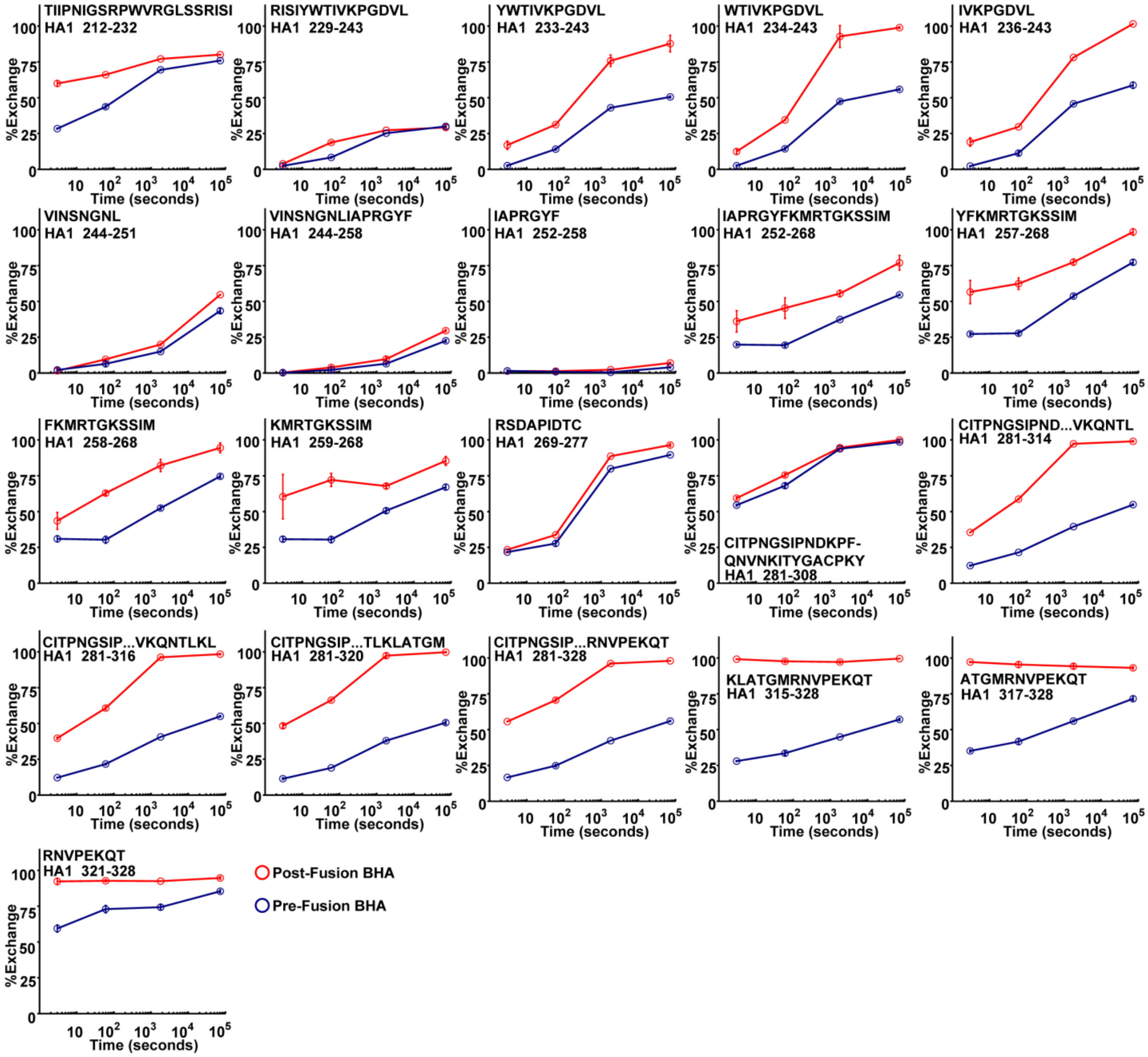
TIIPNIGSRPWVRGLSSRISI HA1 212-232
RISIYWTIVKPGDVL HA1 229-243
YWTIVKPGDVL HA1 233-243
WTIVKPGDVL HA1 234-243
IVKPGDVL HA1 236-243
VINSNGNL HA1 244-251
VINSNGNLIAPRGYF HA1 244-258
IAPRGYF HA1 252-258
IAPRGYFKMRTGKSSIM HA1 252-268
YFKMRTGKSSIM HA1 257-268
FKMRTGKSSIM HA1 258-268
KMRTGKSSIM HA1 259-268
RSDAPIDTC HA1 269-277
CITPNGSIPNDKPF-QNVNKITYGACPKY HA1 281-308
CITPNGSIPND...VKQNTL HA1 281-314
CITPNGSIP...VKQNTLKL HA1 281-316
CITPNGSIP...TLKLATGM HA1 281-320
CITPNGSIP...RNVPEKQT HA1 281-328
KLATGMRNVPEKQT HA1 315-328
ATGMRNVPEKQT HA1 317-328
RNVPEKQT HA1 321-328
%Exchange
0
25
50
75
100
10
10^2
10^3
10^4
10^5
Time (seconds)
Post-Fusion BHA
Pre-Fusion BHA

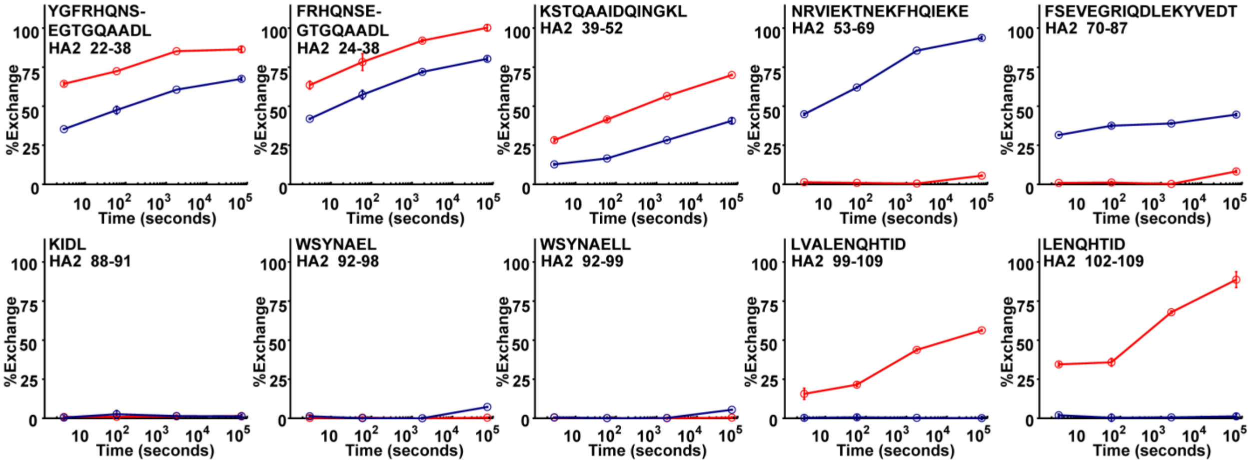
YGFRHQNS-EGTGQAADL HA2 22-38
FRHQNSE-GTGQAADL HA2 24-38
KSTQAAIDQINGKL HA2 39-52
NRVIEKTNEKFHQIEKE HA2 53-69
FSEVEGRIQDLEKYVEDT HA2 70-87
KIDL HA2 88-91
WSYNAEL HA2 92-98
WSYNAELL HA2 92-99
LVALENQHTID HA2 99-109
LENQHTID HA2 102-109
%Exchange
0
25
50
75
100
10
10^2
10^3
10^4
10^5
Time (seconds)

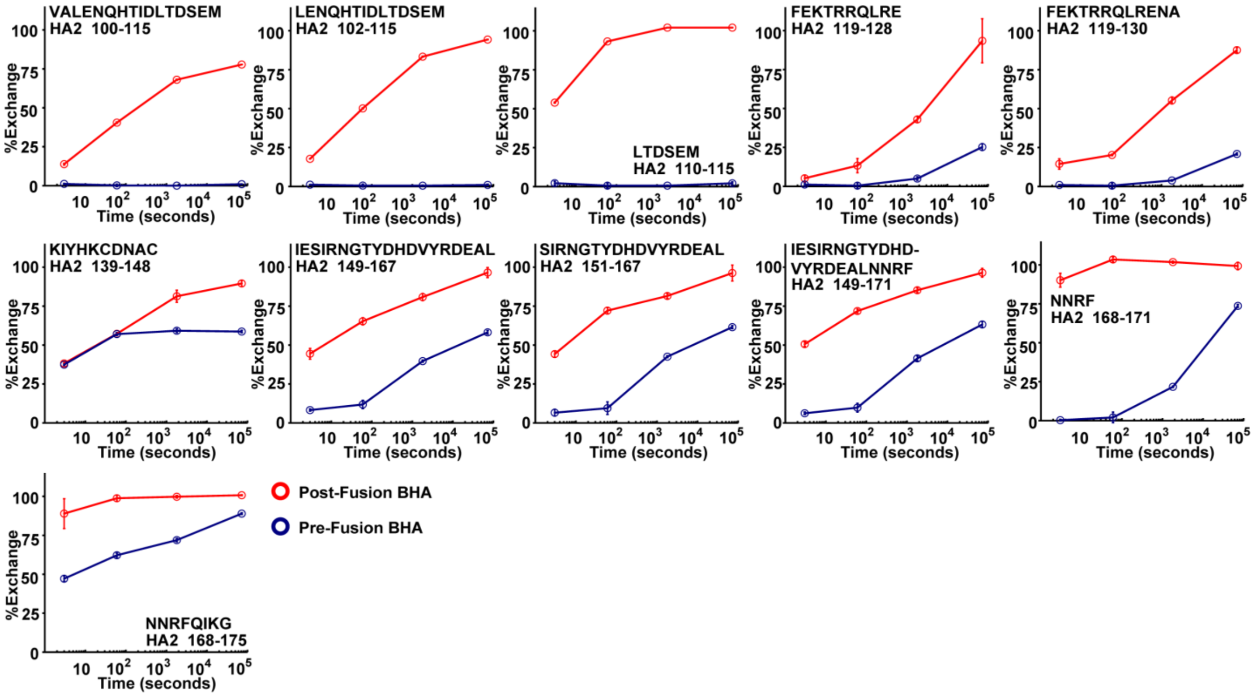

Figure S2.5. Individual HDX plots for all observable peptides of HA1 and HA2 comparing pre- (blue dots) and post-fusion (red dots) BHA. Each plot represents the average from multiple charge states and duplicate measures with the error bars denoting the standard spread between duplicates.

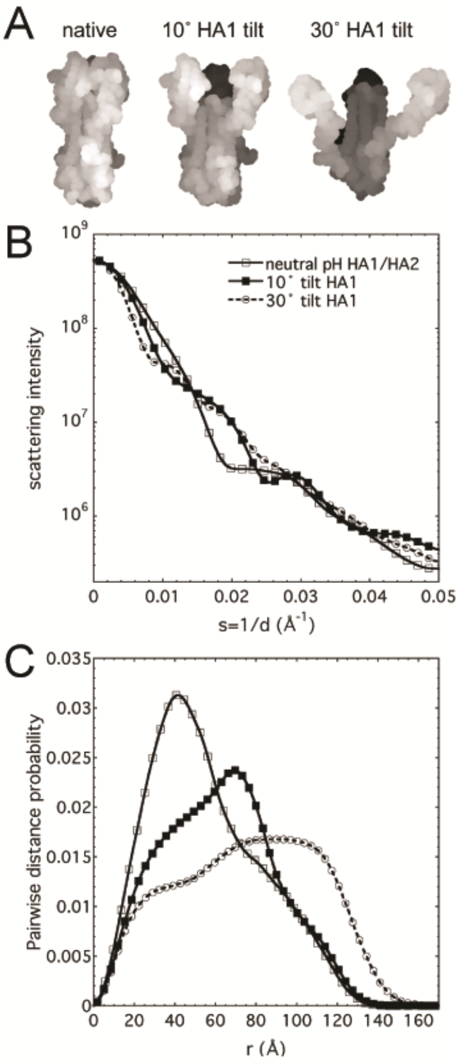

Figure S2.6. Theoretical Small-angle X-ray scattering for Activated BHA. A) Rigid body rotation of HA1 to 10° and 30° tilts from the pre-fusion BHA structure. **B)** Theoretical SAXS patterns of modeled BHA from A) using CRYSOL and GNOM [9,10] showed substantial differences in computed SAXS curves. **C)** Subsequent P(r) pairwise distance distribution plot from SAXS curves in **A)** showed large changes in the mass distribution.

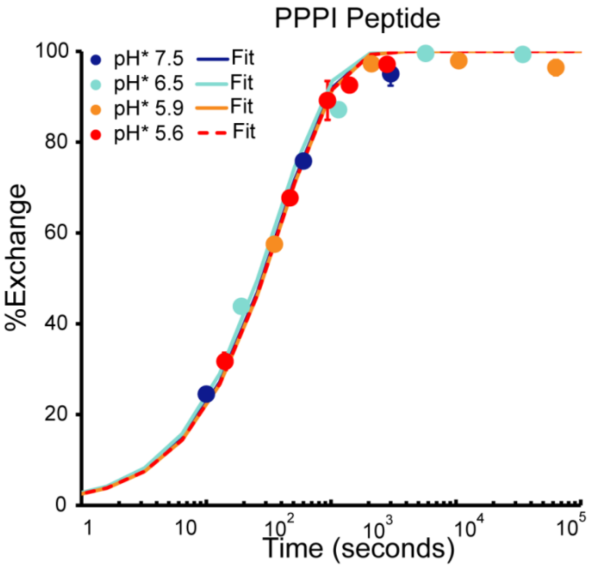

Figure S2.7. Scaled pH-Dependent Exchange Kinetics of Internal Standard PPPI Peptide. Single exponential rates were calculated and scaled for pH* 6.5 (cyan), 5.9 (orange) and 5.6 (red) relative to pH*7.5 (blue) data.[11-13] Each exchange was performed in duplicate and the error bars indicate the standard deviation of both measures in corresponding pH*.

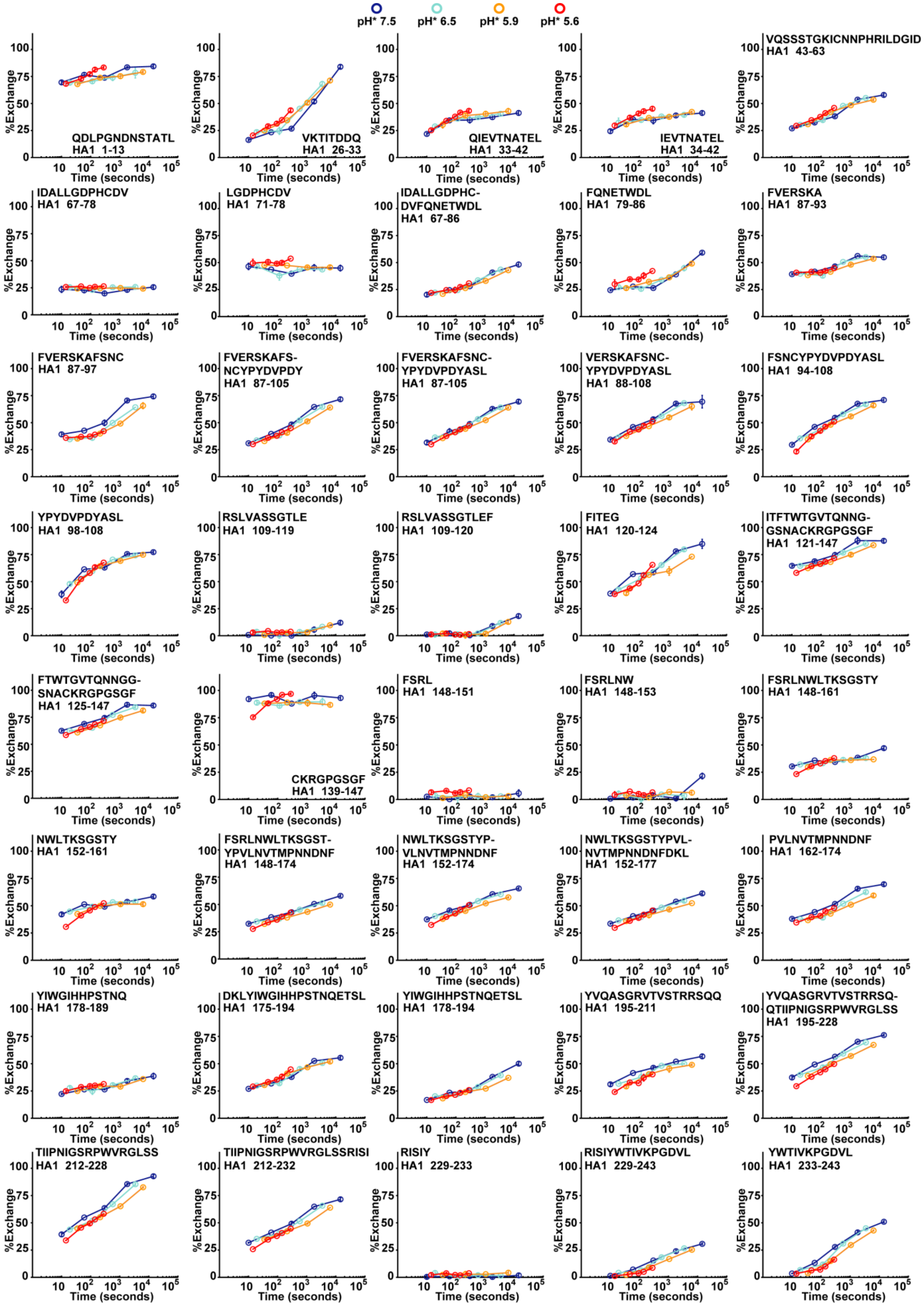
pH* 7.5
pH* 6.5
pH* 5.9
pH* 5.6
%Exchange
Time (seconds)
0
25
50
75
100
10
10^2
10^3
10^4
10^5
QDLPGNDNSTATL HA1 1-13
VKTITDDQ HA1 26-33
QIEVTNATEL HA1 33-42
IEVTNATEL HA1 34-42
VQSSSTGKICNNPHRILDGID HA1 43-63
IDALLGDPHCDV HA1 67-78
LGDPHCDV HA1 71-78
IDALLGDPHC-DVFQNETWDL HA1 67-86
FQNETWDL HA1 79-86
FVERSKA HA1 87-93
FVERSKAFSNC HA1 87-97
FVERSKAFS-NCYPYDVPDY HA1 87-105
FVERSKAFSNC-YPYDVPDYASL HA1 87-105
VERSKAFSNC-YPYDVPDYASL HA1 88-108
FSNCYPYDVPDYASL HA1 94-108
YPYDVPDYASL HA1 98-108
RSLVASSGTLE HA1 109-119
RSLVASSGTLEF HA1 109-120
FITEG HA1 120-124
ITFTWTGVTQNNG-GSNACKRGPGSGF HA1 121-147
FTWTGVTQNNGG-SNACKRGPGSGF HA1 125-147
CKRGPGSGF HA1 139-147
FSRL HA1 148-151
FSRLNW HA1 148-153
FSRLNWLTKSGSTY HA1 148-161
NWLTKSGSTY HA1 152-161
FSRLNWLTKSGST-YPVLNVTMPNNDNF HA1 148-174
NWLTKSGSTYP-VLNVTMPNNDNF HA1 152-174
NWLTKSGSTYPVL-NVTMPNNDNFDKL HA1 152-177
PVLNVTMPNNDNF HA1 162-174
YIWGIHHPSTNQ HA1 178-189
DKLYIWGIHHPSTNQETSL HA1 175-194
YIWGIHHPSTNQETSL HA1 178-194
YVQASGRVTVSTRRSQQ HA1 195-211
YVQASGRVTVSTRRSQ-QTIIPNIGSRPWVRGLSS HA1 195-228
TIIPNIGSRPWVRGLSS HA1 212-228
TIIPNIGSRPWVRGLSSRISI HA1 212-232
RISIY HA1 229-233
RISIYWTIVKPGDVL HA1 229-243
YWTIVKPGDVL HA1 233-243

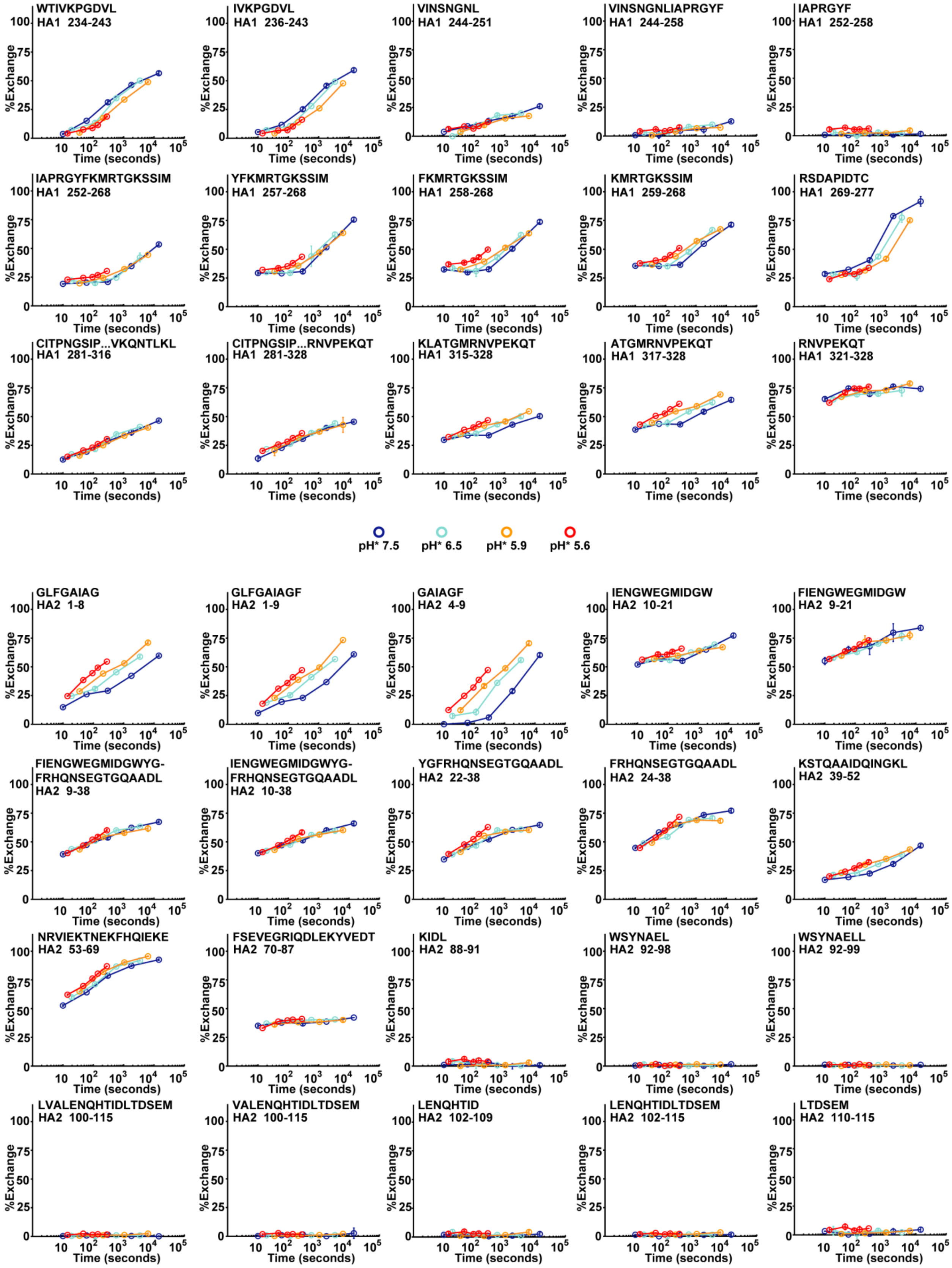
WTIVKPGDVL HA1 234-243
IVKPGDVL HA1 236-243
VINSNGNL HA1 244-251
VINSNGNLIAPRGYF HA1 244-258
IAPRGYF HA1 252-258
IAPRGYFKMRTGKSSIM HA1 252-268
YFKMRTGKSSIM HA1 257-268
FKMRTGKSSIM HA1 258-268
KMRTGKSSIM HA1 259-268
RSDAPIDTC HA1 269-277
CITPNGSIP...VKQNTLKL HA1 281-316
CITPNGSIP...RNVPEKQT HA1 281-328
KLATGMRNVPEKQT HA1 315-328
ATGMRNVPEKQT HA1 317-328
RNVPEKQT HA1 321-328
pH* 7.5
pH* 6.5
pH* 5.9
pH* 5.6
GLFGAIAG HA2 1-8
GLFGAIAGF HA2 1-9
GAIAGF HA2 4-9
IENGWEGMIDGW HA2 10-21
FIENGWEGMIDGW HA2 9-21
FIENGWEGMIDGWYG-FRHQNSEGTGQAADL HA2 9-38
IENGWEGMIDGWYG-FRHQNSEGTGQAADL HA2 10-38
YGFRHQNSEGTGQAADL HA2 22-38
FRHQNSEGTGQAADL HA2 24-38
KSTQAAIDQINGKL HA2 39-52
NRVIEKTNEKFHQIEKE HA2 53-69
FSEVEGRIQDLEKYVEDT HA2 70-87
KIDL HA2 88-91
WSYNAEL HA2 92-98
WSYNAELL HA2 92-99
LVALENQHTIDLTDSEM HA2 100-115
VALENQHTIDLTDSEM HA2 100-115
LENQHTID HA2 102-109
LENQHTIDLTDSEM HA2 102-115
LTDSEM HA2 110-115
%Exchange
0
25
50
75
100
Time (seconds)
10
10^2
10^3
10^4
10^5

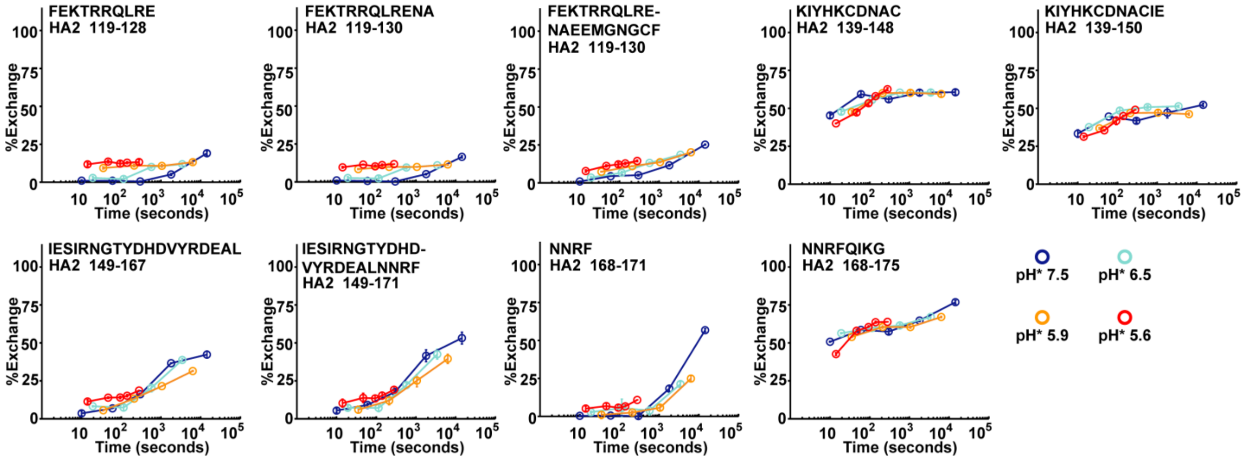

Figure S2.8. Individual HDX Plots for All Observable BHA peptides During Activation. Each plot represents the average from duplicate measurements where error bars indicate the standard deviation for each duplicate. Comparison of exchange data for pH* 7.5 (blue), 6.5 (cyan), 5.9 (orange) and 5.6 (red) where the mildly acidic conditions are scaled (see Figure S2.7) based on the internal PPPI standard for qualitative comparison.

SUPPLEMENTAL FIGURES REFERENCES

1. Wilson, I.A., Skehel, J.J. & Wiley, D.C. Structure of the haemagglutinin membrane glycoprotein of influenza virus at 3 A resolution. *Nature* **289**, 366-373 (1981).
2. Weis, D.D., Engen, J.R. & Kass, I.J. Semi-automated data processing of hydrogen exchange mass spectra using HX-Express. *J Am Soc Mass Spectrom* **17**, 1700-1703 (2006).
3. Guttman, M., Weis, D.D., Engen, J.R. & Lee, K.K. Analysis of overlapped and noisy hydrogen/deuterium exchange mass spectra. *J Am Soc Mass Spectrom* **24**, 1906-1912 (2013).
4. Bullough, P.A., Hughson, F.M., Skehel, J.J. & Wiley, D.C. Structure of influenza haemagglutinin at the pH of membrane fusion. *Nature* **371**, 37-43 (1994).
5. Carr, C.M. & Kim, P.S. A spring-loaded mechanism for the conformational change of influenza hemagglutinin. *Cell* **73**, 823-832 (1993).
6. Skehel, J.J. et al. Changes in the conformation of influenza virus hemagglutinin at the pH optimum of virus-mediated membrane fusion. *Proc Natl Acad Sci U S A* **79**, 968-972 (1982).
7. Ruigrok, R.W. et al. Electron microscopy of the low pH structure of influenza virus haemagglutinin. *EMBO J* **5**, 41-49 (1986).
8. Ruigrok, R.W. et al. Studies on the structure of the influenza virus haemagglutinin at the pH of membrane fusion. *J Gen Virol* **69,** 2785-2795 (1988).
9. Svergun, D., Barberato, C. & Koch, M.H.J. CRYSOL- a Program to Evaluate X-ray Solution Scattering of Biological Macromolecules from Atomic Coordinates. *J. Appl. Cryst.* **28**, 768-773 (1995).
10. Svergun, D.I. Determination of the regularization parameter in indirect-transform methods using perceptual criteria. *J App Cryst* **25**, 495-503 (1992).
11. Zhang, Z., Zhang, A. & Xiao, G. Improved protein hydrogen/deuterium exchange mass spectrometry platform with fully automated data processing. *Anal Chem* **84**, 4942-4949 (2012).

12. Bai, Y., Milne, J.S., Mayne, L. & Englander, S.W. Primary structure effects on peptide group hydrogen exchange. *Proteins* **17**, 75-86 (1993).

13. Connelly, G.P., Bai, Y., Jeng, M.F. & Englander, S.W. Isotope effects in peptide group hydrogen exchange. *Proteins* **17**, 87-92 (1993).